DETERMINATION OF THE ACCURACY AND SENSITIVITY OF INFRARED SENSORS FOR ANTHROPOMETRIC LYMPHEDEMA ASSESSMENT IN CLINICAL ENVIRONMENTS

A Dissertation
Presented to
The Academic Faculty

by

Iris Moying Lu

In Partial Fulfillment
of the Requirements for the Degree
Doctor of Philosophy in Bioinformatics in the
School of Biological Sciences

Georgia Institute of Technology
August 2019

DETERMINATION OF THE ACCURACY AND SENSITIVITY OF INFRARED SENSORS FOR ANTHROPOMETRIC LYMPHEDEMA ASSESSMENT IN CLINICAL ENVIRONMENTS

Approved by:

Dr. J. Brandon Dixon, Advisor
School of Mechanical Engineering
Georgia Institute of Technology

Dr. Fredrik Vannberg
School of Biological Sciences
Georgia Institute of Technology

Dr. Rudolph L. Gleason, Co-advisor
School of Mechanical Engineering
Georgia Institute of Technology

Dr. May D. Wang
Department of Biomedical Engineering
Georgia Institute of Technology

Dr. Eva Lee
School of Industrial and Systems Engineering
Georgia Institute of Technology

Dr. Sheryl Gabram-Mendola
School of Medicine
Emory University

Date Approved: April 9, 2019

To my family and friends who have supported me through this long, windy journey!

ACKNOWLEDGEMENTS

Graduate school has been a journey and has been much more than expected. Over the years, I have grown not only as a scholar but also as a person. It taught me a new level of discipline and greater ability to take life in strides.

I want to thank my extensive support system, because without everyone, I would not be here writing this acknowledgement section. So, here we go.

Thank you to my parents, Ken and Moying Lu. Thank you teaching me the value of an education and constantly pushing me to be and do better than I thought I ever could. Thank you for the decades of sacrifices to give me every opportunity possible to succeed in life. Thank you for giving me two sisters who have been instrumental in my growth, teaching me patience and the ability to guide. While this journey may have taken a bit longer than anticipated, thanks for your support and for pushing me to continue on.

Thank you to my sisters, Sallie and Connie Lu. Thank you for being constant listeners when the pressure of graduate school felt overwhelming. Thanks for keeping me grounded and telling things to me straight. I am so thankful to have you two as my sisters to continue through life together. Sallie and Jake, thanks for all those dinners when life felt too busy to even eat. It means more than you know.

Thank you to my husband, Eric Patterson. Thank you for your never-ending patience. Thanks for supporting my decision to continue my education over the last 12 years. Your constant support during the tough lows and great highs means so much and has

been instrumental in my ability to continue journeying on this path. I am looking forward to continue to do life with you over the next several decades. <3

Thank you to my officially new family, Scott and Dora Patterson and Angelica Howson. Thanks for all the positivity and constantly feeding me.

My friends – some have told me that I have too many and that is probably true but here we go. The besties in alphabetical order by first name (Adelbert, Amy, Andrew, Ben, Eric, Jason, Jessica, Kate, Kelly, Kevin, Keyur, Kris, Quan, Rena, Sarah, Viva, and Vu) – thanks for being such a fun and chill group. Our hangouts are always a great break from the stresses of graduate school and the constant cheering squad has been welcomed. Thank you, my Alpha Gams (Andrea, Alisha, Ariel, Amy, Corinne, Kathy, Liz, Megan, Morgan, Rachel, Susan, Tatiana). Dinners were always so fun to catch up, and learning about what you all are up to is always inspiring. Thank you to my newer friends from graduate school (Anish, Fabrice, Jose, Joshua, Kathleen, Katie, Kim, Kirsten, Liane, Likhit, Linda, Matthew, Mohammad, Scott, Stephen, Susan, Yoshi, and Zhanna). Thanks for keeping me sane and for all the shenanigans. Special shout out to Kirsten and Kathy for the girl lunches to take a break from the craziness and to Josh for being be best lab mate buddy and ensuring I stayed caffeinated. Thank you to Likhit for the great discussions regarding Aim 2. I cannot thank you enough for your work with arm alignment work and the implementation of the PCA, SDF, and regional curvature extraction. Thanks to my life mentor and cheering squad, Sarah Tew. Your constant pep talks have done wonders! Also, thanks to former lab mates (Drs. Jeff, Mike, Timothy, and Tyler) – your advice to get through graduate school was tremendously helpful.

Thank you to my advisor, Dr. J Brandon Dixon for taking me on as a first year and believing in me throughout the whole process. Without that chance, I would not be where I am today. Additionally, thank you to my co-advisor, Dr. Rudy Gleason, who always gave kind words of encouragement. Thank you to the rest of my committee, Drs. Sheryl Gabram-Mendola, Eva Lee, Fredrick Vannberg, and May D. Wang for your advice and pushing my project to new levels with your wonderful insight.

Thank you to all of my collaborators. Without their hard work and support, none of the work in this dissertation would have happened. First, thank you LymphaTech for providing the technology. Specifically, thank you to Mike and Nate; it has been a wonderful experience working with such a driven team tackling an important clinical challenge. Thank you to TurningPoint Breast Rehabilitiation Center, Grady Memorial Hospital, and Benchmark Rehab Partners for providing allowing us to recruit out of your clinic and teaching me so much about the clinical side of what breast cancer survivors endure. Special thanks to Jill Binkley and Rebecca Cowens-Alvarado for their support and teasing out logistics in the study design at TurningPoint. Thank you to the physical therapists (Lauren, Leslie, Carrie, Jessica, Anita, Grayson, and Jyoti) and staff (Karen, Sandy, and Renee) at TurningPoint. Thank you to Dr. Sheryl Gabram-Mendola, her team (Adriana, LeslieAnn, and Karen), and the surgeons of the Breast group at Grady for helping us recruit and scan patients and the general support. Thank you to John Jordi for the support and recruiting and scanning patients at Benchmark.

I would also like to thank my funding sources. Thank you to the Bill and Melinda Gates Foundation for the Phase 1 grant that supported my filariasis work. Thank you to the National Science Foundation for awarding me the Graduate Research Fellowship (GFFP).

Lastly, thank you for the Georgia Research Alliance grant. These last two sources provided me the opportunity to pursue the work described in this dissertation.

It goes without saying that all of those working behind the scenes were immeasurably helpful in ensuring that I can actually graduate. Thanks to my academic advisor, Lisa Redding. You have been such a great resource and such a positive person. Thank you to Laura Paige who helped me through my masters and stayed in contact to make sure I was doing okay throughout the process. Thanks to the rest of the Petit Institute staff (Melissa Raine, Colly Mitchell, Michelle Wong, Randy Johnson, Floyd Wood, Allen Echols, Karen Ethier, Rose Brito, Maria Pinto, and Margie Martin).

TABLE OF CONTENTS

LIST OF TABLES

LIST OF FIGURES

LIST OF SYMBOLS AND ABBREVIATIONS

LE	Lymphedema
QOL	Quality of life
BCRL	Breast cancer related lymphedema
S&S	Signs and symptoms
ICP	Iterative closest point
BMI	Body mass index
SDF	Shape Diameter Function

SUMMARY

Lymphedema is one of most feared side effects of cancer treatments in the United States. This disease leads to swelling of the affected limb and is associated with physical and psychological distress. Disease onset has no clear timeline. At risk patients may develop lymphedema immediately post-treatment or they may wait decades before developing lymphedema. Current medical care for at risk patients does not provide the continuous surveillance necessary for early lymphedema detection. Therefore, more often than not, patients diagnosed with lymphedema are subjected to a lifetime of maintenance, costing thousands of dollars per year in clinical visits and compression garments. In this dissertation, implementation of infrared sensor systems was explored and evaluated against the standard volume measurement tools used in specialized lymphedema clinics. The infrared sensor with the LymphaTech software resulted in good correlation and agreement with current measurement tools while being easier to use and more cost-effective than commercially available systems. Additionally, the efficacy of utilizing local arm geometries for the detection of arm lymphedema was determined. Anthropometric based features were extracted from a 3D point cloud using custom code and applied to train classification models for lymphedema. These features were shown to detect subtle changes in the arm of lymphedema patients with a sensitivity of 61% compared to the current standard volume difference measurement, which has a sensitivity of 33.3%. Clinics not equipped to detect lymphedema could integrate this infrared system and model as a screening tool to improve referral rates to lymphedema clinics.

CHAPTER 1. OVERVIEW AND SPECIFIC AIMS

1.1 Overview

Lymphedema is considered the most feared side effect of cancer treatment for survivors in the United States. Survivors are at a lifetime risk of developing this condition, and those who develop lymphedema will likely live with this condition for the rest of their life. Despite the pervasiveness of lymphedema among the survivor population, little is known about what triggers lymphedema.

The clinical community has developed protocols to detect lymphedema using basic technology and to treat affected survivors. Methods of detecting lymphedema are cumbersome and typically require significant training or financial resources. Therefore, prospective surveillance models, where at risk patients are consistently monitored for signs of lymphedema, are absent in the clinics despite several studies having shown the efficacy and long-term benefits of model implementation. It was found that earlier detection of lymphedema can reduce the extent of maintenance of this disease, but between the lack of continuous monitoring of at risk patients and current detection methods detecting the disease too late in its progression, there is a need for a tool that can begin to close this gap. Continuing with current approaches, the majority of those who develop lymphedema are rendered to a lifetime maintenance of this disease.

The challenge in lymphedema detection is two-fold. First, current measurement methods are either time intensive or expensive. Thus, there is a need for a new measurement method that requires less time to perform and is less expensive to implement in clinics specialized in lymphedema. Secondly, there is a lack of prospective surveillance

for patients at risk for lymphedema. Therefore, there is a need for a system that can easily monitor patients at risk for lymphedema that does not require a specialist and is financially affordable for clinics. New methods of detecting lymphedema that do not require specialized training and new approaches that have the potential to identify lymphedema earlier would address these challenges.

1.2 Specific Aims

I will explore the implementation of novel technologies in clinics that are not specialized to detect lymphedema and new metrics to diagnose lymphedema. The objective is to identify areas of improvement for lymphedema detection to potentially reduce the burden of this disease.

1.2.1 Specific Aim 1: Evaluate the implementation of infrared sensors in clinical settings of patients at risk for and with lymphedema.

This aim explores the efficacy and implementation of an infrared scanning system designed previously in the lab in three different clinical environments.

(a) The infrared system was compared to the breast cancer rehabilitation clinic's gold standard, another optoelectrical scanner, the Perometer. The participants were composed of breast cancer survivors with and without lymphedema (LE) in the arm.

(b) The infrared system was tested in a suburban hospital to gather longitudinal measurements of breast cancer patients pre- and post-operatively with no known lymphedema prior to participating in the study. This clinic does not routinely collect

volume measurements, but the tape measure circumferential method was used to collect measurements in parallel as a comparison.

(c) The infrared system was implemented and compared the standard volume measurement method used at a general rehabilitation clinic that also specializes in lymphedema care. The standard measurement method is the tape measure circumference method. Patients with leg lymphedema were measured longitudinally with both methods.

1.2.2 Specific Aim 2: Determine the efficacy of utilizing local geometrically relevant anthropometric measurements for the detection of arm lymphedema rather than current global volume measurements to detect lymphedema

In this aim, (a) I gathered arm scans of breast cancer survivors with and without lymphedema with a newer iteration of an infrared scanner. (b) Image processing methods were developed to analyze the point clouds generated from these scans, and local geometrical features were extracted from the scans. (c) These features were then used to develop a model to classify lymphedema.

1.3 Outline

This work focuses on the implementation of an infrared sensor system in clinics for arm and leg lymphedema and its ability to classify lymphedema. CHAPTER 2 provides an overview of the lymphatic system and lymphedema, a disease characterized by lymphatic system dysfunction. Clinical causes of lymphedema and current treatments for this disease were discussed. A thorough review of how lymphedema is currently detected is provided, in addition to a review of up-and-coming technologies with promising results found in

literature. The implementation of an infrared sensor system, previously developed in the lab, was explored in three different clinical contexts in CHAPTER 3. These studies showed the system's efficacy in arm and legs in various clinical contexts. In CHAPTER 4, the processing techniques implemented on point clouds collected with the second iteration of the infrared sensor system were discussed. The local anthropometric features were described and were examined in their ability to train a model to classify arm lymphedema. Lastly, CHAPTER 5 discusses the conclusions of this dissertation's work and future work.

CHAPTER 2. BACKGROUND AND SIGNIFICANCE

2.1 Lymphatics System

The lymphatic system is composed of a network of vessels and lymph nodes that present throughout the tissues of the body. It serves three primary roles: (1) maintaining fluid balance, (2) trafficking immune cells, and (3) aiding in lipid absorption.[1–3] Fluid that filters out of the vascular capillaries and does not get reabsorbed is transported through the lymphatic network, outlined in green in Figure 1, back to the vascular system; this volume is approximate 10% of the total fluid volume filtered by the capillaries.

Figure 1 The Lymphatic System represented by the green lines runs throughout the body (Royalty free image from ID 36217306 © Shubhangi Kene | Dreamstime.com)

Unlike the vascular system, the lymphatic system does not have a central pump like the heart. There are intrinsic (lymphatic vessel pumping) and extrinsic (interstitial fluid pressure) factors that propel fluid from the extremities back to the subclavian veins.[4] Fluid in the interstitial space is drained through the lymphatic capillaries, which are composed

of blunt-end collections of lymphatic endothelial cells and basement membrane. These initial lymphatics join to form collecting vessels, composed of an inner layer of lymphatic endothelial cells surrounded by an outer layer of lymphatic smooth muscle cells. Collecting vessels are comprised of serial units of lymphangions, segmented by bileaflet valves. These units pump to propel fluid unidirectionally back towards the vascular system.

When the lymphatic system does not operate properly, a variety of complications can occur. Dysfunction has been implicated in cardiovascular disease, cancer metastasis, obesity, and infection, but the specific mechanisms are not yet known.[5] When the lymphatics is unable to properly remove the protein rich fluid, fluid accumulation occurs, which can lead to lymphedema.

2.2 Lymphedema

2.2.1 Definition, Types, and Causes of Lymphedema

Lymphedema (LE) is a condition that is the result of an imbalance between the vascular capillary exchange and lymph drainage.[6] Lymphedema can be defined as an abnormal accumulation of protein rich fluid built up in the superficial tissue.[7] This insufficiency can be a result of (1) the influx of fluid either due to higher rates of capillary filtration or lower rates of reabsorption or (2) the reduction of drainage in the lymphatic capillaries. While the specific mechanism that results in LE is unknown, there are long-term impacts on those who develop this disease. The physical manifestation of lymphedema is characterized by the swelling of the affected limb as a result of fluid buildup. Over time, this accumulation of protein rich fluid leads to fibrosis and lipid

deposits. While this disease is commonly not fatal, the morbidity severely impacts the quality of life (QOL) of those affected.[8–10]

There are two types of lymphedema, primary and secondary.[11] Primary lymphedema is when lymphedema is not a direct result of another medical condition, and onset can range from birth to adulthood. Congenital lymphedema presents at birth, whereas lymphedema praecox occurs between the ages of 1 to 35 years, and lymphedema tarda occurs after 35 years. Secondary lymphedema is defined as a result of a medical condition, typically due to some occurrence later in life such as cancer treatment or filariasis. In the United States, the most common cause of lymphedema is the result of cancer treatment that disrupts the lymphatic network. Between radiation and surgical interventions, the survivors of cancer are at high risk of developing lymphedema over their lifetime.[12] This disease can occur at any point post-treatment, at any age, and among any gender and racial background. It is important to remember that there are non-cancer related lymphedema, and these cases tend to be underreported.[13] While there are a multitude of studies that show specific activities to be high-risk for development of lymphedema[14–18], the mechanisms of the onset of lymphedema are unclear.

In the United States (US), breast cancer (BC) survivors make up a large portion of lymphedema cases, and BC is the leading cancer diagnosis among women and was expected to account for 30% (or 63,410) of all new cancers in women in 2017.[19] Fortunately, the survival rate has improved over the past couple of decades, but that means there are more survivors who are at a lifetime risk of the common complication of BC treatment, breast cancer-related lymphedema (BCRL).[20] BCRL is a chronic condition that begins with few physical manifestations; as it progresses, changes like the swelling of the

limb and the pitting and thickening of the skin occur.[21] A recent study showed 41.1% of survivors had developed BRCL at the 10 year post axillary lymph node dissection (ALND) surgery.[22] It has been reported that approximately 20-25% of survivors will develop BCRL, even when patients were treated with less invasive surgical treatment techniques.[20,23,24]

Among the breast cancer survivorship community, lymphedema is considered one of the most feared side effects of cancer treatment.[25] The mechanisms of what triggers lymphedema among these survivorship group is unclear. The timing of onset varies greatly among those who develop lymphedema, while a large portion never develops this condition. Because of this large window of onset, continuous monitoring of at risk patients is critical but is severely lacking in the clinics based on the typical follow-up protocols. A decade ago, the cumulative incidence of lymphedema was 42% with 80% occurring in the first two years of diagnosis and 89% in 3 years, ranging from mild to severe.[26,27] As techniques for cancer treatment have become less invasive, risk for lymphedema development has been reduce to 25%.[20] Even though rates of lymphedema onset has fallen, survival rates have increased in a growing cancer population, resulting in an increased number of lymphedema cases. Additionally, studies have shown that health-related QOL decreases in breast cancer survivors with diagnosed lymphedema.[28–30] Another study showed the impact lymphedema had psychologically and socially on those who developed this condition.[31] Therefore, it is important to identify BCRL earlier on, so the disease may be successfully managed with minimized impact on QOL.[32]

Several studies have found that cancer and treatment related risk factors are connected to lymphedema, especially among the cancer survivorship population. The cancer stage is a factor of lymphedema development risk, because it influences the extent

of surgery required to remove all of the positive lymph nodes. The more positive lymph nodes found in surgery correlated with higher with lymphedema development.[33] Type of surgical intervention is long seen as an indicator of risk for lymphedema development. ALNDs are more extensive, removing 5-30 lymph nodes in the axilla region, and has been connected to higher rates of lymphedema development post-treatment, upwards of 56% when combined with radiation.[12,28,34] Sentinel lymph node biopsies (SLNB) are a less invasive surgical technique to remove lymph nodes and has been shown to reduce lymphedema incidence rates but may not be an option for more aggressive cancers.[20]

Non-treatment related factors have also been connected to the development of lymphedema. There have been many tall-tale lifestyle recommendations to minimize risks for lymphedema development, such as avoiding air travel, repetitive motion activities, extreme temperatures, vigorous exercise, and pressure.[35] Infections or injury to the at risk limb has been cited to be a factor of lymphedema development.[34] Obesity is the most commonly noted non-cancer related risk for the development of lymphedema.[36–40] Regardless, these factors are not considered enough to predict lymphedema progression among patients, which means detection is reliant on clinician assessment in conjunction to patient history.[41]

2.2.2 Progression and Classification of Lymphedema

Lymphedema progression has several stages ranging from subclinical to three (3), but these stages are loosely defined in the field. The International Society of Lymphology (ISL) uses a three-stage classification that focuses on the physical changes of the limb (Figure 2).[42] There are no current classifications of lymphedema based on the underlying

causes of lymphedema such as adipocyte deposits, lymph flow characteristics, etc. In the Stage 0, this disease is reversible, but it is difficult to detect clinically since physical changes are modest at best. Lymphatic transport may exhibit insufficiencies, and bioimpedance measurements could capture this change. Bioimpedance measures the resistance to electrical current to determine the composition within the body, as resistance in extracellular fluid is different than that in tissue. As the disease physically manifests in swelling, lymphedema is considered to have progressed to Stage I. The fluid is high in protein content, and pitting may occur. Stage II lymphedema patients have more pronounced swelling, and the condition is no longer reversible. Pitting may subside as excess fat deposits occur and fibrosis starts. In Stage III, skin thickening occurs alongside further swelling.

Lymphedema can also be classified based on severity of volume differences, comparing the affected limb to the contralateral limb. The ISL states that minimal severity can range from a 5-20% increase; moderate is defined as 20-40% increase; and severe is any increases greater than 40%.[42] Stillwell developed a classification for lymphedema that outlines differences of 0-10% to be insignificant, 11-20% to be slight, 21-40% to be moderate, 41-80% to be marked, and greater than 80% to be severe.[43] Other clinics consider mild swelling to be a 5-10% increase. Moderate swelling would be an 11-15% increase. Severe swelling would be an increase greater than 15%.[44] Overall, there are a multitude of systems to classify lymphedema based on volume differences, making detection difficult and inconsistent.

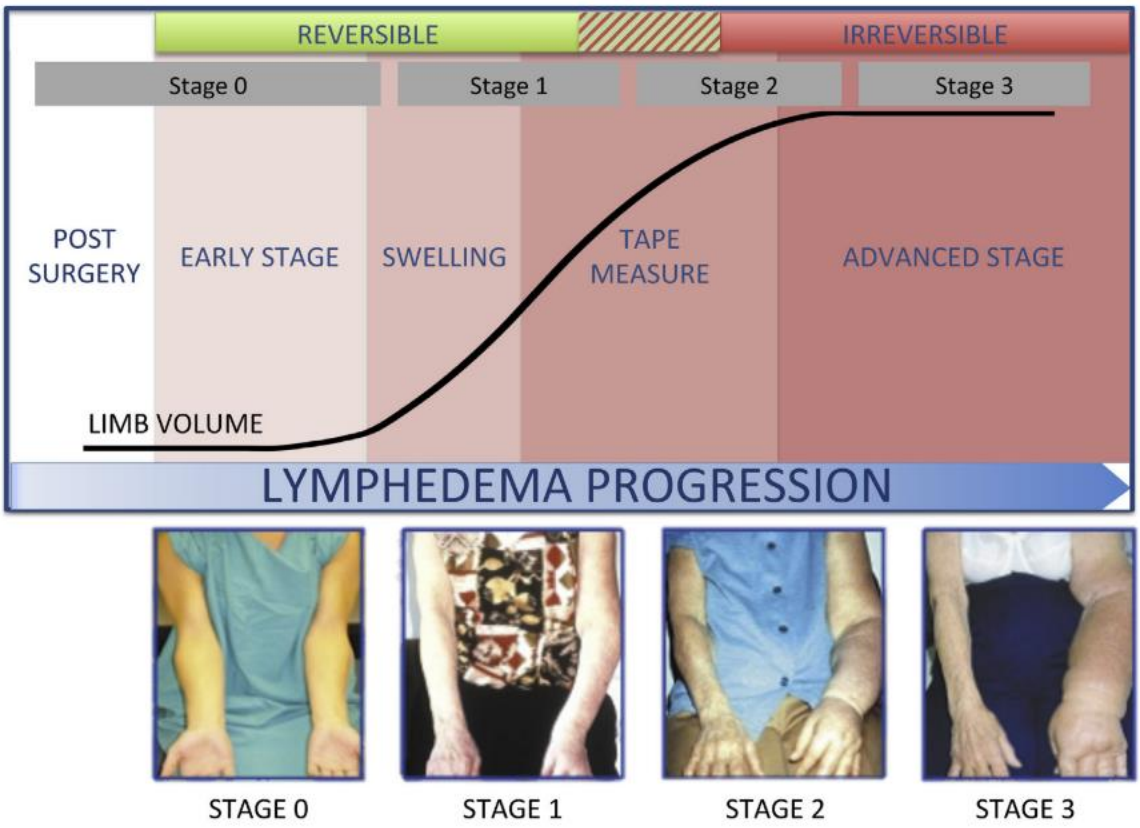

Figure 2 Lymphedema Progression for cancer survivors. Non-cancer related lymphedema progress similarly but the initial event varies. Courtesy of J. Brandon Dixon and Michael Weiler (2015). Images are courtesy of Charles McGarvey and Guenter Klose.

2.2.3 Treatment of Lymphedema

It is important to establish that there is no cure for lymphedema. Once progression of lymphedema begins, intervention is to stop progression and minimize its impact on the patient's QOL Treatment for lymphedema ranges widely from nothing due to the lack of trained therapists to aggressive surgical interventions.

Treatment of lymphedema typically focuses on changes in the limb volume. The gold standard treatment for lymphedema is complete decongestive therapy (CDT). CDT has two phases; Phase 1 is the reduction phase, and Phase 2 is the maintenance phase. More

specifically, the reduction phase focuses on improving the skin of the affected limb and removing the excess fluid built up in the limb through manual lymphatic drainage (MLD). MLD is performed by specially trained therapists. For more aggressive reduction of the limb affected, pneumatic compression have been used with long-term success at maintaining reduced volume.[45–48] In the maintenance phase, the patient is placed on a self-management program that involves wearing compression garments to minimize swelling in the limb. One study showed that the initial fluid volume was the best indicator of the success of therapy treatment for lymphedema.[49] This finding further reinforces the need for prospective surveillance, as therapy can start as soon as swelling can be detected.

Surgical interventions have been developed to treat lymphedema but are reserved for a small number of cases due to its invasiveness and high risk. There are three options: 1) debulking procedures to remove subcutaneous tissues, 2) bypass procedures that facilitates lymph drainage, and 3) prophylactic surgeries.[50] Lymphaticovenular (LV) anastomosis creates a bypass for the lymph to drain to the venous system and typically done as a last attempt at treating lymphedema but can also be performed prophylactically.[51]

While there are treatment options, options are limited and only alleviate some symptoms of lymphedema. Therefore, more research about the underlying mechanisms for lymphedema is critical to a successful move towards finding a cure. In the meantime, better ways to detect lymphedema in order to stop progression can minimize the impact it has on patients' QOL, as advancements in technology allow for new approaches for detection and monitoring.

2.3 Current Clinical Detection of Lymphedema

There are a variety of methods and diagnostic criteria for lymphedema detection and diagnosis. The National Lymphedema Network outlines various methods of diagnosing LE ranging from volumetry to bioimpedance to lymphoscintigraphy to signs and symptoms.[52]

2.3.1 Volume Measurements

The most common method of detection is assessing and tracking volume of the limb of interest. There are many tools to gather volume measurements, but they all have clinical barriers (summarized in Table 1). Tape measures are used to gather circumferential information at a set serial interval along the limb. These circumferential measurements are inputted into a truncated cone formula with either a circular or ellipsoid assumption to calculate a volume. The gold standard is using water displacement, where the region of interest is submerged in a water-filled container, and the volume of water displaced is assumed to equal the volume of the limb submerged. More recently, infrared sensors have been implemented in a variety of systems to measure volume.

The tool often used in clinics is the tape measure method due to its low financial cost. Providers need to invest in training to maintain high intra- and inter-person accuracy and precision, and significant amount of time of the patient visit is dedicated to collecting this volume information. This tool is relatively easy to keep clean by wiping down the tape measure between each patient. Even though this tool is the most common, only clinics that specifically conduct surveillance and treat lymphedema implement this procedure into the workflow.

Water displacement is another tool that does not require a large financial investment. Water displacement is considered the gold standard for volume measurements

with studies showing its high reliability and accuracy.[53,54] This method requires the patient to position oneself and submerge the limb of interest into a tank of water. The volume of water displaced is collected and assumed to be equal to the volume of the limb submerged. While it is the gold standard tool, water displacement is also time consuming, and more importantly, it places patients with open wounds at risk for infection, which can exacerbate lymphedema symptoms. As a result, is not implemented clinically.[27,36]

Infrared sensor systems show a lot of promise as the future volume measurement tool. Many of these systems show high levels of accuracy and precision, while maintaining high levels of hygiene. As with the implementation of technology, some of these systems can be complex requiring more significant financial investment that would preclude clinics from obtaining those tools. Additionally, the footprint of systems requiring dedicated space could also make integration into the clinical workflow difficult.

Table 1 Volume measurement tools comparison

Tool	**Time**	**Tool Cost**	**Hygienic**	**Training**
Tape Measure	High	Low	Moderate	High
Water Displacement	Moderate	Low	Low	Moderate
Infrared Sensors	Low	Moderate to High	High	Low

Clinically, there are a wide variety of diagnostic criteria when measuring limb volume. Two protocols are to either assess (1) limb volume or circumference change, where the same limb is tracked over time, or (2) limb volume or circumference differences, where the limb is compared to the contralateral limb at a specific time point. When assessing limb volume, the diagnostic criteria is a volume change greater than 200mL or a

percent volume difference greater than 10%. When assessing limb circumference, the diagnostic criteria is a circumferential change or difference greater than 2cm. Armer et al showed that when comparing four methods of lymphedema criteria (10% change in volume, 200mL change in volume, 2cm change in circumference, and signs and symptoms), different criteria led to different rates of lymphedema diagnosis ranging from 21-70%.[55] Therefore, the detection of lymphedema is highly variable for clinics that do not specialize in lymphedema detection, where the therapist is trained to use multiple inputs to detect and diagnose lymphedema.

2.3.2 Bioimpedance Spectroscopy (BIS)

Bioimpedance spectroscopy is a method that measures the water content in the tissues. This technology is popular among the fitness industry, but over the last couple decades, it has been used to assess at risk patients of lymphedema. In this measurement, a low frequency electrical current is flowed through the limbs of interest. This current can pass through extracellular space fluid but cannot pass through intracellular fluid. The impedance or opposition to the current can be measured and be inversely related to the amount of fluid in the body. This measurement can identify fluid build-up in subclinical lymphedema cases.[52] The L-DEX (Impedimed Ltd, Australia) is a product often used in studies exploring the use of BIS. The normal range for this device is an L-Dex score between -10 to 10 or a change in score greater than 10. More recently, the Inbody 720 was explored to determine clinical criteria for lymphedema detection but requires further investigation on its ability to predict lymphedema development.[56]

BIS has been shown to have the ability to identify lymphedema earlier in its progression, which could delay disease progression.[57,58] Among breast cancer survivors, the BIS and Perometer measurements were compared with a sensitivity of 73% and specificity of 84% at 6 months post-surgery.[59] Despite the promise of this device, there are some limitations of using a BIS device for lymphedema assessment. There are few studies that report on its accuracy in later stages of lymphedema.[52] Detection is currently limited to unilateral cases of lymphedema, since the contralateral limb is used as a baseline for water volume. This device costs approximately $10,000 with a 5-year lifespan in addition to non-reusable electrodes, limiting this method's usefulness in as clinical surveillance tool. Currently, BIS is difficult to implement in the clinics for surveillance of high-risk populations. The need for prospective surveillance for populations at risk, who may not show symptoms or have complications that would require a clinician, is necessary for the effectiveness of lymphedema detection through BIS.

2.3.3 Lymphoscintigraphy and Near Infrared Imaging

Lymphoscintigraphy is a method that can image lymphatic vessels and look for abnormally functioning lymphatic system. This nuclear imaging technique maps the route of injected radio-labelled proteins in the limb being assessed. While lymphoscintigraphy cannot differentiate between lymphedema versus other causes of insufficiency, it can confirm clinical diagnosis of lymphedema at high levels of sensitivity and specificity.[13,52,60] Therefore, lymphoscintigraphy is the best way to confirm lymphedema, but it would be difficult to prospectively surveillance all at risk patients through this method. Such specialized imaging is expensive and requires training to properly inject and image.

Near infrared imaging can real-time dynamically visualize how the lymphatic vessels are functioning. Similar to lymphoscintigraphy, a dye is injected, and the camera can capture where and how the dye moves in the lymphatic vessels. This system is also expensive, currently limited to most research clinics, and not widely available for prospective surveillance of at risk populations.

2.3.4 Signs and Symptoms

The onset of lymphedema has signs and symptoms (S&S) that patients would experience. These signs include but are not limited to feeling of heaviness, swelling, skin texture changes, reduced mobility, tightness in clothing/jewelry.[26,61]

While this subjective approach has been shown to be effective, it heavily relies on the patient reporting these signs and symptoms.[62] Therefore, patient education on the signs and symptoms of lymphedema and patient compliance are critical to successful detection of lymphedema.[24,63,64] Questionnaires have been developed to help gather this information from patients.[65–67] Nonetheless, lymphedema diagnosis is not often made solely on these questionnaires, and typically require a therapist assessment of the limb. At risk patients who are unaware of such side effects post cancer-treatment may not be properly monitored for lymphedema onset, and standard supportive care would not recognize lymphedema onset until later in its progression when it is no longer reversible. Thus, it is imperative to have a more agnostic tool to aid with lymphedema detection.

2.3.5 Clinical Standards

Lymphedema manifests over a long period of time. This wide range of time for onset makes it difficult to detect and diagnose and lymphedema, because the responsibility lies on no specific field for a patient. It is hard to say whether the responsibility falls on the oncologist on the medical, surgical, or radiological side or on the physical therapist on the rehabilitation side. It could even be the patient's internist's responsibility. Typically, in the field, the physical therapists trained to be aware of lymphedema development have diagnosed its onset, which relies on the patient needing physical therapy and visiting often enough to detect any changes in the limb over a period of time. Clinically, it is not standard protocol to begin measuring every at risk patient at the start of cancer treatment, which compounds the difficulty of lymphedema detection. I strongly believe that the success of prospective surveillance should ideally fall on the team of physicians that treat the patient over the course of cancer care, but the patient's primary care physician is likely to provide the most consistent medical care. Regardless, this task is difficult due to the challenges and specialization associated with being able to detect lymphedema with current tools.

Furthermore, there is a variety of measurement methods and criteria for lymphedema detection and diagnosis. Thus, there is no single universal protocol to detect and diagnose lymphedema, and as a result, a range of diagnosis occurs depending on the method and criteria used.[55] Methods that are considered more accurate and consistent can be difficult to access and/or implement due to financial or spatial costs for a clinic. Therefore, there is a need for a method that combines the accuracy and consistency of the clinical standards, while simplifies the measurement acquisition process and is priced within most clinical budgets for devices. Lowering these barriers to entry for lymphedema monitoring into all clinics can provide the platform for more widespread lymphedema

prospective surveillance for at risk patients. This surveillance could improve patient referrals to physical therapy and rehabilitation clinics with specialized lymphedema care.

Currently, technologies to detect and monitor lymphedema have their drawbacks and could be the cause for a lack of prospective surveillance. To optimize the detection of lymphedema and halt its progression, many studies have shown the need for prospective surveillance in order to recognize early signs of lymphedema.[17,32,68,69] Binkley et al. showed that women find lymphedema more distressing than the cancer itself. Even though ongoing prospective surveillance is shown to be necessary for earlier detection, Binkley et al. found that few women received the necessary referrals to rehabilitative clinics. Many did not have baseline measurements, which complicated the lymphedema detection process.[69,70] As a result, there are many detection criteria that is capable of detecting unilateral lymphedema, but bilateral manifestations of lymphedema are still difficult to detect with current standards until significant swelling of the limbs has occurred.

While tape measure circumference measurements are commonly done, many of these are done in physical therapy environments. This method requires significant training and certification to perform consistent measurements with low intrapersonal variability. Commercially available infrared systems that can measure volume are costly financially and spatially, requiring the finances to acquire the device and the dedicate space for the measurement device. Other methods like BIS and lymphoscintigraphy are financially costly, and therefore are limited to larger hospital settings with the resources available. These challenges need to be overcome in order to implement more widespread surveillance of lymphedema among at risk populations. Additionally, out of the various methods of detection, the more expensive methods are the only ones that can detect bilateral cases of

lymphedema (Table 2). For volume measurements to detect lymphedema, prospective surveillance is necessary but is currently not a standard.

Table 2 Unilateral vs Bilateral detection of lymphedema by methods

	Volume Difference	Volume Change	BIS	Lymphoscintigraphy	S&S
Unilateral LE	X	X	X	X	
Bilateral LE		X	X	X	

Another important aspect to consider is the factors affecting the adoption of the methodology among clinicians. The measurements would need to be easy to use and outputs would need to be informative and useful for their patients. Clinics that are currently not measuring patients for signs of lymphedema may need to be properly incentivized to do so.[71] Therefore, there is still a need for more accessible technology that can assess limb volume to aid in the detection of lymphedema and alleviate the process of monitoring the disease through the duration of therapy.

2.4 Infrared Sensors for Lymphedema Detection

With the advancement of technology, infrared sensors are easier and cheaper to acquire commercially. As a result, more systems have been developed to simplify the volume measurement process. While there have been many infrared systems that have been developed, the most popular commercial tool among lymphedema clinics that utilize such approaches is the Perometer.

2.4.1 Perometer

A commercially available volume measurement tool is the Perometer (Pero-System Messgeräte, Germany), an optoelectronic volumeter that has been shown to be quick and reliable.[72,73] It is composed of a rectangular frame lined with perpendicular photosensors, opposite to light emitting diodes (Figure 3). As the frame moves over the limb being measured, two diameters are acquired for each 3.1 mm thick serial segment, and a volume can be calculated based on a circular or ellipse cross-section.[72]

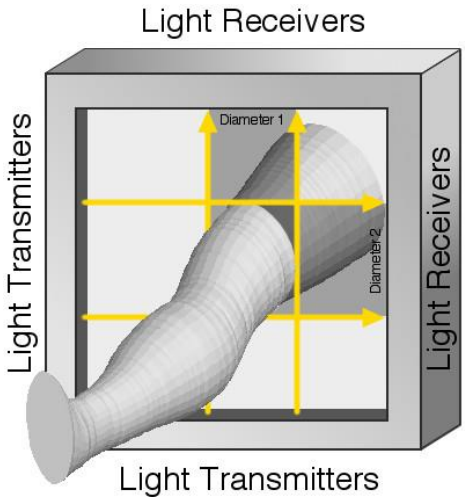

Figure 3 Perometer configuration shows a frame composed of two rows of light transmitters and receivers. When panned over the limb of interest (arm or leg), a volume can be calculated based on the diameters used to calculate cross-sectional area at specific intervals.

Comparing arm volume of healthy and lymphedema patients from sequential circumference method versus the Perometer have demonstrated a correlation of R = 0.985 (R-squared = 0.970) and R = 0.988 (R-squared = 0.976), respectively.[72] In a study comparing the Perometer to circumferential measurements with a tape, the Perometer was found to be more accurate, resulting in smaller standard errors and narrower confidence intervals, and reliable with Cronbach's alpha > 0.9 for experts.[74]

Despite being expensive, Perometers can be found in numerous European clinics due to its consistency and ease of use. Adoption of this method of volume measurement in the United States have been slower as a result of its high financial cost and lack of a reimbursement strategy through the US healthcare system. Additionally, the Perometer has a large spatial footprint, which is an obstacle in clinics where dedicated space for a device whose measurements have yet to become a standardized measure or protocol is difficult to justify.

Another similar device is the Volometer®, which has been used in various studies.[54,75] Studies have shown that optoelectronic volumeters are reliable.[76] Unfortunately, these devices are costly and have seen slow adoption in clinics with many opting to continue using tape measure circumferential measurements, despite it being time consuming and requiring training. Additionally, these volumeters have a large immobile footprint, which can be troublesome to implement in clinics and hospitals where physical space is limited.

2.4.2 Other infrared systems from literature

There are several papers published in literature using infrared systems to measure volume of human limbs. Recently, Moreira *et al* assessed upper arm volume and motion using the Kinect-based system's depth data and skeleton to develop an evaluation tool for upper-limb function. Although arm volume was used to identify patients with reduced arm mobility, volume accuracy was not provided.[77] Since then, there have been several studies that have explored the viability of using these lower cost sensors as a means for limb volume assessment. Ohberg *et al* showed that their three 3D-camera system was

comparable to arm volume performance via water displacement (p=0.270) with it over estimating by approximately 45.25mL.[78] Lu *et al* developed the Iterative Clustered Closest Points (ICCP) algorithm to measure limb volume based on scans taken from a single Kinect sensor rotated around a patient, which also included other sensors such as gyroscopes and accelerometers.[79] Comparing to volumes from water displacement, their system resulted in R = 0.98317 (R-squared = 0.9666). Buffa *et al* validated the used of SkanLab for total arm volume estimation with the Kinect sensor on a rotating detection frame that resulted in a 9.9 mL underestimation compared to water displacement.[80]

More recently, Hameeteman *et al* showed a correlation of R = 0.994 (R-squared = 0.988) when comparing volume from the 5-pod, 15-camera, 3D stereophotogrammetry system to the volume from water displacement.[81] Using the same system, Hoevenaren *et al* showed the use of this system in measuring hand lymphedema reliably, while Verhulst exhibited the reproducibility of the system's ability to measure volume in the hand and forearm.[82,83] Karakashian *et al* scanned arm lymphedema patients by rotating a commercially available camera with color and depth sensors 360° around the arm with high repeatability.[84] Landau *et al* showed a strong correlation with water displacement in 3D arm measurements (R-squared = 0.990) using the Vectra 3D system.[85] While these techniques have achieved a high level of accuracy, many of these systems require significant financial resources, multiple providers assisting with the measurement, and/or substantial physical space due to either a large number of cameras or needing room to rotate the sensor around the patient, and it is likely that all of these factors have played some role in the lack of wide-spread clinical adoption of these approaches. A summary of these methods can be found in Table 3.

Furthermore, a comparison between the iSense, Sense, and Artec Eva 3D scanners were used to scan leg lymphedema patients.[86] Their results showed a correlation of R > 0.92 (R-squared > 0.85) when compared to water displacement. In a recently published study, a 3D infrared depth sensor integrated with a tablet and custom software also indicated promising results when measuring filarial leg lymphedema patients.[87] The study shows a high correlation between LymphaTech device and water displacement (R-squared > 0.98).

Other systems in literature but not on the market (that I am aware of):

Table 3 Summary of volume measurement methodologies in papers

Paper	***Total patients (with LE)***	***Patient BMI (kg/m^2)***	***Number of Sensors***	***Sensor Motion***
Moreira (2015)[77]	48 (24)	N/A	1 Kinect	Stationary
Ohberg (2014)[78]	25 (25)	29.2	3 Kinect	Stationary
Lu (2014)[79]	10 (1)	N/A	1 Kinect	Rotation
Buffa (2015)[80]	30 (0)	23.3	1 Skanlab	Rotation
Hameeteman (2016)[81]	11 (11)	N/A	15 3dMD	Stationary
Hoevenaren (2016)[82]	18 (18)	N/A	15 3dMD	Stationary
Verhulst (2017)[83]	10 (0)	N/A	15 3dMD	Stationary
Karakashian (2017)[84]	24	N/A	1 Xtion Pro 3D	Rotation
Landau (2018)[85]	11 (11)	26.2	1 Vectra 3D	Stationary

BMI, body mass index; LE, lymphedema; N/A, not available.

There are many published systems in literature, but none have reached commercial success in the clinics in the US despite great measurement performance. This lack of integration into the clinics is likely due to other obstacles posed in the clinical workflow. Clinics operate on tight budgets and schedules in already maximized space. Therefore, systems that are too expensive, requiring many sensors and/or accessories impose financial

strain to obtain and maintain. More complex systems are not only potentially more difficult to operate but likely require dedicated spatial footprint that many clinics do not have available. With this in mind, it is not surprising that few published systems have found their place in clinics in the United States.

2.4.3 Our system

In this dissertation, I explore the use of infrared sensors in various clinical settings. The lab developed two different generations of a single infrared sensor system and spun off as LymphaTech, LLC for continued development and expansion into the clinical space. The work in the document assesses the value these infrared sensors bring to the clinics and explores other potential metrics to use for the detection and monitoring of lymphedema.

The first-generation system was composed of a single Microsoft Kinect sensor (Kinect for Windows v2, Microsoft, Washington) connected to a compatible Windows computer with a USB port (Figure 4). Custom code was interfaced with the sensor to pull depth data with a resolution of 640 x 480 pixels to collect scans of patients from the front, back, and sides for leg patients. The whole system is small, light (1656 g for the sensor and laptop), and portable but required enough space between the patient and the sensor to capture enough of the patient for the scan.

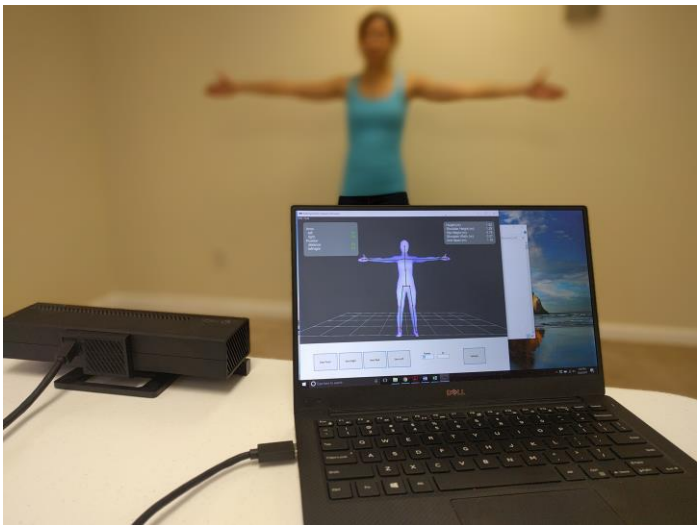

Figure 4 Kinect IR system setup. The sensor is connected to the computer via a USB port; computer captured is the 2015 Dell XPS 13 with the GUI that allows the operator to capture the front, back, right, and left side of the patient seen in the background.

With feedback from the clinics, the second-generation system was composed of a single Structure sensor (Occipital, Boulder, CO) mounted on an iPad Mini 2 (Apple Inc., Cupertino, CA) with a customized software platform designed for scanning lymphedema patients (LymphaTech, Atlanta, GA) (Figure 5). The sensor provides depth data with a resolution of 640 x 480 pixels and is precise to half of a millimeter when taken at 40 cm away. Custom code interfaces with the sensor to acquire the point cloud of the limb scanned. In contrast with the first-generation, a single .OBJ file is outputted for each scan, and each scan captures an individual arm resulting in two files per patient for each arm. As a result, 3-dimensional scans of the arm are possible and provide higher resolution information. This entire system is smaller (200 x 134.7 x 36.5mm), lighter (totalling 426g for the sensor and iPad), and more portable as a single combined device than the first generation. In addition to ease of movement of the system in a clinical setting, it also requires less space to capture arm scans.

Figure 5 Structure sensor system set up with the sensor (behind the iPad) connected to the iPad through the lightning port. The tablet displays a box to indicate a region of interest and the captured information is painted in white as seen in the image.

This dissertation will explore the implementation of the first generation of the device in various clinical settings and will compare it against the clinic's standard of measurement. With the second generation, I will investigate the possibility of using local features of arms to delineate healthy and lymphedema arms as opposed to volume, which is the current standard for detection.

CHAPTER 3. AIM 1

3.1 Introduction

Despite the breadth of techniques that can be used to detect and monitor lymphedema, the most common technique in the United States is using tape measures and collecting circumferential measurements at evenly spaced intervals. Limited infrared sensor systems have been implemented in clinics despite their of ease of use, which is likely due to unaccounted challenges.

Accurate volume measurements are critical for adoption in the clinics, but there are other factors to consider. The financial cost of the system is important, including not only the device but also any associated subscription and training necessary to maintain accuracy. The spatial requirement is a limitation as clinics tend to be small and are overcrowded.[88] Therefore, finding a sufficient amount of space to dedicate to lymphedema detection equipment can be difficult.

While there have been infrared systems that have been shown to be potential replacements for the tape measure circumference method for volume measurement, there are few reports of these systems used in the clinical environment. Therefore, evaluation of its successful implementation in these settings is unknown. Furthermore, the lack of widespread integration of these systems into clinics begs the questions of how successful these systems are in the clinical spaces and what are the challenges these spaces presenting.

This chapter navigates three different situations where the Kinect IR system was used and compared to the clinic's best practices for lymphedema detection and monitoring

to explore its clinical efficacy. In Objective 1A, I explore the use of the Kinect IR system in a breast cancer rehabilitation center among patients with and without lymphedema. This location has a Perometer, which has been shown to be highly accurate. In Objective 1B, the Kinect IR system is implemented in a breast cancer clinic at a local public hospital of Atlanta, GA, where patients are scanned pre- and post-operatively. Typically, no screening of lymphedema is performed at this center. Lastly, in Objective 1C, the Kinect IR system is integrated into a physical therapy clinic where patients have lower limb lymphedema, and the typical measurement performed uses a tape measure to collect circumference measurements.

3.2 Objective 1A: Assessment of arm swelling among breast cancer survivors with an infrared system in a specialized breast cancer rehabilitation clinic

There are many approaches to clinically diagnose and measure BCRL, but the most common is using a volumetric measurement.[26,89] A common tool to make volumetric measurements is with a tape measure, where circumferential measurements are taken along the arm at evenly spaced intervals. Using the circumference measurements, a truncated cone geometry, circular or elliptical, is assumed for volume calculations. This method is the most common method performed in clinics and does not require expensive equipment but can be time consuming and requires training to reduce intra-operator variability.[90]

The aim of this study is to show that a single stationary Kinect for Windows v2 IR sensor, in conjunction with a custom image processing algorithm, is a tool that can be implemented in a clinical setting to calculate arm volume among breast cancer survivors with the requisite clinical accuracy. This system is easy-to-use, has a small footprint, is

non-invasive, is faster than the commonly used circumferential measurements technique, and is an inexpensive alternative in terms of time, cost, and space when compared to other systems and devices used to detect, measure, and monitor lymphedema. This combination of accuracy and small footprint allows for simple implementation in clinical settings, where dedicated rooms are a limited resource and would be difficult to integrate into the workflow.

3.2.1 Methods

3.2.1.1 Participants

The women in this study previously had breast cancer and underwent treatment. These women were referred to TurningPoint Breast Cancer Rehabilitation by their physicians for post-treatment rehabilitation and have been undergoing treatment at the rehabilitation center for various periods of time when they were recruited for this study from the center. Seventy-three (73) women at varying stages post-surgery participated in this study, and thirty (30) of these women have been clinically diagnosed with lymphedema in the arm between the wrist and shoulder. Diagnosis was determined by a notation of the I97.2 code for lymphedema symptoms in the patient's chart with the exception of lymphedema manifesting in the chest and/or hand, which were not included as a lymphedema case for this study.

Women receiving physical therapy treatment at TurningPoint Breast Cancer Rehabilitation were recruited for this study by therapists at the center based on the inclusion and exclusion criteria. Participants were required to be female breast cancer survivors who may have undergone surgery, chemotherapy, and/or radiation. They must be able to stand

unassisted for one minute and must possess all four limbs. Women recruited did not need to be diagnosed with lymphedema to participate, and they must be 18 years or older. Prior to participating in the study, all participants provided a written informed consent.

3.2.1.2 Measurement Acquisition Procedures

In a single visit, the patient was measured once with a single Kinect IR sensor (Kinect for Windows v2, Microsoft, Washington) and twice with a Perometer in a consecutive manner, using a horizontal measurement frame. Women were asked to wear taut sleeveless tops with no jewelry on their arms, although rings were permitted since arm volumes consisted of measurements from the wrist to the shoulder.

Measurements taken by the Kinect IR system required the patient to walk to the delineated spot marked on the ground (approximately 1.8 m in front of the sensor) with the arms held out, parallel to the ground seen in Figure 1. When in the correct position, the software program used for acquisition would visually paint the cartooned version of the patient blue, indicating that the patient was in the correct position and ready to be scanned. The software algorithm required each patient's limb to be horizontal to the sensor with a tolerance of 10 degrees to ensure separation of the arm and the trunk of the body. When in an incorrect position, the cartooned patient was painted red and a prompt in the program was given to correctly position the patient. The front and back of the patients were scanned in this position for approximately 30 seconds to acquire up to 30 frames. Each frame is captured and a .PLY is immediately generated in real-time before capturing the next frame. The .PLY files are saved to be processed at a later date (Figure 6).

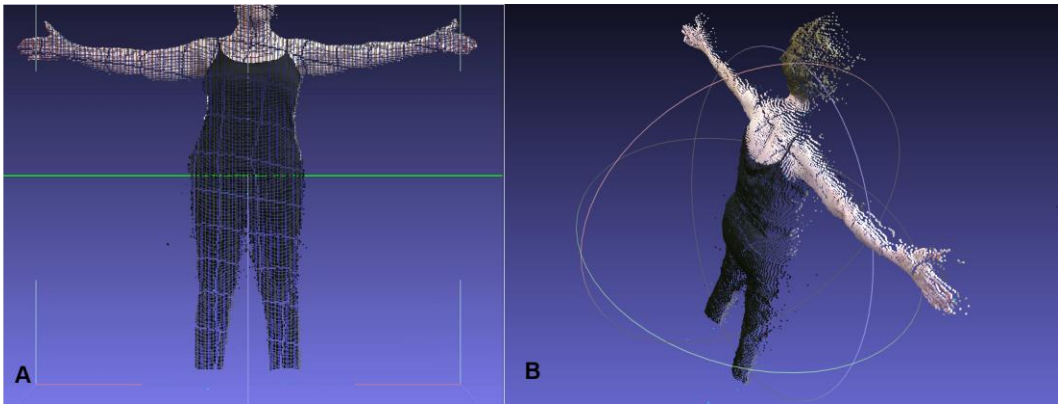

Figure 6 Kinect IR System arm scans. The (A) front and the (B) back scans are taken and pseudo arm volumes are calculated for the right and left.

For Perometer measurements, the patient was positioned next to the device with the patient's arm of interest extended straight, resting the finger tips on a support at the end. The frame of sensors and receivers on the Perometer was moved forward once and back into position once per scan per arm. For each set of scans (of the right and left arms), the volume measurements were collected from the Pero-System database. The wrist for each of these scans were manually identified to gather arm volume from the wrist to shoulder. The user identified the wrist by locating the point just before an increased slope that would indicate the start of the carpometacarpal joint that would lead to the thumb.

Background information regarding patient breast cancer history were taken from the patient's electronic record. A summary of the patient characteristics can be found in Table 4.

Table 4 TurningPoint participant characteristics (n=73)

Personal data	*Mean (stdev)*
Age (years)	60.1 (10.6)
BMI (kg/m^2)	26.5 (5.6)*
Time since BC surgery (months)	39.9 (62.6)
BC Treatment	*Number (%)*
ALND	6 (8.2)
Lumpectomy	

Mastectomy	18 (24.7)
Radiation	59 (80.8)
Chemotherapy	42 (57.5)
	41 (56.2)
BCRL	*Number Yes (%)*
Clinical	28 (38.4)
10% Volume difference	--
Perometer	9 (12.3)
Kinect	17 (23.3)
200mL difference	--
Perometer	13 (17.8)
Kinect	21 (28.8)

* Average does not include the three patients who were missing BMI information from their electronic records.

3.2.1.3 Scan Processing

Scans, composed of sequential frames, were post-processed by custom algorithms written in MATLAB (version R2015b, MathWorks) to calculate the final left and right arm volumes.

For each patient, the front and back scans had to be filtered to remove noisy data points in the point cloud of the whole body. To do so, the point cloud was centered at the origin by taking the mean location of the data points in the point cloud. Then, the location, color, and joints identified using the Kinect sensor and Kinect SDK were extracted. The point cloud was filtered using a nearest neighbor algorithm with a distance of 0.015 and degree of four; this filter removed the flyaway points that can be seen in the raw point clouds.

Next, the arms were segmented from the rest of the body captured in the scans. The shoulder was auto-detected for each frame, and the rest of the arm from the shoulder to thumb was segmented, outlined in Figure 7A. The identification of the shoulders in the

front and back scans resulted in four segments – front-left, front-right, back-left, and back-right. For each segment, the upper and lower boundary points of the arms of interest were then smoothed twice using a 3-point moving average filter. This step further cleaned noisy data points the arm segment of the point cloud. The script then prompted the manual identification of the wrist in each of the four arm segments, which determined where the arm was truncated for volume analysis. The x-coordinate of the wrist was manually identified (seen in Figure 7B) for each of the four segments on the first frame, and these coordinates were used for the subsequent frames to process and truncate the arm from the shoulder to the wrist.

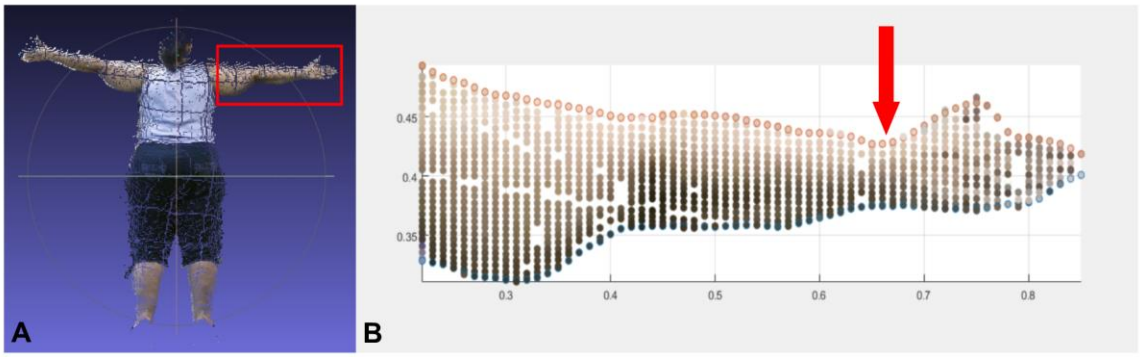

Figure 7 Kinect IR System Wrist Identification. The arm is isolated and the code prompts for the wrist identification during the scan processing process.

Final left and right arm volumes of each frame were calculated by using the pseudo-volumes for the front-left, front-right, back-left, and back-right segments. The pseudo-volumes were calculated using 1cm slices along the arm times the calculated area in the y-z plane assuming a circular cross-section. Although I analyzed all the frames acquired, it was found that ten consecutive frames resulted in a consistent arm volume output per patient (data not shown). This amount was determined by calculating (over a range in the number of frames) the cumulative volume average, which is the sum of the volume per

frame divided by the number of frames considered. Then, I analyzed the change in normalized cumulative volume averages by calculating the difference in consecutive cumulative volume averages divided by the initial frame of the sequence. The results indicated that the volumes stabilized after five consecutive frames. Therefore, I determined that ten frames were sufficient for calculating arm volumes. The set of ten consecutive frames, for each of the four arm segments, with the smallest standard deviation of the angles of the arm (towards the sensor) was used to calculate the pseudo-volumes of the front-left, front-right, back-left, and back-right segments. The average of the pseudo-volumes of the front-left and back-left was calculated for the left arm volume; the same process was applied for the right arm volume.

The volumes from the two Perometer scans were taken after adjusting the arm length in both sets of scans to ensure the same regions of the arms were analyzed with the exception of fifteen (15) patients who had one Perometer reading due to limitation of time or fatigue. An average was calculated from the two Perometer scans when applicable to calculate a right and left arm volume for a patient that was used for analysis in this study.

Arm lengths for a single participant were matched within each modality in addition to being matched between modalities in order to fairly draw comparisons between the Perometer and Kinect IR system. Normalized arm volumes were calculated by taking the arm volume of interest and dividing it by the arm length of that patient, resulting in an arm volume/length metric.

3.2.1.4 Statistical Analysis

Linear regression analyses were performed to determine the level of correlation between the Perometer and the Kinect IR system. Additionally, to assess the agreement of the Perometer and the IR system, a Bland-Altman plot was generated, where the percent volume difference and volume differences between the right and left arm from Kinect was subtracted from the volume from Perometer. In clinical settings, a threshold of 10% in arm volume difference or a 200mL difference would indicate lymphedema. Therefore, using the Cohen's kappa agreement for categorical data, the outcomes for each modality were compared using each threshold.[91,92] To compare LE and non LE patients, arm LE diagnosis was determined from the patient's charts, and Mann-Whitney tests were performed. Data analysis were run using Prism 6 for Windows (version 6.07, GraphPad Software).

3.2.2 Results

While the arm lengths were internally matched for both the Perometer and the Kinect IR system, an initial comparison between the modalities was performed in which the arm length was not fixed between Perometer and Kinect. As expected, the correlation of the volumes initially calculated from these two modalities showed weaker correlation, with an R-squared = 0.7785 (Figure 8A). In order to remove the effect of differences in arm length acquired between the two modalities without having to actually match the length of arm acquired between the two methods, the arm volumes were then normalized to the arm lengths of the respective scans, which improved the correlation to a value of 0.8350 (Figure 8B and did not require accurate registration of the defined "wrist to shoulder" distances measured between the two parameters.

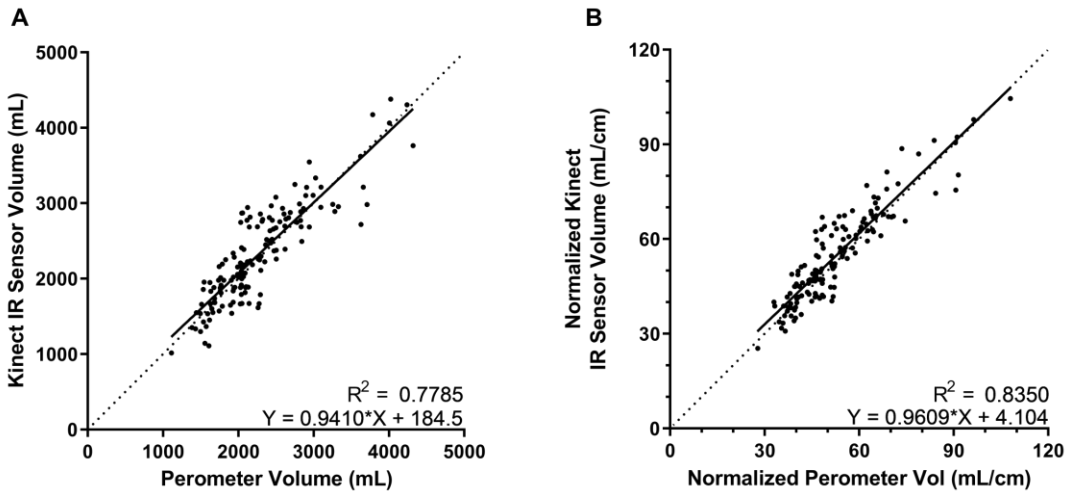

Figure 8 Correlation without matching arm length between modalities

When the arm lengths between the two modalities were matched, the correlation in arm volume gave an R-squared value of 0.8799 (Figure 9A). Meanwhile, normalizing the arm volumes to the now matched arm lengths produced an improvement to from the normalization in Figure 8B, but a drop in the R-squared value to 0.8676 (Figure 9B) from the matched arm lengths in Figure 9A. As anticipated, the correlation is stronger when matching the arm lengths for each modality to compare arm volumes between them, however merely normalizing the volume by the arm length works surprisingly well to correct for differences between arm lengths without having to match them.

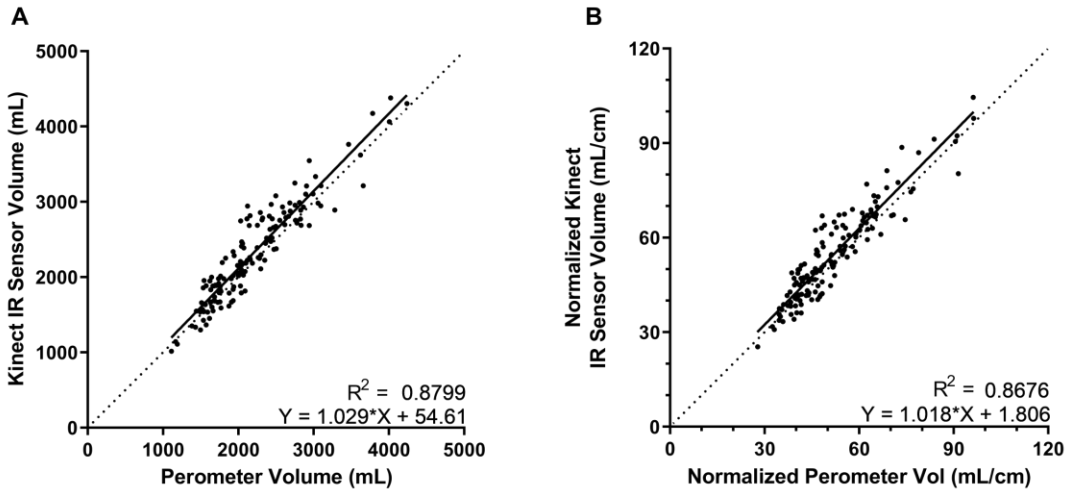

Figure 9 Correlation after matching arm lengths

The absolute volume agreement analysis resulted in a difference of -117.6 ± 228.6mL. To determine agreement between more clinically relevant measurements, Figure 10A compared the percent arm volume differences between the right and left arms measured by the Perometer and the Kinect IR system when arm lengths were matched. The Bland-Altman analysis resulted in a difference of -0.4657 ± 6.006%, meaning the Perometer and the Kinect IR system produced similar percent volume differences. For another clinically relevant metric, Figure 10B compares the arm volume difference (right arm volume – left arm volume) measured by the Perometer and Kinect IR system. The Bland-Altman analysis showed a difference of 6.016 ± 132.7mL, where Perometer and the Kinect IR system produced similar volume differences.

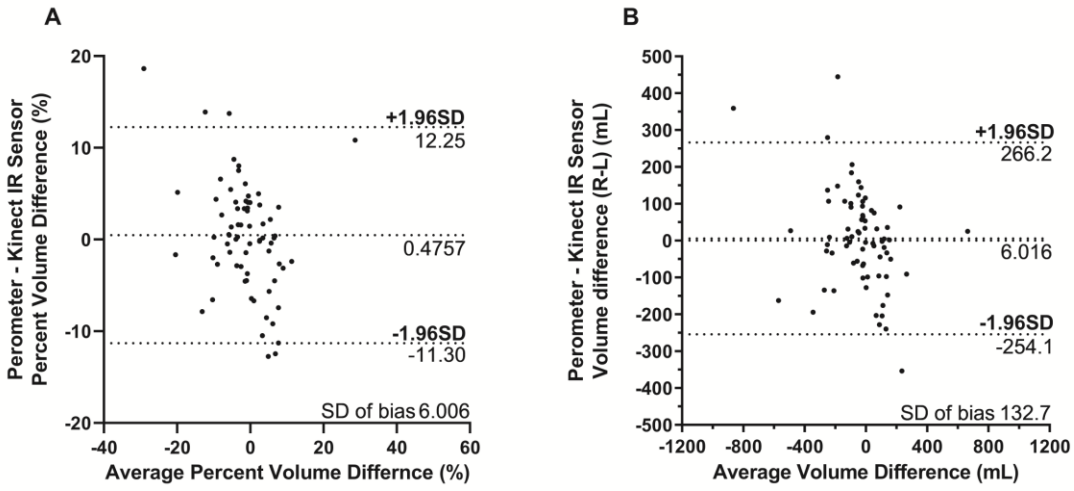

Figure 10 Bland Altman plots

To assess the clinical agreement between the two modalities, the Cohen's kappa agreement coefficient was calculated. Cohen's kappa ranges from 0 to 1, where 0 indicates that any agreement is equivalent to chance and 1 indicates perfect agreement.[92] Based on a diagnosis of 10% arm volume difference, the kappa was 0.2663, which is deemed a "fair agreement". When considering a lymphedema analysis based on 200mL difference between left and right arm volumes, the kappa was 0.5475, which is deemed a "moderate agreement". The agreement strength varied with the method of clinical diagnosis, but both showed a fair agreement between the two modalities.

Interestingly, the percent difference in arm volume when comparing the left and right arm of a participant between the two modalities showed an R-squared value of 0.5950 (Figure 11A). When the absolute percent difference data were segmented based on Perometer measurements (<5%, 5-10%, >10%) to identify where the lack of variation originated, I found that the most variation fell within the first segment, <5% difference. The R-squared value for absolute Perometer measurements less than 5% was <0.0001

(Figure 12A). The other two segments where the absolute percent difference was 5-10% or greater than 10% had R-squared values of 0.6277 (Figure 12B) and 0.7098 (Figure 12C), respectively. The volume difference between the left and right arm correlation between the Perometer and Kinect IR system resulted in an R-squared value of 0.6732 (Figure 11B).

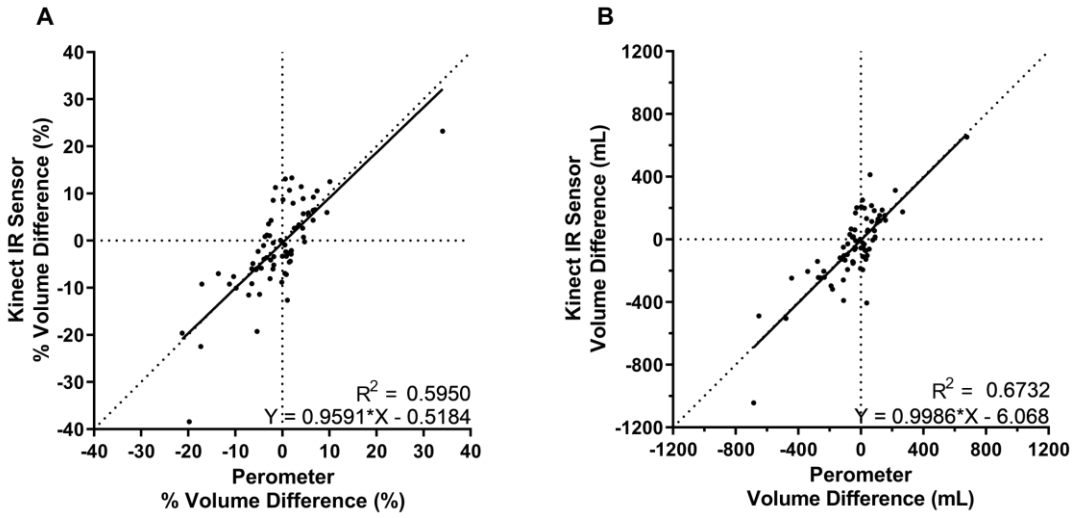

Figure 11 Percent Volume Difference and Volume Difference Comparison

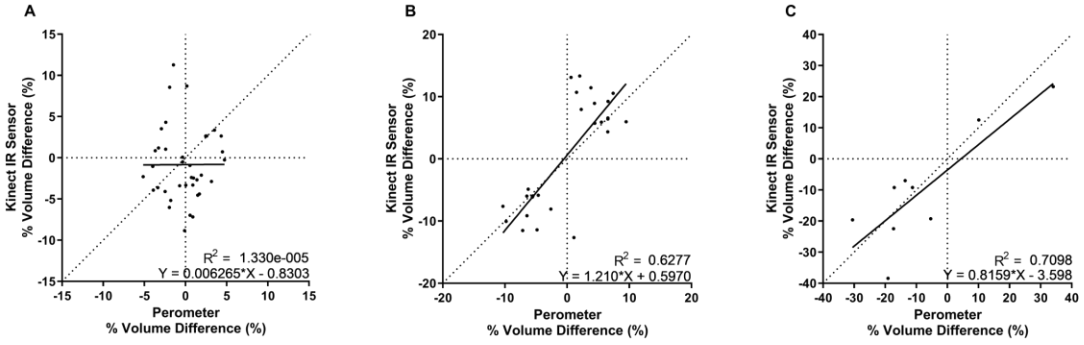

Figure 12 Percent Volume Difference

When comparing patients with lymphedema to those without lymphedema, there was no significant difference in percent volume differences (p=0.2806), while there was a significantly greater volume difference (p=0.0309) between the right and left arm for women with lymphedema (Figure 13A-B). For this comparison, percent difference was defined as the larger arm volume minus the smaller arm volume divided by the smaller arm volume. The volume difference was defined as the larger arm volume minus the smaller arm volume. This adjustment in calculation made the analysis comparing those with and without lymphedema agnostic to whether the right or left side was larger.

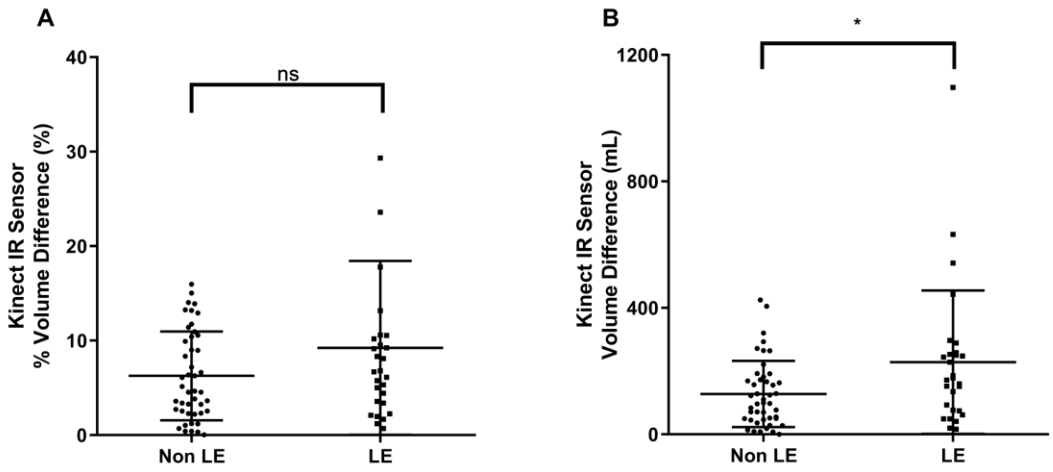

Figure 13 Non-LE vs LE (A) Percent Volume Difference and (B) Volume Difference comparison

3.2.3 Discussion and Conclusion

It has been shown and recommended by an expert panel convened by the American Society of Breast Surgeons that taking preoperative measurements has been helpful with the diagnosis of lymphedema, yet it is not performed regularly in the clinic.[32,44,69,93] More often than not, prospective surveillance of those at risk for developing lymphedema is not

done. This lack of information is driven in part by the insufficient resources required to make meaningful measurements (i.e. properly trained staff with the dedicated time to perform tape measurement evaluations or expensive volume acquisition hardware) that cause challenges for a clinic to implement the measurement into the work flow. As a result, baseline and immediate post-treatment volume measurements are missing. When post-treatment volumes are necessary and finally taken, there is no frame of reference to understand the significance of the measurement. Since these change-over-time measurements are rarely available, percent difference and absolute volume difference between the affected and contralateral arm are metrics used to assess lymphedema and its severity when the patient is referred to a lymphedema clinic. Patients who have had ongoing therapy for swelling may be misdiagnosed, as they may not exhibit the physical hallmarks of lymphedema. Additionally, patients suffering from bilateral lymphedema may not be diagnosed until significant swelling occurs due to the limitations of current lymphedema metrics. If a method for volume surveillance before and after treatment can easily be integrated to the work flow, then these baseline measurements can be recorded and used to monitor for lymphedema onset for everyone at risk.

Typical tools used to assess arm volume include taking circumferential measurements, water displacement, and infrared sensors. This study explored the use of a single infrared sensor and processing algorithm to calculate the arm volume. This method was shown to be capable of quickly capturing scans that produced accurate arm volumes. Compared to other 3D scanner systems, this proposed device had many benefits without compromising the accuracy that is necessary for clinical implementation (Figure 9A, Figure 11A-B). While there was variation in percent difference between the two modalities,

the variation occurs primarily when the percent difference between arms is less than 5%, which is a range more prone to errors due to subtle changes in volume. It is unclear whether these changes are a result of the Perometer or the Kinect IR system.

Additionally, the agreement analysis showed that the bias between the Perometer and the Kinect IR system was minimal when assessing the percent volume difference and volume difference, which are two common measurements for lymphedema (Figure 10). This agreement indicated that moving between the two modalities in a clinic would not require much of an offset. The system remains a low-cost and small footprint device due to a single camera system that interfaces with a basic computer via USB and does not require rotation around the patient. The simplicity in the acquisition process means that the system could be easily performed in clinics but also in the home of patients as self-measurements are possible without an additional person. This acquisition setup requires a smaller footprint that leads to simplified implementation in the physical space limitations of clinical settings, which can help move the field towards taking prospective measurements.

Patients with and without clinically diagnosed lymphedema were compared. The lack of difference between the two groups in percent volume (Figure 13A) was likely a result of lymphedema patients undergoing therapy, including the wearing of compression garments, and thus were actively managing their swelling. However, when the absolute volume difference was compared, the two groups were statistically significant. Other papers have noted the lack of consistency among metrics used to detect lymphedema, so the discrepancy between the two measurements was not surprising.[55] In addition, the study indicated there were a small number of women who are not clinically diagnosed with

lymphedema but have metrics (whether determined by Perometer or the Kinect IR system) that exceeded traditional thresholds used for lymphedema diagnosis; these women had percent volume differences greater than 10% and volume differences greater than 200mL. So, while volume measurements can be helpful as an initial screen, it can be difficult to detect lymphedema based solely on a single volume measurement. Therefore, having a system that can be easily integrated into a clinical workflow would allow for more longitudinal measurements of a patient at risk, including pre-operative baseline measurements, providing more information for detection and would provide a platform that could refer patients to lymphedema specialists.

While there are many advantages to the system used in this study, there are a few limitations when compared to other systems. The cost of the technology was approximately $950 ($150 and $800 for the sensor and computer, respectively), which is cheaper than the Perometer but can be reduced by purchasing a more inexpensive computer. Because a dedicated laptop is not necessary, the computer can be multi-purposed to meet other clinical needs. With that stated, the market price for this system is unknown since the analysis software is not included. It is worth noting that the specific Kinect sensor model has been discontinued, but there are other viable infrared sensors that can be integrated with this system.

Additionally, this current system cannot calculate volume based on an elliptical cross-section, but studies have shown that only under extreme deviations would assuming a circular cross section lead to differences greater than 5%.[94] Using clinically relevant measurements, the agreement analysis (Figure 6A-B) indicates a standard deviation of bias smaller than clinical thresholds utilizing percent volume difference and volume difference.

Studies have reported a standard deviation of bias up to 4.3% for arm volumes (corresponded to 69.4mL) and 345.4 mL for leg volumes when comparing the Perometer and sequential circumferential tape measurements.[72,95] While the study reported a slightly larger standard deviation of bias, this system is considerably more affordable than the comparison. Additionally, it is difficult to directly compare the study results with published studies since those studies compared the Perometer against tape measure circumference measurements while I compared the system to the Perometer. One study even reported that experts performing repeated volume Perometer measurements on a healthy volunteer arm had a standard error of 38.99mL compared to tape measure standard error of 25.00mL.[74] Based on this study, it is difficult to determine which system contributed to the larger standard deviation of bias, but the deviation is comparable to published comparisons.

Despite the current limitations, the Kinect IR system has many advantages, especially for clinical applications. The Kinect IR system was shown to have a good correlation and clinical agreement with the Perometer, which was shown to have a high correlation with commonly used circumference measurement methods.[72] The use of Kinect IR system required no physical contact with the patient, which is optimal compared to other volumetric tools such as water displacement and circumferential tape measurements. Because there is just a single Kinect IR sensor plugged into a laptop, the spatial footprint required for this system is smaller than some of the proposed systems that either require multiple sensors or enough radial distance for the sensor to be moved around the patient to capture the limb of interest. This study was able to implement this system in a rehabilitation center to gather scans with minimal impact on the workflow of the center. The Kinect system is quicker than taking circumferential measurements with a tape measure. The

scanning acquisition takes approximately a minute plus transitioning time to move into position for a total of about two minutes. Meanwhile, tape measure circumferential measurements have been reported to take 7 minutes[87] but can take longer as this method was reported as having a "high" operating time.[77] The Kinect system takes minutes to acquire all the necessary scans at its current development stage and could be reduced once the protocol is optimized. This system is a tool that has many advantages that make it a great improvement for arm volume measurements in clinical settings by saving time, reducing cost, being accurate compared to the Perometer, and providing a stepping stone towards a more prospective approach to lymphedema diagnosis.

The volume measurement tool developed in this study can calculate volume and compare percent volume difference and volume difference between arms in a clinical setting of patients with or at risk of BCRL. This system is low-cost and highly correlates with the previously developed Perometer system. The system with existing Kinect sensors or other compatible sensors can be implemented in clinics and be used as a tool to detect and monitor lymphedema. In the next steps, immediate analysis of the scans will be integrated with the system to allow physicians and therapists to make decisions regarding patient care immediately. To further validate the ease of implementation in clinics, expanding the number of clinics and operators is needed. For long-term management of lymphedema cases, gathering longitudinal data to show changes in arm volume over time would show the system's ability to monitor changes during a patient's rehabilitation journey.

3.3 Objective 1B: Evaluation of an infrared system to track arm swelling in the breast surgical oncology team of a public hospital

This study aims to show how a single stationary Kinect IR sensor with a custom image processing algorithm can be a tool implemented in a clinical setting to measure changes over the course of breast cancer treatment. The implementation of this system in a public hospital of a major city provided feedback about challenges unique to a fast-pace clinical setting among a patient group who has just begun their cancer treatment journey and are therefore less concerned about the side-effects of their treatment and more worried about the cancer itself. This inexpensive alternative system is reasonably priced but also reduces the amount of measurement time, decreases the associated training needed, and has a small physical system footprint in the clinical space.

3.3.1 Methods

3.3.1.1 Participants

All participants in this study had been diagnosed with breast cancer for the first time but had not undergone treatment when recruited to participate in the study. Those who participated in this study were at varying stages between 0-III of unilateral cancer. To participate, patients must possess all four limbs, be able to lift their arms laterally by 75°, and be able to stand on their own for 5 minutes at a time. Patients who had a prior history of breast cancer and its associated treatments (i.e. axillary surgery or radiation) were excluded from this study. Breast cancer diagnoses of inoperable cancer, stage IV, and bilateral disease were not included. Patients were all measured pre-operatively and post-operatively at least once.

There were 106 patients screened based on reviewing the charts from of the breast clinic at Grady Memorial Hospital, who were eligible to participate in the study. Eighty-

three patients either declined or missed their appointment and therefore could not be recruited. The other 23 patients were recruited and consented. Two patients withdrew prior to completing the study. The personal and cancer history of the remaining 21 patients were summarized in Table 5. Seventeen patients had pre-operative scans that could be processed to calculate volume. Six patients had pre-operative scans that could not be processed due to articles of clothing covering portions of the arm; therefore, accurate measurements could not be performed. A final fifteen patients had post-operative scans, while others were lost in the follow-up process and thus, a post-operative scan was missing for those patients.

Table 5 Grady participant characteristics (n=21)

Personal Data	***Mean (Standard Deviation)***
Age (years)	54 (12.9)
BMI (km/m^2)	29.4 (5.7)
Breast Cancer (BC) History	***Count (%)***
Stage 0	1 (4.8)
Stage 1	8 (38.1)
Stage 2	8 (38.1)
Stage 3	4 (19.0)
BC Treatment	***Count Yes (%)***
Neoadjuvant chemotherapy	12 (57)
Radiotherapy	0 (0)
Surgery	21 (100)
Partial mastectomy/lumpectomy	9 (42.9)
Total mastectomy, unilateral	5 (23.8)
Total mastectomy, bilateral	3 (14.3)
Modified radical mastectomy	4 (19.0)

3.3.1.2 Measurement Acquisition

The arm was measured with two techniques: the tape measure circumferential measurements and the Kinect IR system.

The tape measure circumferential measurements were performed by positioning the patient lying down on her back on a table. A tape measure was taped down starting at the ulnar styloid up to the shoulder. With a second tape measure, circumferential measurements were recorded at every 4cm starting at the ulnar styloid and up to the shoulder.

The Kinect IR system was performed in the same procedure described in 3.2.1.2 Measurement Acquisition Procedures.

3.3.1.3 Measurement Processing

The circumference measurements taken with the tape measure for each patient was inputted to calculate the arm volume using the truncated cone technique. The scans from the Kinect IR system were processed in the same procedure described in 3.2.1.3 Scan Processing.

To track the change in arm volumes of each participant through their treatment, I normalized change in volume, shown in Equation 1. This measurement was tracked for both the side affected and unaffected by breast cancer. To better understand the difference of these changes, the difference between the normalized change in the affected arm and the normalized change in the unaffected arm was determined, as seen in Equation 2.

$$Normalized\ change\ in\ volume = \frac{(volume_{post-op} - volume_{pre-op})}{volume_{pre-op}}$$

Equation 1 Normalized Change in volume over Cancer Treatment

$$Difference\ in\ Normalized\ Volume\ Change = \frac{(volume_{post,aff} - volume_{pre,aff})}{volume_{pre,aff}} - \frac{(volume_{post,unaff} - volume_{pre,unaff})}{volume_{pre,unaff}}$$

Equation 2 Difference in Normalized Volume Change over Cancer Treatment

3.3.1.4 Statistical Analysis

Linear regression analyses were performed to determine the level of correlation between the tape measure method and the Kinect IR system. Additionally, to assess the agreement of the tape measure method and the IR system, a Bland-Altman plot was generated, where the circumference and volume of the right and left arms from Kinect were subtracted from the circumference and volume from tape measure method, respectively. Data analyses were run using Prism 6 for Windows (version 6.07, GraphPad Software).

3.3.2 Results

The arm lengths between the tape measure and Kinect IR system were matched. The correlation analysis of the circumferences at 4cm intervals along the arm from the tape measure method and Kinect IR resulted in a R-squared = 0.9000 and a slope of 1.035 (Figure 14A). Similarly, the volume calculated using the tape measure circumferential method and the Kinect IR system resulted in a R-squared = 0.8518 and a slope of 1.057 (Figure 14B). These correlations of determination indicate that the circumferences and volumes are highly correlative between the two measurement methods. As the slope approaches 1.00, the two methods near perfect agreement.

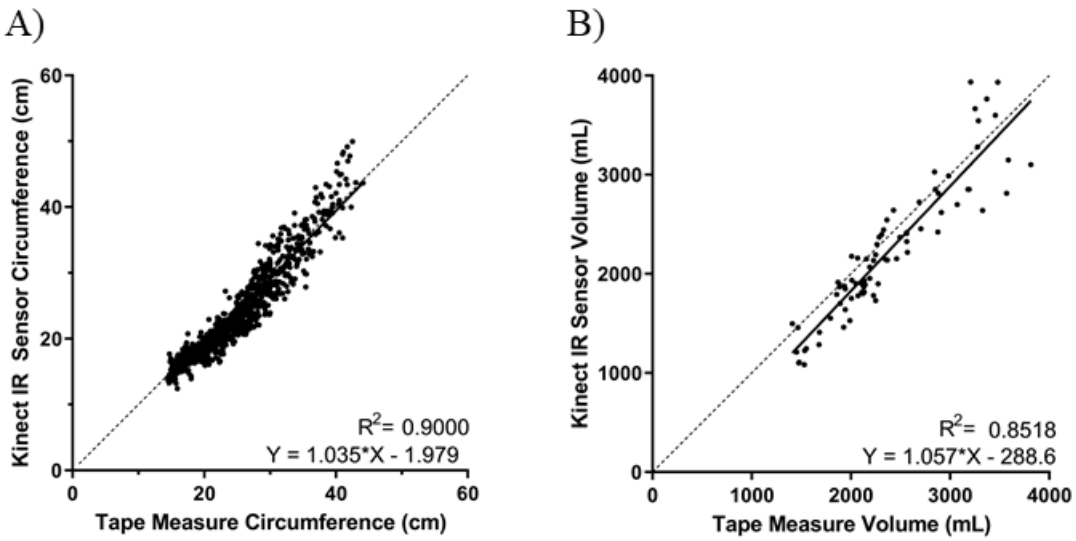

Figure 14 Correlation of Circumference and Volume

For this study, there were three operators that were trained to take measurements with the tape measure and the Kinect IR system. Breaking down the volume correlation based on each operator, there is some variation (Figure 15). The coefficients of determination were comparable to that between Perometer and the Kinect IR system for two out of the three operators.[96]

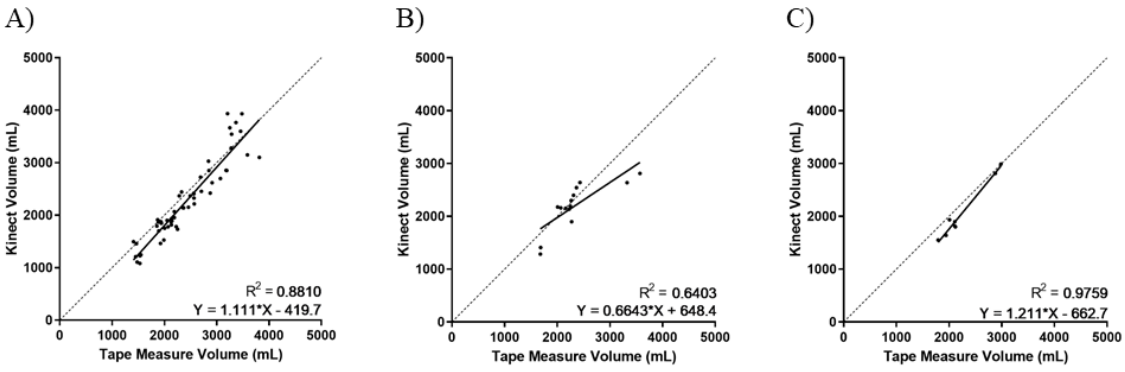

Figure 15 Correlation of Volume segmented by user

The Bland-Altman agreement analysis resulted in fair agreements between the tape measure and the Kinect IR system. The absolute circumference agreement analysis resulted in a difference of 1.086 ± 2.249cm (Figure 16A), and the volume agreement analysis resulted in a difference of 153.1 ± 264.5mL (Figure 16B).

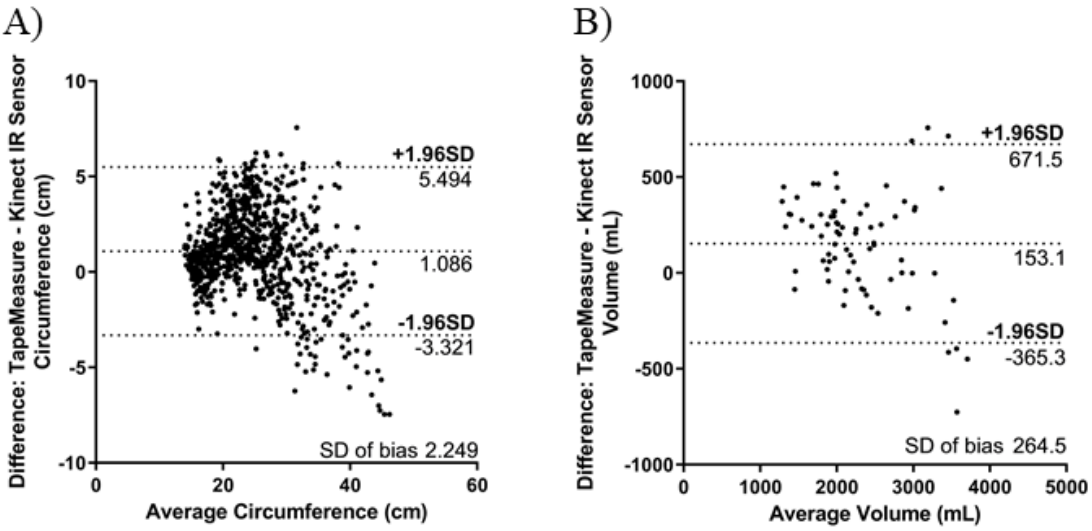

Figure 16 Bland Altman Plot of Circumference and Volume

For the 15 patients with a follow-up scan, the normalized change in volume for the affected and unaffected breast cancer sides were analyzed over time. On the affected side,

most patients experienced an increase in volume of approximately 10%. Compared to the affected side, the unaffected side had more patients that experienced smaller volume changes, and more patients that experienced a reduction in volume post-surgery. To see how one side changed compared to the other to ensure that changes were not due to overall body change such as weight gain or loss, the difference in change in normalized volume was calculated. Again, most of patients saw a modest increase in volume in their affected side. The single, known lymphedema patient that was diagnosed with lymphedema at a lymphedema clinic had the largest difference in normalized change in volume. Statistical analyses were not performed due to low sample set.

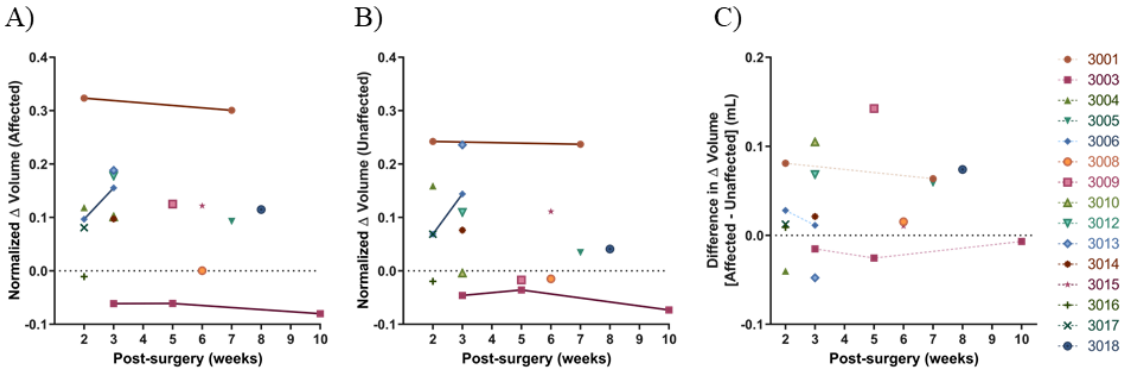

Figure 17 The normalized changes in volume for the A) affected cancer side and the B) unaffected cancer side were tracked over time post-cancer surgery. C) The difference in the change in volume of breast cancer patients were tracked over time.

3.3.3 Discussion and Conclusion

Currently, prospective surveillance among breast cancer patients pre- or post-treatment is not performed. This lack of surveillance is due to a combination of the difficulty in performing such measurements without either significant financial investment

or significant training for the clinical staff and the non-ubiquitous collection of this data in the field that leads to the lack of measurement. The Kinect IR system was tested in this environment against the tape measure method and was shown to be a strong candidate for implementation. The measurements performed with the Kinect IR system were quicker and easier to collect by the operators. The correlations of the volumes of each method taken by each individual operator indicated that there was variability among tape measurement skillsets.

Variability was shown in the correlation between the tape measure and Kinect IR system volume measurements among the operators. This variability in volume correlations is speculated to be due to the tape measure circumferential measurement. Many previous studies showed that the tape measure method requires training and experience to minimize intra-operator variability, much less inter-operator variability.[73]

The Bland-Altman agreement analysis showed that if measurements are made with both the tape measure and Kinect IR system, there would need to be an offset used in order to compare circumferences and/or volumes. In general, the tape measure reported larger circumferences and volumes. It is also interesting to note that at larger circumferences and volumes, the differences in metrics between the two modalities become larger, indicating that there is more variation among larger arms. This variability could be a result of the arm shape being difficult to measure with the tape measure because of various surface textures or due to either arm shape deviating from the circular or ellipse cross-section assumption when calculating volume.

Unexpectedly, enrollment into the study was low with less than 22% enrolled. It is hypothesized that the need to move to a different room to have the measurements taken negatively impacted the enrollment. Patients stated they did not want to lose their place in the checkout process at the end of their visit, despite stating that participation had no impact on their place in checkout. A more portable system would be ideal in clinical environments where checkout processes are less visible to patients. If the system was fully integrated into the workflow, then the patient would be less inclined to refuse measurement with the system.

While the majority of patients had at least a single follow-up measurement, consistent follow-up measurements were difficult and depended on the number of surgical follow-up appointments. The eight patients with no post-treatment measurement were a result of logistical challenges in followings patients to their post-treatment follow-up. Many of the surgeons of patients enrolled in the study perform a single follow-up, and the medical oncology team performed the subsequent follow-ups. Since the medical team is separate from the surgical oncology team and located in a different wing of the hospital, this study was limited in the number of follow-up measurements taken. This study's next steps would be to involve the whole oncology team for the patient so more longitudinal measurements could be performed. For the unilateral cases, having longitudinal data would provide enough information to note any asymmetrical arm changes over time. This richer dataset could provide insight into how well the metric of difference in change in normalized volume of the affected and unaffected cancer side would perform in detecting potential lymphedema cases. Then, patients could promptly be referred to a lymphedema trained therapist to treat lymphedema before the disease progresses too far.

The Kinect IR system was implemented in a busy, public hospital setting to test whether breast cancer patients could have their arms monitored in a longitudinal setting. This system is low-cost and has been shown to highly correlate with the previously developed Perometer system.[96] While this pilot study highlighted logistical challenges, the enrollment size would need to increase in order to gather more longitudinal data of pre- and post-treatment measurements, which can provide information regarding how swelling progresses over time after treatment. The next iteration of the system would ideally be more portable so that the measurements could be performed in the patient's room. This change would ease the follow-up measurement process. Ultimately, this implementation into the hospital workflow could allow for detection of lymphedema and referral for lymphedema treatment.

3.4 Objective 1C: Exploring the implementation of infrared sensor system for monitoring leg lymphedema in a rehabilitation clinic

Lower limb lymphedema may be a permanent and debilitating disease that severely impacts one's QOL.[10,97] There are various methods of clinically diagnosing and measuring lower limb lymphedema, but the most common is taking a volumetric measurement[98] or assessing signs and symptoms[68,99]. A common tool used to measure leg volume is with a tape measurement taking the circumferences along the leg at evenly spaced intervals.[100] This technique is time and labor intensive. While the "gold standard" for volumetric measurement is water displacement, the challenges regarding hygiene have resulted in limited to no use in clinics.[62] Various systems have been developed for upper extremity lymphedema using infrared technologies that require different numbers of sensors or rotation during scan acquisitions, which can be difficult to implement in clinics.[78–

[80,82,84,85,101] The commercially available Perometer is available in a horizontal and vertical version; while the vertical model aids in the consistency of leg measurements, the frame size of 47cm limits the size of leg lymphedema that can be measured.

Traditional assessment of lymphedema treatment outcomes has been measured by some reduction in volume, and details like circumferential changes over time have not been used.[102] Volume measurement alone is a generalization of the lower limb and does not assess the uniformity of reduction or lack thereof. Recently, a study assessed the treatment of intermittent pneumatic compression by comparing lower limb circumferences over time at five specific levels along the leg.[45] More granularity would provide more detail, but the five segments were a good start to understand where the volume reduction occurs.

This study aims to show how a single stationary Kinect IR sensor with a custom image processing algorithm can be a tool implemented in a clinical setting to measure changes in response to therapy of lower limb volume of leg lymphedema patients with the requisite clinical accuracy. The system is easy-to-use, has a small footprint, is non-invasive, and is quicker than the traditional tools used for circumferential measurements. A larger number of circumferential measurements within a limb can be obtained without the extra time that would be involved with using standard methods such as the tape measure. This inexpensive alternative reduces not only cost but also time and has a small physical system footprint in the clinical space.

3.4.1 Methods

3.4.1.1 Participants

Men and women who suffered from various stages of lymphedema and were undergoing physical therapy at BenchMark Rehab Partners, LLC, were recruited for this study. The inclusion criteria required the participant to be able to stand on their own for at least one minute and to possess all four limbs. While all adults were eligible, no minors (<18 years old) were recruited for this study. Patients receiving physical therapy treatment at BenchMark were recruited for this study by the therapist at the center based on the criteria. Prior to participating in the study, all interested patients provided a written informed consent.

3.4.1.2 Physical Therapy Protocol

Lymphedema treatment is varied among each patient depending on diagnosis and treatment needs. There are a few consistent components that each patient can use for treatment: education, compression, skin care, exercise, manual therapy, and volumetric measurements. Each patient was measured at the beginning of therapy for baseline volume of affected and unaffected extremities. The involved extremity was then measured weekly to determine differences in volume and changes in size. The patient was then treated with compression bandaging of the leg from distal to proximal, to increase the efficiency of the veins and lymphatics for volume reduction. Patients then began exercises that will increase muscle pump action and hypertrophy of muscles to push against the bandages.[103] Manual therapy was also applied to further increase lymph volume uptake. Volumetric measurements were done only on the affected leg after the first week, but if both were affected then both were measured each time. When volume reached a plateau or had clinically reduced to normal or near normal volumes, the patient was then measured for appropriate compression garments.

3.4.1.3 Measurement Acquisition

Recruited patients were measured at each visit upon consent by a certified therapist with the tape measure, which was the clinic's standard method of measurement, and the Kinect IR system. This study was approved by the Institutional Review Board at the Georgia Institute of Technology (IRB H15203). Single point and longitudinal measurements were gathered at BenchMark. The patients were asked to remove socks, shoes, and pants that would obscure the leg measurements; ankle socks were permitted.

For the Kinect IR system measurements, the patient was asked to walk to the delineated spot on the ground (about 1.8 m in front of the sensor). The feet were spaced about shoulder width apart to ensure separation of the legs as seen in Figure 18. When in the correct positioning, the software interface visually indicated this correct positioning by painting the cartooned version of the patient blue. In the background, there were parameters built in to ensure that the legs were fully separated, although actual separation becomes more difficult to achieve with larger volume legs. When in an incorrect positioning, the cartooned patient in the software display would be painted red. The patient was scanned from the front (Figure 18A), left side (Figure 18B), back (Figure 18C), and right side (Figure 18D) in this body positioning for approximately 30 seconds per side. Ten frames per side were used to calculate leg volumes post-hoc, and the process is further described in the next section.

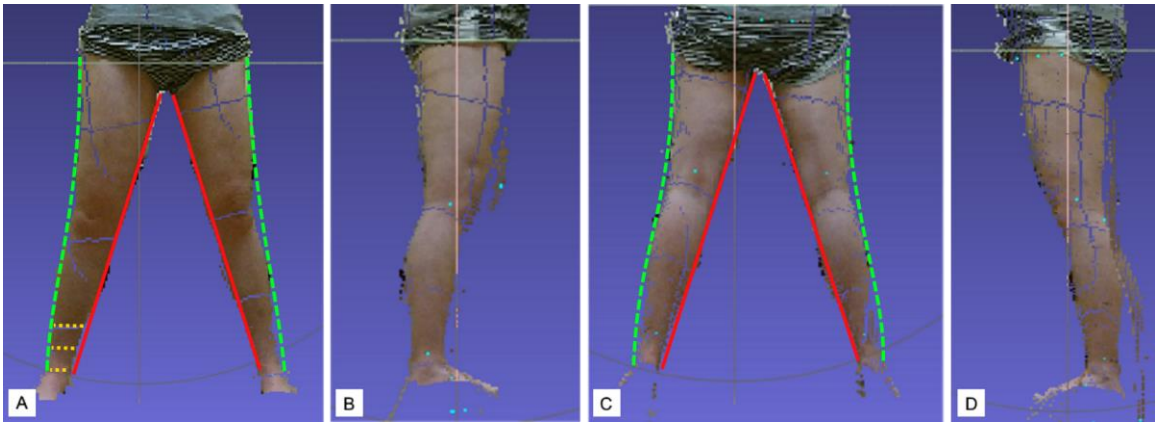

Figure 18 Kinect IR system leg scans. The (A) front, (B) right, (C) back, and (D) left scans are used to calculate the right and left leg volumes.

When taking measurements with a tape measure, the patient was positioned on a table, where the trained therapist could take circumference measurements every four centimeters along the leg, starting at the ankle.

3.4.1.4 Scan Processing – Volume Calculation

Kinect IR System

Leg volumes were calculated from the point clouds gathered by the Kinect IR system (Figure 18A-D). To compare the volumes calculated with the Kinect IR system with the volume from the tape measure measurements, the leg of the IR scan was truncated so that the length of the leg matched the length determined by the therapist measurements. First, the right and left legs were segmented in the front and back scans with customized code. More specifically, the code identified the location where the legs anatomically meet and isolated the left leg and right leg in each of the front and back scans. If the leg length captured with the tape measurements was longer than the scan's leg length, then the code produced an error message, because it was assumed that there was not enough separation

between the legs during the scan to enable complete isolation of the legs. In such an instance, the legs were manually isolated by visually determining the boundary between the two legs.

Once the right and left legs were segmented, the legs were truncated to match the leg length defined by the tape measure method. First, the legs were truncated at the ankle, set at 10cm from the ground to match the tape measurement protocol, and then up the leg at the y-coordinate equal to the sum of 0.1m and the tape measure leg length. The boundary points of the individual legs were identified and were smoothed using a 5-point moving average filter, resulting in a point cloud of the right and the left leg from the front and back scans.

Once the left and right legs were segmented and truncated in the front and back scans, the diameters (represented by the dotted yellow lines in Figure 1) were calculated by taking the difference of the x-coordinate of inner and outer boundaries (represented by the solid red and dashed green lines respectively in Figure 1) of each leg at every 1cm interval along the leg. The average of the diameter calculated from the front, d_{front}, and back, d_{back}, scans was used to determine the major axis of the ellipse used to calculate the circumference at each axial location on the leg. The diameters from the left and right leg scans, d_{side}, were used to determine the minor axis of the respective leg. These diameters were calculated by finding the distance between the front and back boundary along the leg. The ellipse circumference formula Equation 3 uses the radius of the major and minor axes to calculate the circumference of the leg at each location, *i*, along the leg.

$$circumference_i = \pi * (0.5 * \left(\left(d_{front,i} + d_{back,i}\right) + d_{side,i}\right))$$

Equation 3 Leg circumference based on the ellipse formula

To compare to the tape measure method, the disc method was used to calculate the volume at 4 cm intervals using the circumferences calculated previously. The disc method formula uses the area of each slice taken every 4 cm and multiplies it by the length (4 cm) to calculate the volume of that segment. These segments are summed to give the total volume. Subsequently, percent volume difference and volume difference were calculated based on the right and left leg volumes.

Tape Measure

The leg volume was calculated from the circumference measurements taken with the tape measure every 4 cm by a trained therapist. Circumference values were input into software by Academy of Lymphatic Studies (ACOLS) to calculate the volume, which is based on the disc method, and the resulting percent difference in volume and volume difference.

Other Clinical Measures

Clinical metrics used are percent volume difference and volume difference. The ACOLS software calculates these metrics based on the affected side in unilateral cases and the larger side in bilateral cases. For better comparisons with the Kinect IR system, I recalculated these metrics. Volume difference was the right leg volume subtracted by the left leg volumes, and the percent volume difference is the volume difference divided by the right leg volume multiplied by 100%.

3.4.1.5 Leg Change over Therapy

To assess how volume changed along the leg in response to routine treatment, changes in volume were tracked from one visit to the next using both modalities. I calculated the average absolute percent error of volumes, which was 6.5%, between the tape measure method and the Kinect IR system. Based on this threshold, each leg was classified as having undergone (a) no change or less than 6.5% change in either direction, (b) increased in volume by 6.5%, or (c) reduction in volume by 6.5% over the course of therapy. Then, the change in circumference was calculated between the initial and last therapy visit. Using the measurements taken with the Kinect, change in circumference was calculated as the difference in circumferences measured at the first and last visit, divided by the circumferences in the initial visit, and multiplied by 100%:

$$Change\ in\ circumference_x = \frac{(circ_i - circ_1)}{circ_1} * 100\%$$

Equation 4 Change in Circumference over therapy

Where *x* represents the position along the leg, $circ_i$ represents the circumference at the last visit and $circ_1$ represents the circumference at the initial visit.

3.4.1.6 Statistical Data Analysis

Linear regression analyses were performed to compare the degree of correlation between the Kinect IR system and the tape measure for leg circumference, leg volume, percent volume difference, and volume difference. To assess the agreement of the two methods, a Bland-Altman plot was created for circumference and volume. This plot is composed of the percent difference in either circumference or volume ([Tape Measure – Kinect IR system] / average volume) over average circumference or volume of the two

modalities, respectively. To evaluate circumferential changes along the leg, the Wilcoxon matched-pairs signed rank test with a Bonferroni correction was performed on positions with three or more samples to determine whether statistically significant changes in circumferences occurred across the patient population. For patients with a reduction in leg volume, the modified alpha was 0.0011, and for those with an increase in leg volume, the modified alpha was 0.0005. All the analysis was performed using Prism 8 for Windows (version 8.0.2, GraphPad Software).

3.4.2 Results

Thirty-eight (38) patients at a range of time points of post-lymphedema onset had leg lymphedema and participated in the study (Table 6). The patients were composed of 12 males and 26 females. Of the participants, seven were unilateral cases and 31 were bilateral cases. Fifteen participants had a single visit, and 23 participants had more than one visit, averaging 3.9 visits over the duration of 25 days (3.5 weeks).

Table 6 Benchmark participant characteristics (n=38)

Gender	***Count (%)***
Male	12 (32)
Gender	26 (68)
Affected Side	***Count (%)***
Unilateral	7 (18)
Bilateral	31 (82)

The standard tape measure circumference measurement method and the Kinect IR system were compared. The correlation of leg circumferences and correlation of volumes along the leg between the two modalities were strong with an R-square = 0.9522 (Figure 19A) and R-square = 0.9847 (Figure 19B), respectively. The linear regression coefficients comparing circumferences and volumes from the two modalities were 1.028 and 1.067,

respectively. An R-square value of 1.000 would indicate perfect correlation between the tape measure and the Kinect IR system, and a coefficient of 1 with an intercept of 0 would indicate perfect agreement. The agreement analysis resulted in a circumference percent difference bias of 1.492 ± 6.302% (0.3971 ± 2.601cm) (Figure 20A) and a volume percent difference bias of 3.558 ± 7.888% (50.39 ± 518.2mL) (Figure 20B) between the tape measure and Kinect IR system. A bias of 0.000 would indicate perfect agreement between the two modalities. Additionally, I assessed the correlation of clinically relevant metrics such as percent volume difference and volume difference. The analysis resulted in fair correlations for percent volume difference with an R-square = 0.6282 (Figure 21A) and volume difference with an R-square = 0.6518 (Figure 21B).

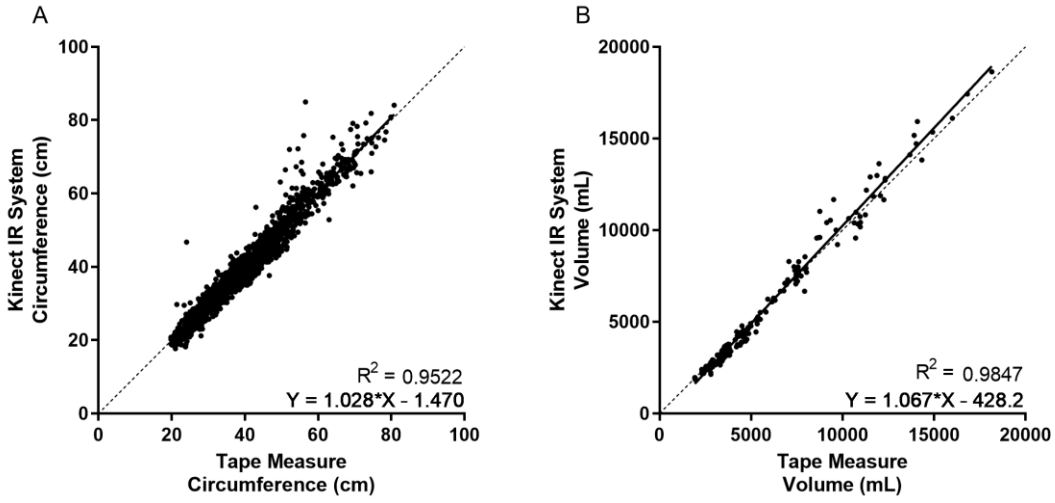

Figure 19 Correlation of leg Circumferences and Volumes

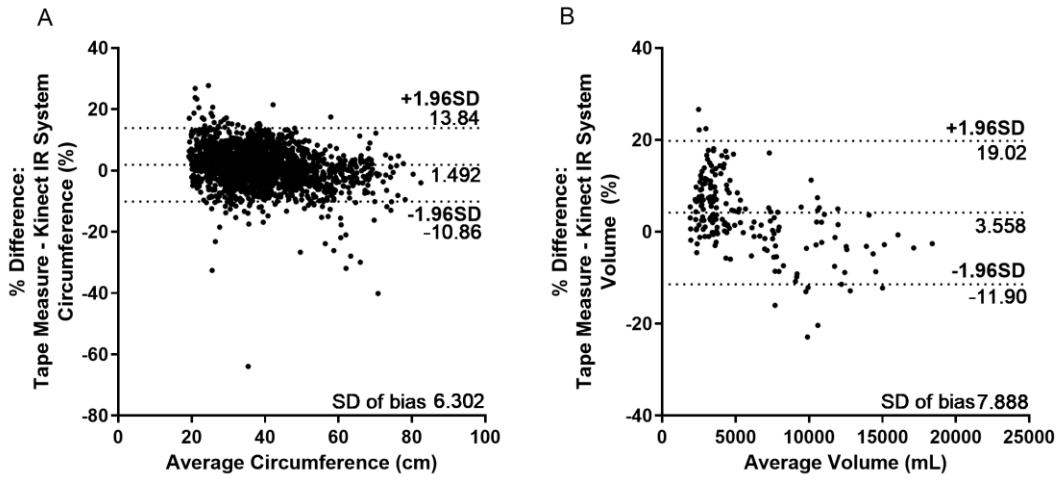

Figure 20 Bland Altman Plots of leg circumference and volume

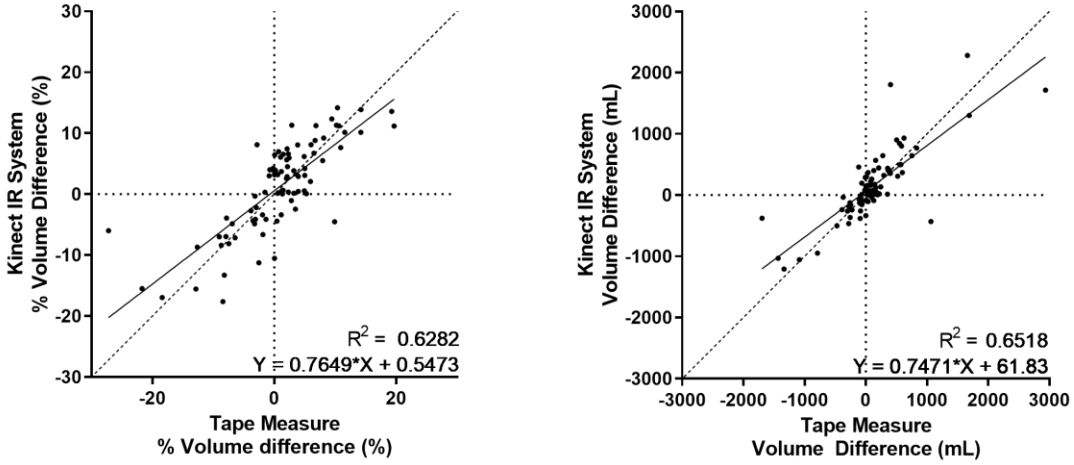

Figure 21 Percent volume difference and volume difference

Interestingly, I noted that a change in leg volume did not change uniformly along the leg over the course of therapy. There were 23 participants that had more than one measurement, meaning 46 legs were analyzed to assess change from therapy. While 23 legs had no notable changes in volume, meaning changes less than 6.5%, five legs

increased in volume and 18 legs had a reduction in volume. For legs that underwent a reduction in volume, the largest reduction in leg circumferences were distal to the body, closer to the ankles. Specifically, there was significant reduction in circumferences when comparing the changes at 4cm from the ankle to 24cm ($p = 0.0007$) and 28cm ($p = 0.0001$), 8cm to 32cm ($p = 0.0090$), and 12cm to 32cm ($p = 0.0090$) up the leg (Figure 22A). For legs that increased in total volume after therapy, the greatest changes were found at the most distal and most proximal of the leg to the body, but these regional changes were not significantly different.

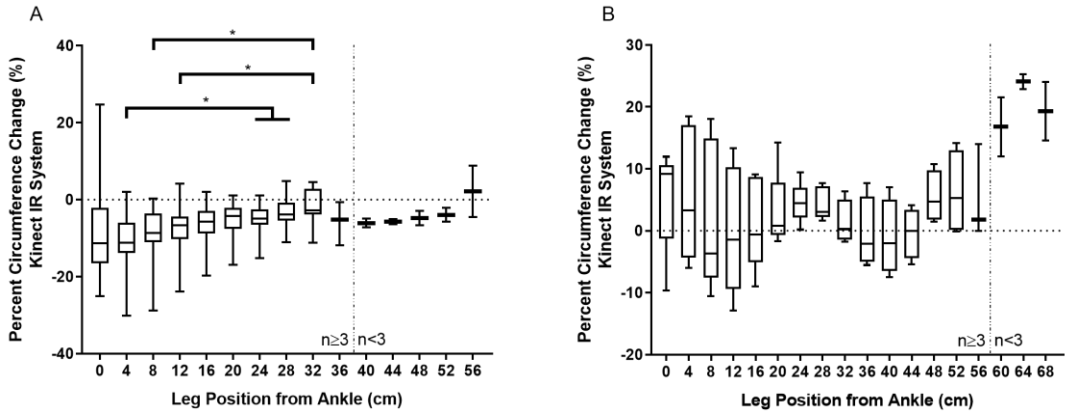

Figure 22 Circumference Change in Legs with Volume Change greater than 6.5%. (A) Legs had a reduction in leg volume and (B) legs had an increase in leg volume.

For legs with a reduction in leg volume greater than 6.5%, I analyzed the percent change in circumference taken by the Kinect system in Figure 23. While there was no difference found in the percent circumference change in patients with bilateral lymphedema, there was a significant difference found when comparing regional leg circumference changes of patients with unilateral lymphedema. Specifically, at 4cm above

the ankle, there was significant reduction in circumference compared to the circumferecnes at 24cm (p=0.0391) and 28cm (p=0.0234) above the ankle.

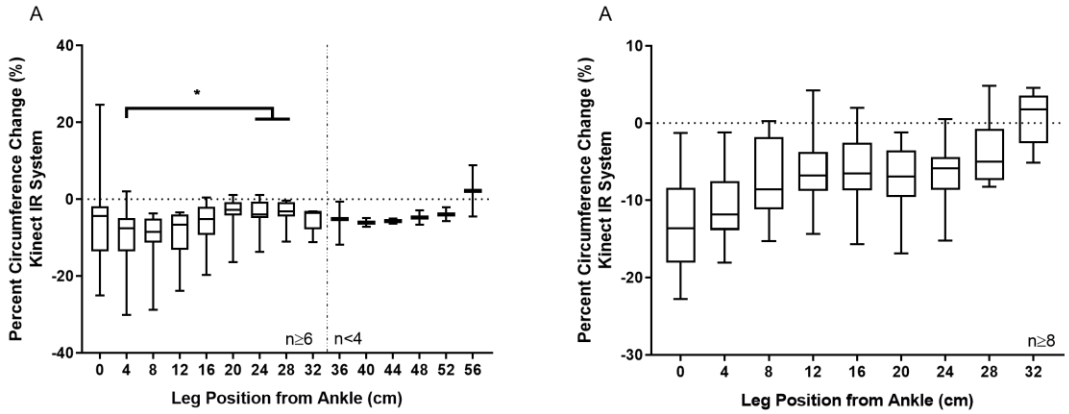

Figure 23 Reduction in leg volume for (A) unilateral cases compared to (B) bilateral cases of lymphedema

3.4.3 Discussion and Conclusion

While there are methods to track lymphedema in its progression and its response to physical therapy treatments, there is room for technological improvement to aid with clinical implementation to save time and to promote continued monitoring. This study shows that circumference and volume strongly correlated when comparing the tape measure method and the Kinect IR system. Also, in this study, the therapist collected all the scans after a brief training session during regular patient treatment visit, which indicates that clinical implementation is realistic and logistically possible with minimal training.

The Kinect IR system has various strengths and weaknesses. The system is quick and requires less training to operate. While length of time for acquisition was not specifically recorded in this study, other studies have shown that tape measurements of the leg circumferences can take up to 7.5 minutes[87], in comparison the Kinect IR system

currently takes an estimated 4-5 minutes but was shortened with increased familiarity and could be further shortened by reducing the number of frames taken of each side. This time savings provides the therapist with time to focus on therapy as opposed to making manual measurements with the tape measure. Additionally, this study assessed whether the changes in limb volume over the course of therapy was uniformly distributed on the leg. This granularity of detail can help inform therapists of which locations within the limb are being particularly responsive to therapy and can also identify potential problem areas where fluid is not sufficiently draining. While there are many strengths, there are also a few limitations to the system. The system results in a slightly weaker correlation when the circumferences (>60cm) and volumes (>7000mL) are larger. This limitation is also reflected in the agreement analysis, as the differences between the two modalities are larger for limbs with larger circumferences and volumes. This data may indicate that at these larger measurements, the leg shape may deviate from the assumed cross-sectional shape.

Many studies have reported various ways of assessing effectiveness of treatment of lymphedema with volumetric measurements being the most common[100,102]. There are multitudes of modalities to measure volume that vary in financial cost, labor intensity, hygienic risk, and length of testing. Interestingly, there has been little attention on the assessment of more regional changes over the course of therapy to gain a better understanding of where changes in swelling occurred. The Kinect IR system balances its cost with the reduction in scanning time and reduced training for acquisition. It is worth noting that this model of the Kinect IR sensor has been discontinued, but other comparable infrared sensors can be integrated with the software, and thus the approach of applying detailed morphological analysis of 3D point clouds to determine localized volume changes

in response to therapy is agnostic to the particular sensor being used. A study has shown promising volume measurements using portable infrared technology among filarial patients in Sri Lanka that can be translated for lymphedema patients under therapy.[87] In fact, this new scanner technology (LymphaTech, Atlanta, GA) has replaced the use of the Kinect scanner in the clinical implementation of limb volume tracking at BenchMark Rehab Partners in Chattanooga, where the data presented here was collected.

Assessing regional circumferential changes along the legs under treatment for lymphedema in this study showed that the resulting volume reductions were not uniform along the leg. While volume has been a good indicator of efficacy of the treatment, this approach does not detail whether reduction occurs uniformly along the leg or in specific regions. Therefore, analyzing specific regions provides more granular information that can inform future treatments. The results showed that when analyzing regional changes over the course of therapy for lymphedema, there was significant reduction of leg volume at regions more proximal to the body. Legs that underwent an increase in volume over time had no significant regional differences in volume change, but because this increase was a rare event in the study, the sample size of this group was very small and likely underpowered. While assessing changes in this small set of patients, volume increases seemed to occur at the most proximal and distal regions of the leg, which correlates to where the therapeutic compression garment ends. Additionally, fluid buildup in the leg despite therapy could be an indication of lymph blockage more downstream to the leg. In addition to informing therapists of where the leg is responding to therapy, this implementation could expedite the overall duration of therapy for volume reduction, and future studies could investigate its potential in this regard.

The Kinect IR system is a good alternative to the tape measure method used in clinics to monitor the change in leg volume over the course of therapy. It is capable of tracking patients over time. Again, this system is low-cost and highly correlates with the tape measurement method. Furthermore, all these scans were collected by the clinician, demonstrating the ease of use and implementation in the clinic. Because of the time-consuming nature of measuring with a tape measure, non-affected legs were measured only at the initial visit and are assumed to be constant over the course of therapy. This Kinect IR system quickly measures both legs; any changes in the non-affected leg could potentially be informative with general body changes. In the next steps, analysis of local changes in the leg to *inform* treatment could show whether this approach could result in greater reduction in the affected limbs.

3.5 Conclusion

Through this aim, I explored the implementation of the Kinect IR system in multiple clinical settings. The clinical environments ranged from specific rehabilitation centers to a large public hospital. Participants included lymphedema and non-lymphedema cases of the arms and legs. While arm lymphedema patients were all unilateral cases, leg lymphedema cases included unilateral and bilateral cases. The Kinect IR system measurements were taken either by the researcher or the clinician involved in the specific study. Comparisons were made with the clinic's measurement standard, either the Perometer or the tape measure circumference measurement method.

Through these studies, the analysis showed that the Kinect IR system correlated and agreed well with the clinic's measurement standard. In addition, the Kinect IR system

was quicker, taking no more than 4-5 minutes to collect measurements, and was easier to operate. The implementation into the rehabilitation clinic's workflow had fewer challenges due to more spatial area. The patient population in these environments was also educated about lymphedema since they were further along in their oncology journey. Challenges in the hospital study indicated factors that, if changed, would ease the implementation process such as portability.

With the discontinuation of the Kinect IR sensor model, the system was updated. The next iteration went from a Kinect IR sensor connected to a computer (Figure 4) to the Structure sensor connected to the iPad mini 2 (Figure 5). While the cost of the system itself remained approximately the same, there were many benefits with the second iteration of the system. The Structure system is more portable and completely handheld. Arm patients rest their hands on a stand during the scanning process, eliminating fatigue associated with holding the arms in the air and minimizing any motion associated with fatigue. Additionally, a single arm is scanned at a time reducing the amount of open space necessary to acquire scans. Although the arms are scanned separately, the overall measurement time remains approximately the same, taking about 1 minute of scan time per arm. This system outputs a high-resolution 3D scan of the arm, as opposed to partial scans resulting from the Kinect IR system. As a result, there are more opportunities to explore questions regarding lymphedema. With the right dataset, I could explore if there are other measurements that can be more meaningful when identifying limbs with lymphedema.

CHAPTER 4. AIM 2

4.1 Introduction

Traditional methods of diagnosing and monitoring lymphedema use volume of the limb. Because prospective surveillance is not standard among the patients who are at risk, there is no baseline measurement of volume when the patient goes into therapy. With no baseline, it can be difficult to detect lymphedema. Common alternatives such as volume difference, where both arm volumes are compared, can detect unilateral lymphedema, but significant swelling must occur before bilateral lymphedema is detected as both limbs could swell simultaneously.

Studies have explored features aside from volume in conjunction with the use of machine learning to detect lymphedema in patients. Moreira *et al.* evaluated upper body function and its ability to classify lymphedema in patients from non-lymphedema patients.[77] They showed features such as range of motion and arm widths had greater influences in its functional assessment. More recently, the Fu group has developed a model that takes in self-reported symptoms, and clinical analytics to predict lymphedema appears promising with nearly 94% accuracy, 96% sensitivity, and 91% specificity rates.[104] Meanwhile, Armer *et al.* showed that continued surveillance of both limb measurements and symptoms is critical as lymphedema incidences can present as volume changes despite lymphedema symptoms decreasing.[105] New measurements for detecting lymphedema are intriguing and a viable approach.

New approaches can take advantage of technological advances and utilize 3D scans taken by infrared sensors. Rather than assessing global metrics like volume, more detailed

local geometries can be explored.[84] To determine whether these local geometry measurements have any potential value, I assessed the measurement's capacity to classify lymphedema patients and their arms by training and testing classification models. Ultimately, the final model can be used in clinics with limited lymphedema background and specialization seeing patients who are at risk for developing lymphedema.

In this aim, features were engineered based on metrics that are descriptive of the local anthropometric geometries of the arm. Healthy and lymphedema arms undergoing therapy were scanned using the second-generation system using the Structure sensor and LymphaTech acquisition software. These features were used to train classification models to identify lymphedema cases, and the sensitivity and accuracy of the models were assessed.

4.2 Methods

4.2.1 Participants

All women in this study previously had breast cancer and underwent treatment at least once. Their physicians referred these women to TurningPoint Breast Cancer Rehabilitation for post-treatment rehabilitation. Those who participated in this study were at various stages post-treatment of breast cancer and were undergoing rehabilitation for varying periods of time ranging from new patient to returning patient for many years.

Women who were receiving physical therapy treatment from TurningPoint Breast Cancer Rehabilitation were recruited for this study by the therapists based on the inclusion and exclusion criteria. All participants were required to be adult (18 years or older), female

breast cancer survivors, who may have undergone any combination of surgery, chemotherapy, and/or radiation. Participants must have all four limbs and must be able to stand without assistance for one minute. These women did not have to be diagnosed with lymphedema to participate. All patients provided a written informed consent prior to participating in the study.

4.2.2 Structure Measurement

Participants were scanned once per side, totalling twice including the right and left sides, with a single Structure sensor (Occipital, Boulder, CO) mounted on an iPad Mini 2 (Apple Inc., Cupertino, CA) as seen in Figure 5. Women were asked to wear taut sleeveless tops and to remove jewelry on their arms, although rings were permitted, to ensure that the wrist to axilla region was unobstructed.

Participants were asked to stand with a single arm raised and extended to create a 90-degree angle with the body, resting their hand on a pole adjusted to the height of their axilla. As the participant stands still for approximately one minute, the scanner panned the Structure device around the arm of interest to capture the 3D scan (Figure 24). As the sensor collected depth data of the arm, the LymphaTech software paints over the completed area with a solid color, differentiating it from what is remaining to be captured. Each arm was scanned, resulting in two .OBJ files of the right and left arms per patient. The session per patient took at most 5 minutes from positioning the participants to completion. The lymphedema status of participants was reported by the participant's caring therapist.

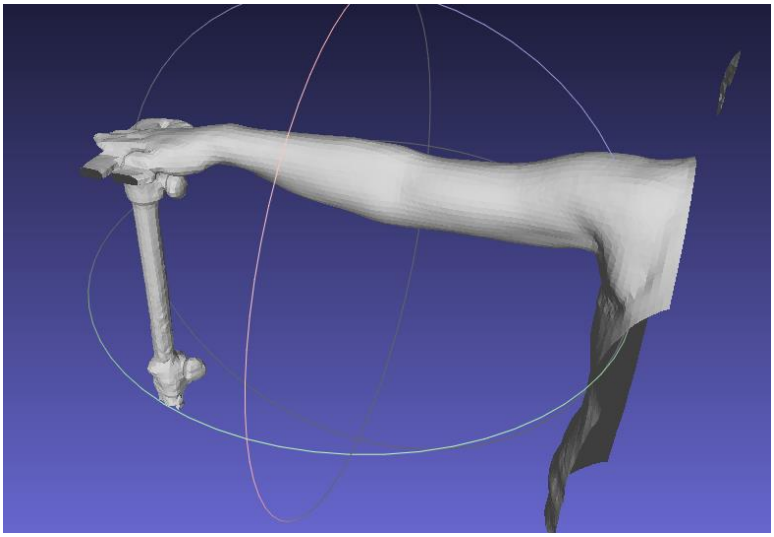

Figure 24 Structure system arm scan

4.2.3 Feature Development

The .OBJ files were pre-processed in two major steps for feature engineering. Firstly, the point cloud needed to be segmented to capture only the portions of the arm between the shoulder and the wrist, which would be used for further analysis. The .OBJ file collected was read into Matlab R2017b as an object composed of an array of vertices and their corresponding normals in the x-, y-, and z- components (Figure 25A). Because the scan captures portions of the trunk and the hand in addition to the arm, defined as the wrist to the shoulder, the object was truncated. This process included identifying the axilla (associated with the shoulder position) and the wrist as described below. Next, this arm .OBJ was inputted into a feature extraction code that outputs a list of features extracted. Extracted features were used as inputs to train a model.

4.2.3.1 Data Segmentation

The region of interest is the arm bounded by the wrist and the axilla. The axilla detection was automated by rotating the object by $5\pi/6$. The rotation ensures that the axilla is located at the maximal y-coordinate point. A boundary line was created to represent the underside of the arm, and the point associated with the maximum y-coordinate in this boundary corresponded with the axilla location, denoted as the blue circle in Figure 25B. The original point cloud was filtered so any x-coordinate greater than the x-coordinate of the axilla is removed, where along the x-coordinate the object starts from the hand and moves to the wrist, elbow, axilla, and then trunk (Figure 25C). Next, the object was rotated back to its original orientation, and the wrist is identified.

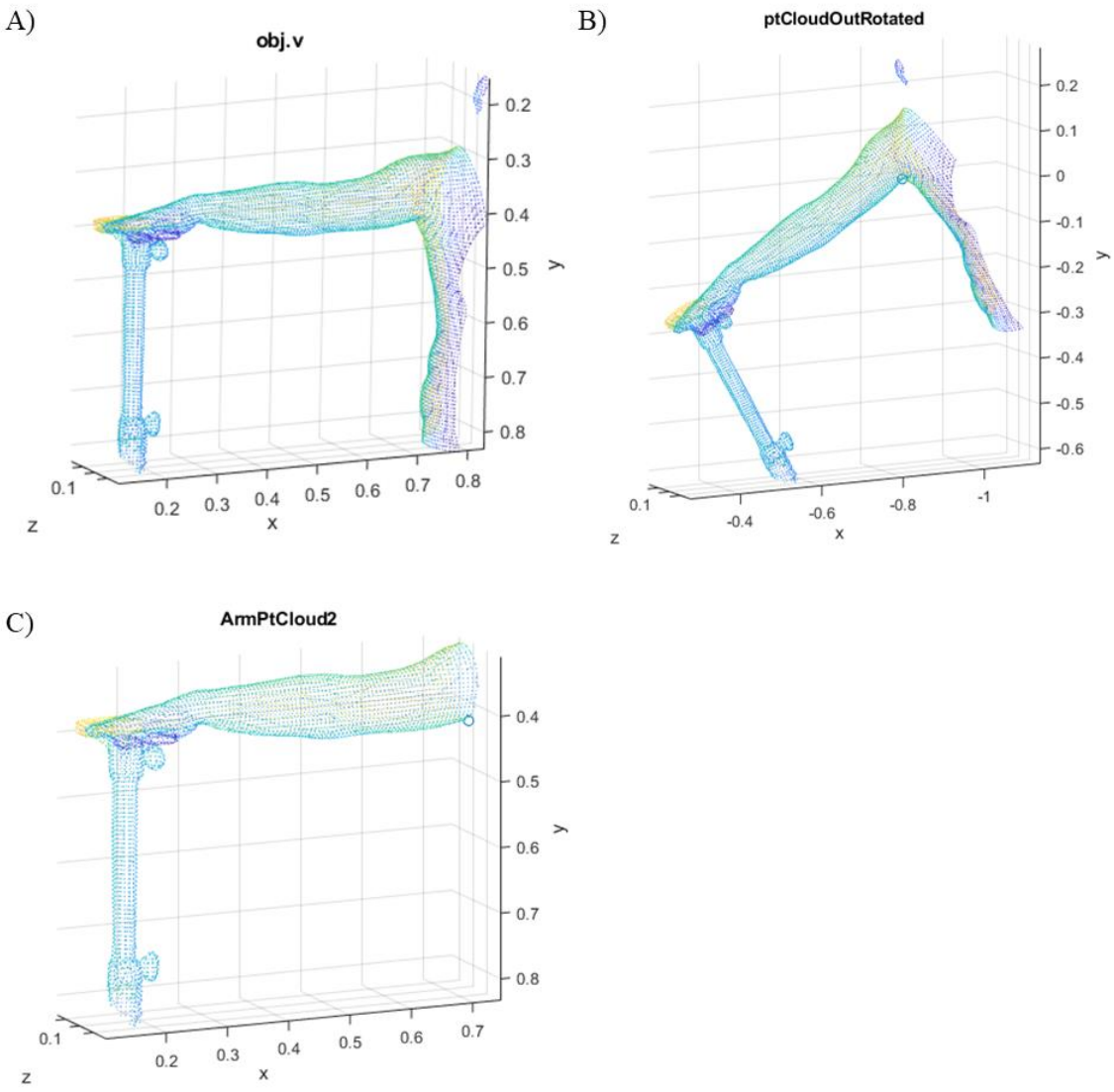

Figure 25 Process of removing the trunk. A) Plots the original .OBJ file showing that the pole, hand, arm, and trunk of the patient is captured. B) The object is rotated for automated axilla identification, where the axilla is represented by the blue circle ("o"). C) The body/trunk is identified and removed from the object file, leaving the pole, hand, and arm. The blue circle represents the identified axilla again.

The wrist was manually identified by the researcher three times at spaced out intervals over the course of two months. The wrist detection was to the closest centimeter, to determine the final x-coordinate of the wrist. This wrist identification process was done

in an interactive figure display, where the user could rotate the .OBJ (of the hand through the axilla) and then clicked on the wrist region in the .OBJ displayed. The x-coordinate to the nearest centimeter of the location of the click was recorded. Of the three identifications, the final x-coordinate of the wrist was determined based on the following rules. If there was one unique x-coordinate, then it became the final x-coordinate. If there were two unique x-coordinates, then the mode of the x-coordinates was taken for the final x-coordinate. If all three x-coordinates were unique, then the median x-coordinate was taken as the final x-coordinate. These outcomes were summarized in Table 11. The final x-coordinate of the wrist was recorded and inputted in the TruncateArm_FINAL.m (A.1.1 TruncateArm.m) function to output the final .OBJ file of the arm from the wrist to the axilla visualized in Figure 26.

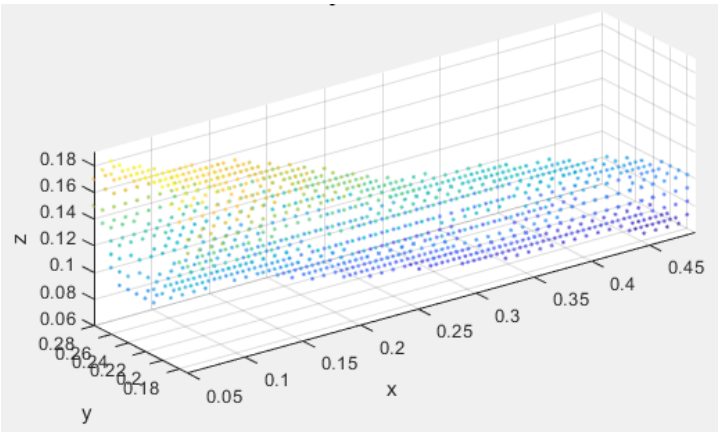

Figure 26 A representative image of a point cloud of an arm from the shoulder to the wrist.

Despite best efforts to position arms parallel to the ground, some scans of arms were sloped and non-aligned as seen in Figure 27A, where the left arm point cloud is in yellow and the right arm point cloud is in blue. Therefore, the arms were aligned. This alignment started by generating a cylindrical point cloud centered around the positive x-

axis. The left and right arm point clouds were aligned to this cylinder using a point-to-point iterative closest point (ICP) algorithm, which used the cylinder as a fixed point of reference seen in Figure 27B. This step transformed the arm point cloud to be parallel to the x-axis. The left and right arm point clouds were transformed by rotating and translating the point clouds to match the cylinder reference. The transformation process iteratively minimized the error, which is the sum of the squared differences between the coordinates of the matched pairs of the left and right arm point clouds with the cylinder point cloud. Lastly, the left and right arm point clouds were aligned with each other using the ICP algorithm, setting the left arm point cloud as the reference point cloud for the right point cloud. The final alignment of the left and right arm point clouds is represented in Figure 27C. This final .OBJ was inputted in the feature extraction function to derive the list of features for each arm.

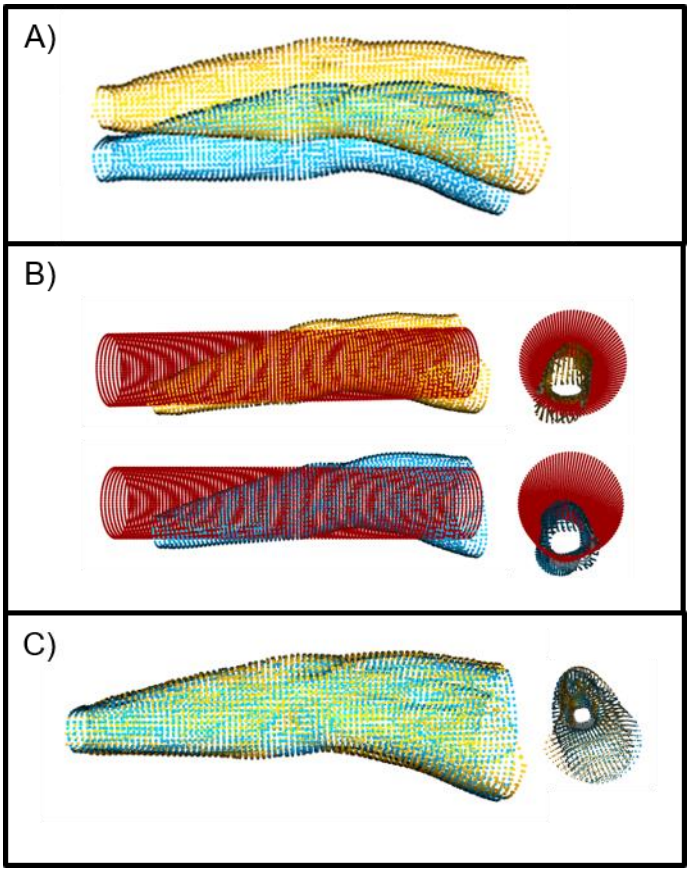

Figure 27 Arm alignment process is represented in these images. A) The image shows the initial arm position, where the left arm corresponds to the yellow arm and the right arm corresponds to the blue arm. B) The arms are aligned with the cylinder drawn along the x-axis before C) the right arm is aligned to the left again for the final alignment.

4.2.3.2 Transforming Data

Aside from volume, various metrics were determined to represent local geometries that might differentiate a healthy arm versus a lymphedema arm. During the progression of lymphedema, the arms change regionally. Therefore, features should also assess specific regional changes in metrics to capture non-uniform changes. Table 12 outlines the features.

The angles of the forearms were calculated based on the first third of the arm from the wrist. Two lines were created in both the x-y and x-z planes by fitting a first-degree

polynomial via a least-squares approach to the upper and lower edges (blue and red lines, respectively in Figure 28) of the arm in that plane. An angle between the two lines, denoted in the yellow arc in Figure 28, in each plane was calculated in degrees. Specifically, the angle was calculated by taking the inverse tangent in degrees of the upper line and lower line, and the sum of the absolute value of the two angles was the final forearm angle.

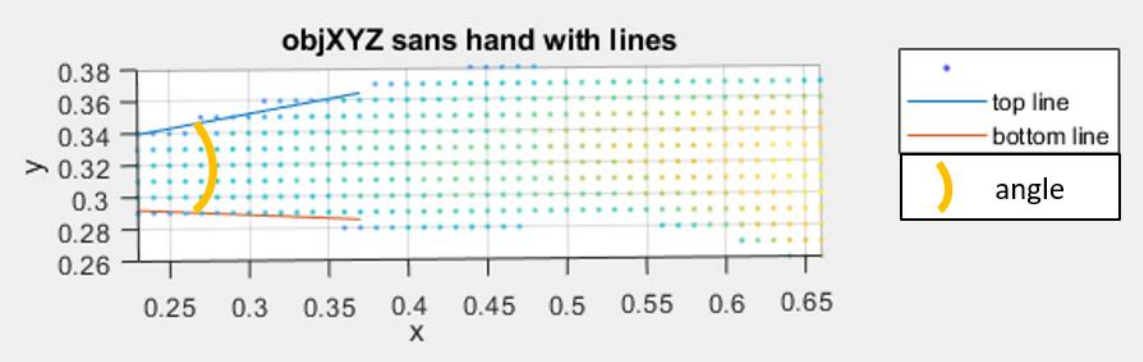

Figure 28 The forearm angle is denoted by the yellow arc and is formed by the tapering of the forearm as the wrist is approached. This figure is a representative image of this forearm angle in the x-y plane. The forearm angle was also calculated for the x-z plane.

The regional curvature data were composed of minimum, maximum, mean, and gaussian curvature information for each specific region outlined in Figure 29. These features were feasible due to the alignment of the arms so that features of a region of the left arm matched that of the right arm. Each arm was divided into 36 regions where curvature data was calculated. The arm was segmented in the sagittal plane along the arm (in the x-direction) into six segments. Each of these segments was then divided in the axial plane into top and bottom halves at the mid-point of the arm. Then, these halves were separated into thirds in the coronal plane, creating a front, mid, and back region, where the front region corresponds to the anterior side of the body. The various curvature features were then calculated for each region.

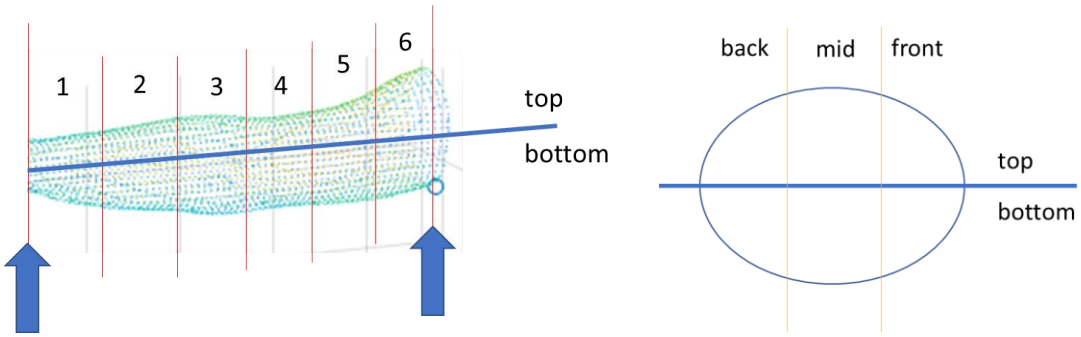

Figure 29 Arm regions for curvature features (minimum curvature, mean curvature, maximum curvature, and gaussian curvature) were outlined above for a total of 36 regions. The arm was divided into six regions in the sagittal plane along the arm in the x-direction. Each slice was then divided into a top and bottom region at the mid-point of the arm in the axial plane. Then, the halves were subsequently divided into thirds in the coronal plane, creating a front, mid, and back section where the front corresponds to the anterior side of the body.

The arm scans contained a 3D point cloud composed of vertices, where triangular faces exist among the points. The principal component analysis (PCA) was performed on these local face centers. This process was an orthogonal transformation of the x-, y-, and z-components of the face centers. The covariance was calculated, and the eigenvalues were represented as s1, s2, and s3.

Statistical measurements of features that have an output for each vertex or for each slice, set at a thickness of 1cm, along the arm of the scan were calculated to gain a better understanding of the feature distribution. Assuming a unimodal distribution, the average, median, standard deviation, range, skewness, and kurtosis were calculated. The average was calculated by summing the feature at each point or slice and dividing by the number of points and slice. The median was calculated by ordering the measurements and taking the value in the middle. The standard deviation described the amount of variation that exists

from the mean. The range was calculated by taking the difference between the maximum and minimum values. The skewness measured the symmetry of the feature dataset, and the closer to zero the skewness was, the more symmetrical the data was. The kurtosis measured how much of the data fell near the tails of a normal distribution, and a positive kurtosis indicates a "heavy-tail" dataset, meaning more data was near the tails or are outliers. A negative kurtosis indicates a "light-tail" where the dataset fell near the mean and had few outliers. Both skewness and kurtosis were calculated based on the mean, standard deviation, and number of points (i.e. the number of vertices or number of slices, depending on the feature).

As mentioned previously, the arm scans are composed of vertices and their corresponding normal. Each normal was composed of its x-, y-, and z-components, and each component was treated as an individual feature. The unimodal statistical measurements were calculated per arm scan, resulting in an understanding of the distribution of each feature per arm. When plotting the distribution of the normal y-coordinate and z-coordinate, the data appeared to have a beta distribution. Therefore, the shape parameters, alpha and beta, were calculated utilizing the Matlab function that fits the beta probability distribution to the normal y-component and normal z-component for each arm scan.

A curvature was calculated for each vertex in an arm scan. To estimate these curvatures, the nine (9) closest points to each vertex was determined by the knnsearch function in Matlab. The eigenvectors and eigenvalues were computed for the surface created by the nine neighbors and the vertex itself. The estimated curvature was calculated by dividing the smallest eigenvalue by the sum of the three eigenvalues.[106,107] The

unimodal statistical measurements were calculated per arm. In addition, when plotting the distribution of the curvatures for each vertex, an inverse gaussian distribution was noted and therefore, the shape parameter lambda was calculated utilizing the Matlab function that fits the inverse gaussian distribution to the curvatures for each arm scan.

The perimeter, area, and circularity were calculated at 1cm slice thickness. The slices were created by starting at the wrist x-coordinate and binning vertices at every 1cm interval. In each 1cm bin, the vertices were plotted in the y-z plane and a boundary function in Matlab was applied to create a boundary around the vertices as shown in Figure 30A. The function outputs a vector of point indices that represent the boundary around the vertices that were input into the function. The shrink factor of the boundary function was set to 0.5, which controls how compact the boundary is. Occasionally, the boundary function produced an erratic fit, resulting in an incorrect perimeter, area, and circularity. Therefore, when the circularity was greater than 2, the shrink factor was set to 0.1.

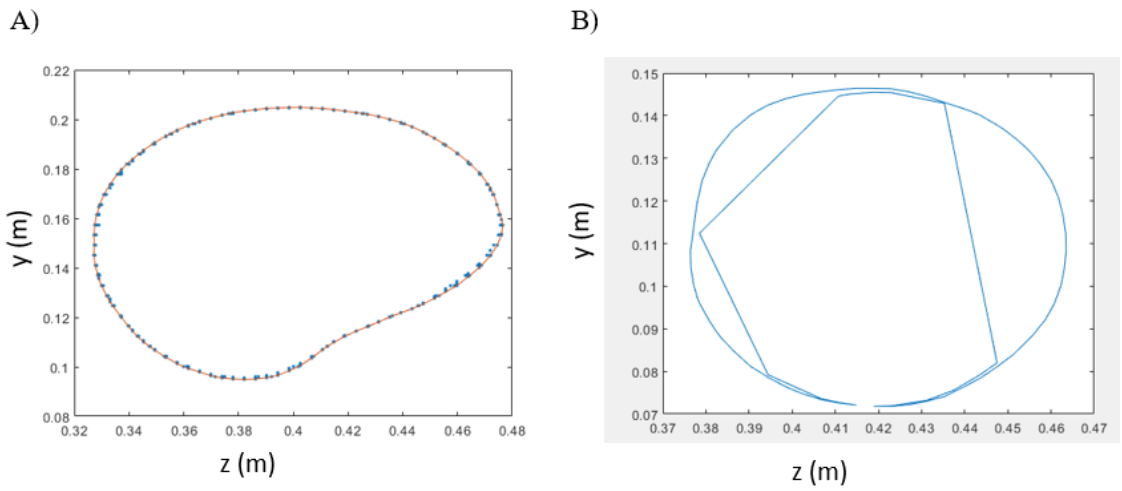

Figure 30 A) The image represents a one cm thick segment of the arm composed of the vertices (blue dots) and a boundary that was fit to the vertices (red line). B) This image represents when the boundary fit was erratic.

Based on the boundary output, the perimeter was calculated by summing the distance between the points in the boundary output vector. The area was then calculated using the polyarea function in Matlab, which returns the area of a polygon that was specified by the vertices. Lastly, circularity was calculated based on Equation 5, where a circularity value of 1 represents a perfect circle.

$$circularity = \frac{perimeter^2}{4 \times \pi \times area}$$

Equation 5 Circularity equation

When calculating volume clinically, circumferences are measured at 4 cm intervals, which segment the arm into a number of slices equal to the arm length divided by 4 cm. This Structure sensor provides point cloud coordinates to the tenth of a millimeter. Volume calculations used the disc method, which multiplies the area of each slice by the slice

thickness to calculate the slice volume. These slices were summed to compute the total volume.

Traditional slice thickness is 4cm, but this system is capable of calculating volume with thinner slices. Therefore, I calculated volume at various slice thickness for every arm to determine which thickness is optimal for volume calculations. As the slices became thinner, fewer data points from the arm scan were available for the area calculation, and thus set a limitation to how thin the slices could be. The slice thicknesses ranged from 0.05 cm to 10cm. The correlation coefficient was calculated for each paired slice thickness, and the results are summarized in the volume correlation matrix in Table 7. Then, it was determined that 1 cm provided the best balance between the number of data points per slice and the number of slices at fine enough intervals.

Table 7 Correlation Matrix that represents the correlation coefficients of the arm volumes calculated based on various slice thicknesses

Thickness (m)	0.0005	0.0010	0.0050	0.0100	0.0200	0.0300	0.0400	0.0500	0.0800	0.1000
0.0005	1									
0.0010	0.9981	1								
0.0050	0.8102	0.8006	1							
0.0100	0.5260	0.5076	0.8949	1						
0.0200	0.5859	0.5680	0.9245	0.9910	1					
0.0300	0.5738	0.5560	0.9189	0.9917	0.9972	1				
0.0400	0.5801	0.5631	0.9217	0.9898	0.9961	0.9961	1			
0.0500	0.5719	0.5585	0.9150	0.9864	0.9923	0.9924	0.9921	1		
0.0800	0.5866	0.5715	0.9212	0.9811	0.9884	0.9894	0.9901	0.9881	1	
0.1000	0.5809	0.5657	0.9158	0.9809	0.9879	0.9896	0.9897	0.9873	0.9923	1

To gain a better understanding how different regions of the arm may differ, ratios of the perimeters and ratios of the circularities were calculated. In order to do so, the 3D point cloud of the arm was segmented into six equal regions similar to the region shown in

Figure 29A, resulting in seven locations (represented by the red, vertical lines) where a 1cm slice was taken and compared to other slices that are more distal (closer to the wrist).

Additionally, arm length was calculated by taking the difference of the x-coordinates at the shoulder and wrist. This measurement was used then to calculate an average cross-sectional area for each arm by dividing the arm volume by the arm length. This measurement can provide a sense of body mass index. For a patient of a specific height, arm length is within some range that is proportionate to the patient's height. Therefore, as the volume of the arm for a specified arm length, it can be assumed that the patient has a larger body mass.

Lastly, the shape diameter function (SDF) was computed based on cones of 120° for each vertex. SDF provided a relationship between the arm volume with its surface boundary.[108] The cone was centered in the inward normal direction at each vertex, and ray are sent within the boundaries of the cone to the other side of the arm. The SDF was calculated to be the weighted average of the lengths of the rays that was within one standard deviation of the median of all lengths. The unimodal statistical measurements were calculated for all the SDF values for an arm scan.

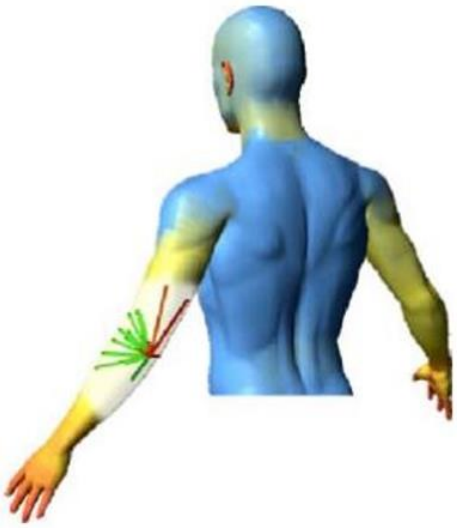

Figure 31 Visual representation of a cone of rays. Images are courtesy of Lior Shapira *et al.* (2008).

The naming nomenclature of the features took the base features (i.e. perimeter, circumference, etc.) and appended the statistical analysis (i.e. average, range, etc.). If there were specific parts of the arms that were compared, then those were appended to the feature name. For the perimeter and circularity ratios, the seven slices were named 1 through 7 with slice 1 corresponding to the first slice starting at the wrist and slice 7 corresponding to the last slice closest to the shoulder. The ratios were calculated so the perimeter or circularity of a slice closer to the shoulder is divided by the slice closer to the wrist. Thus, a perimeter ratio of "2to1" would mean slice 2 was divided by slice 1 and named "periRatio_2to1". For the regions, the six segments were numbered 1 through 6 starting from the wrist (Figure 29A). The top and bottom halves were noted as "T" or "B", respectively. The front, mid, and back thirds would be appended to the end. As an example, the front third of the bottom half of region 1 of the gaussian curvature feature would be denoted as "curvature_gaussian_RB1front".

4.2.3.3 Feature Development for Patient

In addition to developing the feature vector for the individual arms, features were developed for the patient. The difference between the arms for each feature was calculated. The specific differences depended on how the patients were classified. Two approaches were taken. I developed a model for two-classes where I defined the dataset into two labels, lymphedema and non-lymphedema. A three-class model was developed where the dataset was divided into three labels: right lymphedema, left lymphedema, and non-lymphedema. For two classes, the difference of each feature was taken between the larger volume arm and the smaller volume arm, denoted by appending "DiffLS" to the end of the feature name. For three classes, the difference of each feature was calculated between the right arm and the left arm, denoted by appending "DiffRL" to the end of the feature name.

To properly compare features of the right and left arm, the arms should be equal in length in order to be able to compare measurements such as volume between the two arms. A longer arm may artificially skew features for that arm, and when comparing it with the contralateral may exacerbate or reduce the differences seen between the arms. Therefore, these arms are matched in length for the feature development process for patient level models. Specifically, for the volume feature, the arm lengths of the right and left were matched to the shorter arm and the volume was recalculated for the arm that was shortened.

4.2.4 Classification model

Models were developed to either classify the patient or the arms. To classify patients, two approaches were taken. First, two classes were assumed: the patient either was healthy or had lymphedema. The second approach assumed three classes that

delineated which arm had lymphedema, resulting in the following classifications: lymphedema in the left arm, lymphedema in the right arm, and no lymphedema. With both approaches to patient classification, it was assumed that there were no bilateral lymphedema cases, which is true for this dataset. Only women at risk for unilateral lymphedema or with only unilateral lymphedema were recruited to participate in this study. To classify arms, two classifications were possible: healthy or lymphedema. This method was implemented because with a patient classification approach, bilateral lymphedema cases are missed as a result of both arms undergoing changes. Therefore, if a model could classify arms individually without needing to compare to the other arm, then this subset of lymphedema patients could be identified. These models were tested and evaluated for their ability to classify correctly.

The dataset was divided into a training set and testing set. The training dataset was chosen by using a random number generator with a uniform distribution to identify the arms or patients that would be used, and the remaining arms or patients became the testing dataset. It is important to note that for this split, the rate of lymphedema was maintained in the training and testing sets. For the arm classification, this split was 25% / 75% for training and testing. For the two-class patient classification, the split was also 25% / 75% for training and testing. Lastly, for the three-class patient classification, the split was 50% / 50% for training and testing.

4.2.4.1 Feature Selection

The features were reduced based on running a statistical test on the difference groups. A t-test was performed for datasets of two classifications, and the Kruskal-Wallis

test was performed for datasets of three classifications. This step of the analysis was performed solely on the training set to ensure that the testing set data did not inform the features selected. The alpha threshold was set to 0.10 so any feature with a p-value less than alpha was kept and used within the training dataset.

4.2.4.2 Training Model and Evaluation

Using Matlab, the training dataset was passed through various standard machine learning algorithms with a 5-fold cross validation. This cross validation means that the training set was partitioned into five randomly chosen subsets of approximately equal size. One subset was used to validate the model that was trained by the remaining four subsets per round. This validation was done for each of the five subsets for a total of five rounds as illustrated in Figure 32. The average of the errors of each round was minimized to calculate the parameters of each feature for the final model.

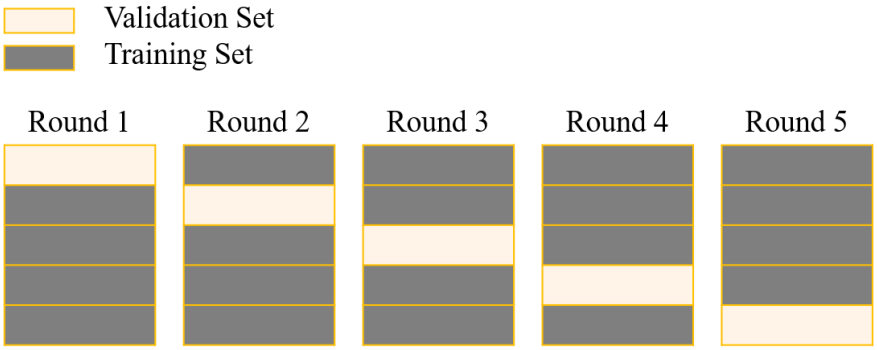

Figure 32 Five-fold cross validation illustration

The performance of the trained model was assessed, and the most promising models were tested with the testing dataset. Two metrics used to evaluate the potential trained models to test were sensitivity and specificity. Sensitivity is the true positive rate or the

number of lymphedema cases correctly identified by the model over the total number of actual lymphedema cases. Specificity is the true negative rate or the number of healthy cases correctly identified by the model over the total number of actual healthy cases. While both of these are important, sensitivity is more important as the goal is to be able to identify the lymphedema cases for referral to a lymphedema specialist, who can diagnose and treat lymphedema onset. Even though specificity was a secondary metric when evaluating the model, it was not completely sacrificed because that would be no better than clinically assuming everyone would develop lymphedema, which is not the case. Accuracy, which is the rate of correctly identified healthy and lymphedema cases, was calculated when evaluating trained models, but the metric can be misleading since lymphedema occurs at a rate lower than 50%. Therefore, accuracy was also a secondary metric used to evaluate the trained model.

In order to test the classification, the testing set was inputted into the trained models and the outcomes were evaluated based on the sensitivity, specificity, and accuracy. As a benchmark, the sensitivity, specificity, and accuracy of the clinical metrics, volume difference and percent volume difference were calculated and assumed as the gold standard. Once the models were evaluated, the features that were used to train the well-performing models were aggregated.

4.3 Results

One hundred (100) female patients participated in the study at various time points post breast cancer treatment. While the majority of women did not have lymphedema, the thirty-six (36) women who did have lymphedema had unilateral presentation of

lymphedema and had been undergoing therapy to treat the swelling. The thirty-six (36) lymphedema cases contained twenty-six (26) patients who had swelling in the left arm and ten (10) who had swelling in the right arm. These characteristics can be found summarized in Table 8.

Table 8 TurningPoint participant characteristics (n=100)

Gender	***Count (%)***
Male	0 (0)
Female	100 (100)
BCRL	***Count (%)***
Clinical	36 (36)
Left	26 (26)
Right	10 (10)
200 mL difference	21 (21)
10% volume difference	12 (12)

As described earlier, there are two criteria used with arm volumes to determine lymphedema. One of the standard methods of measurement for lymphedema detection is the absolute value of the volume difference between the two arms that is greater than 200mL. For this dataset, the performance of this metric resulted in an accuracy level of 67%. The sensitivity rate is 33%, and specificity rate is 86%. An analysis of how accuracy, sensitivity, and specificity change as the critical value threshold changes is summarized in Table 9 and Figure 33. As sensitivity improves, specificity and accuracy rates decline. For a sensitivity rate of 50% on this dataset, the critical threshold for volume difference would need to be set at 100mL. This threshold also results in a specificity rate of 50% and accuracy rate of 50%.

Table 9 Critical values for Volume Difference of arms to classify lymphedema

Critical value (mL)	200	150	100	75	50
Sensitivity (%)	33.3	36.1	50	66.7	77.8
Specificity (%)	85.9	68.8	50	35.9	28.1
Accuracy (%)	67	57	50	47	46

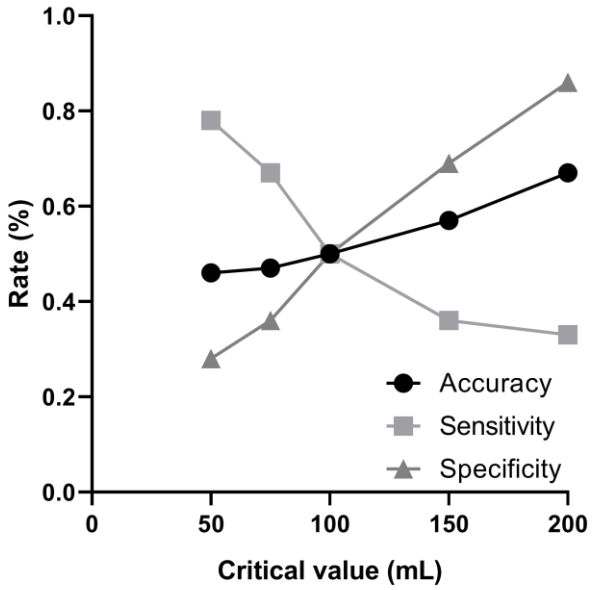

Figure 33 Critical threshold value for volume difference (larger arm – smaller arm) and the resulting accuracy, sensitivity, and specificity rates as the result.

The other standard methods of measurement for lymphedema detection is the absolute value of the percent volume difference between the two arms of greater than 10%. Percent difference was calculated based on the difference of the larger and smaller volumes, which are then divided by the smaller arm's volume. For this dataset, the performance of this metric resulted in an accuracy level of 68%. The sensitivity rate is 27.8%, and specificity rate is 90.6%. An analysis of how accuracy, sensitivity, and specificity change as the critical value threshold changes is summarized in Table 10 and

Figure 34. Again, as sensitivity improves, specificity and accuracy rates decline. For a sensitivity rate of 58.3% on this dataset, the critical threshold for percent volume difference would need to be set at 3%, which is below the error associated with many volume measurement approaches. This threshold also results in a specificity rate of 28.1% and accuracy rate of 42%. These clinical standards were used as the gold standard to compare against the models developed.

Table 10 Critical values (sensitivity, specificity, and accuracy rates) for Percent Volume Difference for lymphedema classification

Critical value (%)	10	9	8	7	6	5	4	3	2
Sensitivity (%)	27.8	27.8	30.6	38.9	41.7	41.7	41.7	58.3	75.0
Specificity (%)	90.6	87.5	82.8	71.9	65.6	56.3	43.8	32.8	28.1
Accuracy (%)	68.0	66.0	64.0	60.0	57.0	51.0	43.0	42.0	45.0

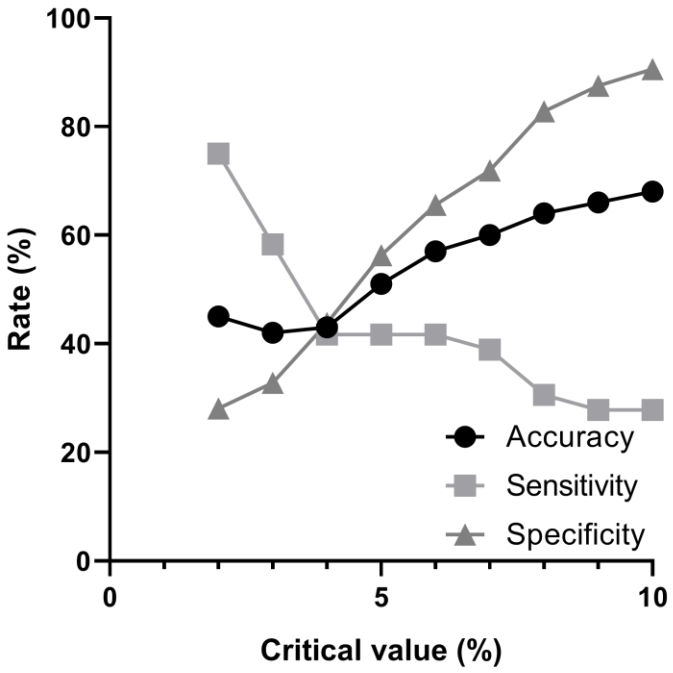

Figure 34 Critical value for percent volume difference for classifying lymphedema. Percent different was calculated to be the difference of the larger volume arm minus the smaller volume arm, divided by the smaller volume arm.

4.3.1 Feature Development

4.3.1.1 Data Segmentation

When the scans were filtered to ensure that only the arm from the shoulder to the wrist were kept, the wrist was manually identified. The three wrist identifications were analysed to determine its consistency. The average standard deviation of the three identifications for all the scans was 0.44cm. Seventy-two (72) scans had the same x-coordinate identified as the wrist point for all three attempts. One hundred eleven (111) scans had two unique x-coordinates identified as the wrist. Seventeen (17) scans had three unique x-coordinates identified as the wrist. The maximum range of x-coordinates when manually identified was 3 cm, which occurred for two scans. For twenty-five (25) scans,

the range was 2cm. There was a 1cm range for 101 scans. These ranges are summarized in Table 11.

Table 11 Ranges of the x-coordinate deviation from manual identification of the wrist

Range (cm)	**0**	**1**	**2**	**3**
# scans	72	101	25	2

4.3.1.2 Features for Patient Classification

When the right and left arm lengths were compared, small differences in length were found. Most patients in this study had arm lengths that varied less than 4cm between the two arms with the majority having a difference less than or equal to 2cm (Figure 35). This finding aligned with what clinicians have found anecdotally when measuring arms via the tape measurement method, measuring every 4cm; clinicians would measure one arm of a patient 4cm longer than the other and would calculate volumes for both arms based on the shorter arm length. The same approach was taken in this study when calculating volume differences for a patient.

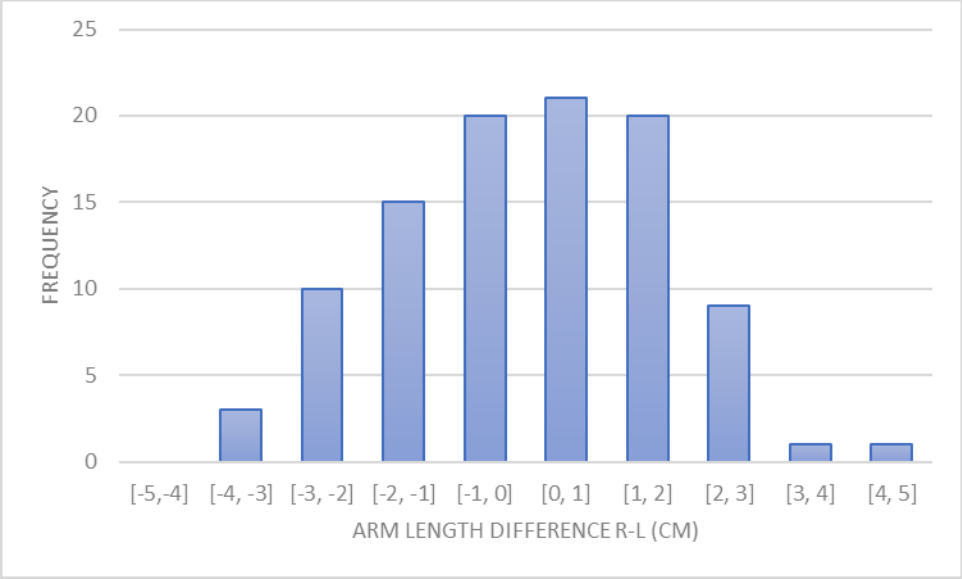

Figure 35 Arm length differences (right-left) indicates the majority of patients in this study had arms of similar length, with most falling within 4 centimeters of each other.

4.3.2 Model Results

The clinical metrics of volume difference and percent volume difference for detecting lymphedema were used to calculate how well it would be able to identify healthy and lymphedema cases. These outcomes were used as a baseline for the evaluations of the trained models. Volume difference between the right and left arm had a sensitivity of 38.9%, specificity of 89.1%, and an accuracy of 71%. Meanwhile, percent volume difference between the right and left arm resulted in a sensitivity of 27.8%, specificity of 96.9%, and an accuracy of 72%.

4.3.2.1 Features for Patient Classification

During the feature selection process of the three-class model, seventeen (17) features have p-values less than the alpha threshold. The features and its p-values are listed

in Table 13. Of all the trained models, the best performing was the trained quadratic discriminant model, which resulted in a sensitivity of 61%, specificity of 78%, and an accuracy of 72% (Figure 36). The complete list of trained models and tested models can be found in the appendix in Table 14 and Table 15, respectively. Interestingly, when the quadratic discriminant model was trained with the same set of features listed in Table 13 but removing Volume_diffRL, the test dataset performance improved slightly. The sensitivity maintained at 61%, but specificity improved to 84% and accuracy improved to 76%.

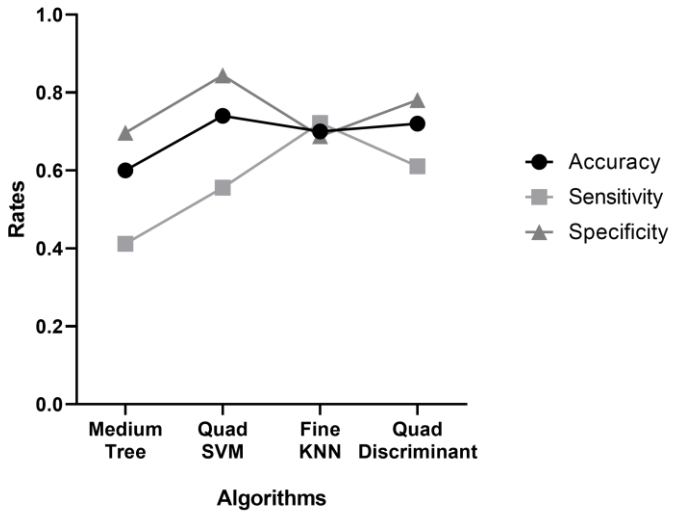

Figure 36 Evaluation of performance of trained model to classify patients based on 3 classes

I developed two models for identifying patients, one with two-classes and the second with three-classes. During the feature selection process of the two-class model, three features have p-values less than the alpha threshold. These features and their p-values are outlined in Table 16. Of all the trained models, the best performing was the trained medium tree model, which resulted in a sensitivity of 44%, specificity of 73%, and an

accuracy of 63% (Figure 37). The complete list of trained models and tested models can be found in the appendix in Table 17 and Table 18, respectively.

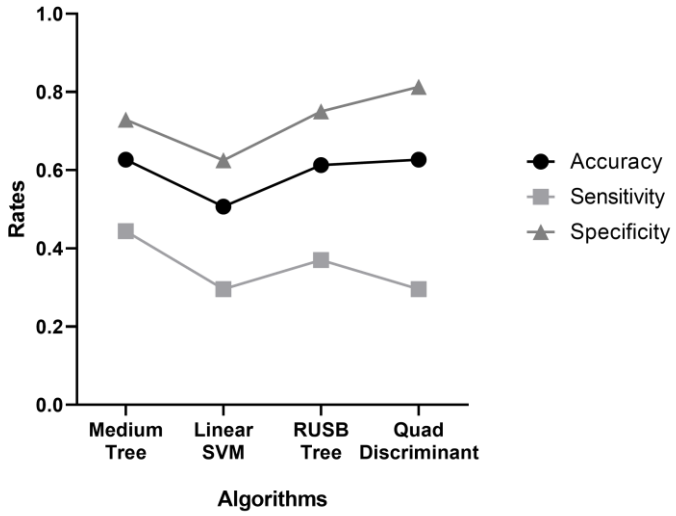

Figure 37 Evaluation of performance of trained model to classify patients based on 2 classes

4.3.2.2 Features for Arm Classification

During the feature selection process, twenty (20) features have p-values less than the alpha threshold. The features and p-values can be found in Table 19. Of all the trained models, the best performing was the trained RUSBoost tree model, which resulted in a sensitivity of 52%, specificity of 72%, and an accuracy of 69% (Figure 38). The complete list of trained models and tested models can be found in the appendix in Table 20 and Table 21, respectively. Interestingly, when the RUSBoosted Tree model was trained with the same set of features listed in Table 19 but removing Volume, the test dataset performance improved slightly. The sensitivity increased to 55.6%, but specificity decreased to 66.7% and accuracy decreased to 64.7%.

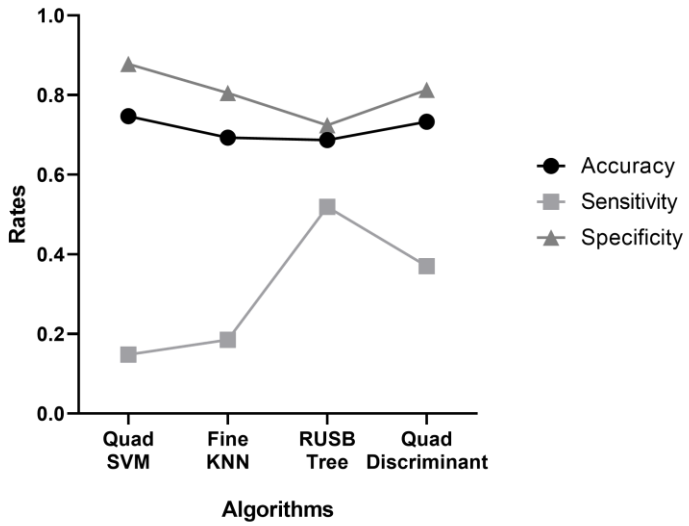

Figure 38 Evaluation of performance of trained models for arm classification

4.4 Discussion and Conclusion

Currently, clinics specialized in lymphedema diagnosis and treatment use many inputs to diagnose lymphedema. The greater challenge is ensuring that at risk patients are being referred to these clinics prior to lymphedema development. Despite the many techniques available to detect and monitor lymphedema, surveillance of patients at risk of developing lymphedema is poor. There is a need for a system that can be easily implemented in clinics that can help clinicians refer patients to specialized lymphedema clinics without large financial investments and with minimal training to know when to refer patients. Utilizing technological advances, more information can be collected and analyzed to develop new metrics to use to detect lymphedema. It is currently known that using volumetric measurements and their derivatives is a limiting factor of when lymphedema can be detected.[55,109,110] This study developed and explored novel metrics as potential additions to volume that were created from a 3D scan of the arm. I was able to identify

some interesting metrics that have aided in a trained model's ability to differentiate subtle differences between a healthy and a lymphedema case.

This study showed that for this sample of patients, using volume difference alone resulted in poor sensitivity (33.3%), meaning many lymphedema patients were not classified as lymphedema patients based on this measurement. This low volume difference in arm volumes is representative of early stage lymphedema patients. This model was able to detect lymphedema patients at a much higher sensitivity (61%), and overall accuracy improved, albeit the sensitivity dropped approximately 5%. For the volume difference measurement to match the model's sensitivity, the threshold would need to be reduced, which would also reduce accuracy and specificity. Specifically, to achieve a comparable sensitivity of 60%, the threshold needed for this data set would be around an 80 mL difference in volume, which would drop specificity below 40%.

Similarly, the threshold for percent volume difference would need to be set at 3% for lymphedema detection, but sensitivity would drop to less than 33%. In comparison, this model performance was stronger with a specificity of 78% when the model sensitivity was 60%. Further steps need to be taken to test the applicability of this model on patients immediately following cancer therapy, but prior to lymphedema detection, to assess if these classification algorithms would have a similar efficacy when compared to patients from this cohort, who were already diagnosed and are being actively treated for lymphedema. Simplifying the model to two classes did not improve the ability to detect lymphedema as shown in Figure 37.

The features that were used to train the patient 3-class model represented various local shapes of the arm. The average, median, and standard deviation of the perimeters and areas of each 1cm slice of the right and left arms describe how normal the distribution of the arm slices are. Additionally, the ratio of the perimeters of specific regions of along the length of the arm indicates that the relative size of the arm along the arm is different between lymphedema patients and non-lymphedema patients. Furthermore, the ratio of circularity of specific regions along the arm shows that swelling among lymphedema patients is different than the ratios on non-lymphedema patient arms. The mean, median, and lambda parameter to describe the inverse Gaussian distribution of vertex curvature continued to suggest that the arm shape differs when the arm is undergoing lymphedema onset.

In conjunction with these local geometry-derived features, volume difference was a feature that passed through the feature filtering step. Interestingly, removing this single feature did not negatively impact the sensitivity of the trained model and even improved specificity, which indicated that volume difference as a feature had little weight in the trained model. Meanwhile, the average cross-sectional area of the arm as a feature to train the model could mean that the overall body mass of the patient is implicated in lymphedema detection.

When the features were filtered for the training of the patient 2-class model, three features were identified, which were forearm angle, the standard deviation of the normal x-coordinates, and the arm length. None of these features were filtered in the patient 3-class model and the lower performance of the patient 2-class model indicated that these features are less important for the detection of arm lymphedema.

The features that were filtered to train the arm model had many that overlapped with the features used to train the well-performing patient 3-class model except no difference between the right and left arms were taken. These features were descriptive of the shape of the arm like perimeter, area, circularity, and curvature but also included the vertices' normals, which could potentially explain the poorer sensitivity rates that the arm classification model resulted in when testing on the testing set.

While the arm classification model did not perform as well as the patient 3-class model, I explored the ability to classify individual arms, because patient classification is primarily beneficial for unilateral cases. Therefore, the subset of lymphedema patients who have bilateral manifestation of lymphedema are difficult to detect and diagnose. It is important to note that none of the patients in this cohort had bilateral lymphedema. There are currently no methods to classify bilateral lymphedema outside of the clinical centers with specialized lymphedema expertise. This study was the first to show some ability to detect lymphedema among arms, without requiring the paired arm to serve as a reference, but that model was not able to perform at the same level as the patient classification model as indicated by the sensitivity and specific.

To appropriately determine the efficacy to detect and diagnose lymphedema with the Structure sensor, a rich dataset of long-term scans of patients from pre-treatment to periodic post-treatment for two to five years is needed. Such an ideal dataset does not exist as this scanning device is new on the market. Fortunately, I could collect scans of patients ranging in time post-treatment and in physical therapy progress. Patients with lymphedema are undergoing active therapy for their arm. Thus, the traditional volume difference is unable to identify the difference between a lymphedema arm and a healthy arm.

Through this aim, I explored the capacity of using the local geometries of an arm to identify lymphedema among female breast cancer survivors who are undergoing therapy as a result of the cancer treatment and/or for lymphedema. The Structure system was used to collect high resolution 3D scans of the patient arms and custom codes were developed to engineer features based on these scans. These features were used to train classification algorithms, and the most promising models were tested. Outcomes were evaluated to determine the performance of the models on the testing dataset. The features used to train the well-performing models show that these local features together can detect lymphedema and provide a foundation for features to further explore to determine if it has the capability to detect this disease earlier on in its progression. Rather than waiting for the arm to swell to a critical threshold, changes in these features that represent local geometries in well-performing models could be an earlier indicator to watch for in the clinical setting.

CHAPTER 5. CONCLUSION AND FUTURE DIRECTIONS

5.1 Summary

The implementation of an infrared sensor system as a substitute for lymphedema detection and monitoring is critical and a useful system for the lymphedema field. The systems used in this dissertation showed potential as a replacement for methods currently used in the clinics, tape measure circumferential measurements and the Perometer. These studies were one of the first that I am aware of where the system was implemented in clinics and performed by clinicians. I demonstrated that the Kinect system correlated and agreed well with the Perometer, which studies have shown to be a reliable tool limb measurement for volume. Because clinicians were successfully acquiring scans, it showed promise in its integration in the clinical space. Additionally, I determined a method of assessing change in volume for patients with a unilateral risk for lymphedema development.

In the second aim, an updated iteration of the infrared sensor system was implemented. Studies have shown its accuracy and reliability compared to clinical measurement standards.[111,112] I was able to focus on the potential applications of acquiring a true 3D scan of the arms. Specifically, I explored whether there are other metrics to use aside from volume to detect lymphedema. Rather than looking at the arm on global scale, I developed measurements that represent the local features of the arm that may manifest differently between healthy arms and lymphedema arms. I showed that using local features improves the ability to classify an arm as either healthy or lymphedematous compared to the gold standard of arm volume and its variant measurements like volume difference or percent difference in volume between the affected and unaffected arm. I believe that the

most exciting finding is to be able to identify arms as healthy or lymphedematous at an improved rate compared to the ability to detect whether a patient has lymphedema. This ability opens opportunities to detect bilateral lymphedema, which is an underserved demographic within an already underserved disease – lymphedema. While there is more work to determine the predictive value of these local measurements, it is a fundamental step towards lymphedema detection and with the right set of scans, the validity of the metrics determined in this dissertation can be assessed along with its predictive capabilities.

5.2 Limitations

There are several limitations in this work that can provide more validation regarding the implementation of infrared systems in the clinic and what metrics can be used in the detection and monitoring of lymphedema. First and foremost, given the time constraints and the lack of a dataset already available, the datasets collected for each study in this body of work were limited. The longitudinal dataset in aim 1B did not extend far enough post-operatively. Therefore, the incidence rates of lymphedema in the study was much lower than what is found in the breast cancer survivor population. The datasets in aim 1A and in aim 2 did not have any longitudinal component. All patients were scanned at a single time point. While there was a healthy mix of lymphedema and non-lymphedema patients, the patients who had lymphedema were being actively treated for lymphedema and were at various stages of treatment.

Additionally, in the first aim of the dissertation, the Kinect IR system did not output a true 3D scan of the limbs of interest. To explore local metrics would have been difficult as a limb was represented in two or three scans for the arms and legs respectively. While

the studies showed the Kinect IR system was a good alternative to current clinical tools for measuring volume, in order to compare the volume output on the Kinect IR system with other tools, an offset would be required. While calculating volume can still be done with good correlation and agreement with the clinical standards, the extent of its applications in this field was limited. Additionally, the Kinect's commercial discontinuation would require an alternative infrared sensor for long-term implementation in the field.

The largest limitation of this work is the sets of scans that could be gathered and their sample sizes. Because an existing dataset did not exist, all the samples were collected over the course of this dissertation and the rate of consent was a limiting factor. Especially in Aim 1B, this study had the lowest rate of attrition to the study. Due to the rate of breast cancer diagnosis at Grady Memorial Hospital combined with the consent rate, the medical team and I had a difficult time recruiting participants. I believe that the study logistical set up requiring patients to move to a dedicated room while waiting to check out of their appointment hindered the attrition rate. In future studies with the updated Structure system, the scans can occur in the patient's room as a result of the portability of the system.

While this iteration overcomes the portability issue and can output a true 3D representation of the limb, the system relatively expensive to the most common volumetric measurement tool, the tape measure. The price is not known, but the cost of materials would be approximately $1,300.[87] I believe that despite its cost, the benefits and the time saved compared to the cheaper alternative, the tape measure, overcomes this financial obstacle.

5.3 Future Considerations

Based on the results and feedback through the studies in this work, the implementation of the Structure system is feasible and would be an impactful next step. The Structure sensor is more portable than its predecessor, which would remove the requirement for a dedicated space or room for the scan. Therefore, the integration of this system into the clinical workflow could be more seamless. The impact of this integration is two-fold. First, studies gathering these scans would likely have a better attrition rate as the patient would not be required to move to a dedicated room. Secondly, clinicians are likely to start collecting these scans for patients who are at risk of developing lymphedema. Studies have outlined the implications of performing prospective surveillance with the early detection of the disease leading to better quality of life and the reduction of healthcare cost associated with managing lymphedema, which can be thousands of dollars. [44,105,113,114]

As clinics adopt this technology, more data can be collected on patients who are at risk for developing lymphedema and longitudinal scans could be collected. In addition to these scans, clinician diagnosis of lymphedema would ideally be collected in parallel. Therefore, these scans can be used to evaluate the metrics developed in this work on its potential to identify lymphedema onset earlier on in its progression. More specifically, it could be determined at which point the metrics from the scans would classify an arm as having developed lymphedema compared to when the clinician would make this determination. The ideal long-term implementation would be for this system to be used by at risk patients at home so prospective monitoring could be more easily performed.

Overall, I believe that the impact of integrating infrared sensors can overcome some of the obstacles in the field of lymphedema and positively impact not only the lives of lymphedema patients but also those at risk for developing this disease.

APPENDIX A. MATLAB CODE

A.1 Aim 2 Code

A.1.1 TruncateArm.m

```
%% TRUNCATEARM.M
%% THIS FUNCTION TRUNCATES THE INITIAL SCAN .OBJ AT THE ARMPIT AND
WRIST IN PREPARATION FOR THE FEATURE EXTRACTION
%%Read in object
ID = [{'1001'} {'1002'} {'1003'} {'1004'} {'1005'} {'1006'} {'1007'}
{'1008'} {'1009'} {'1010'} {'1011'} {'1012'} {'1013'} {'1014'} {'1015'}
{'1016'} {'1017'} {'1018'} {'1019'} {'1020'} {'1021'} {'1022'} {'1023'}
{'1024'} {'1025'} {'1026'} {'1027'} {'1028'} {'1029'} {'1030'} {'1031'}
{'1032'} {'1033'} {'1034'} {'1035'} {'1036'} {'1037'} {'1038'} {'1039'}
{'1040'} {'1041'} {'1042'} {'1043'} {'1044'} {'1045'} {'1046'} {'1047'}
{'1048'} {'1049'} {'1050'} {'1051'} {'1052'} {'1053'} {'1054'} {'1055'}
{'1056'} {'1057'} {'1058'} {'1059'} {'1060'} {'1061'} {'1062'} {'1063'}
{'1064'} {'1065'} {'1066'} {'1067'} {'1068'} {'1069'} {'1070'} {'1071'}
{'1072'} {'1073'} {'1074'} {'1075'} {'1076'} {'1077'} {'1078'} {'1079'}
{'1080'} {'1081'} {'1082'} {'1083'} {'1084'} {'1085'} {'1086'} {'1087'}
{'1088'} {'1089'} {'1090'} {'1091'} {'1092'} {'1093'} {'1094'} {'1095'}
{'1096'} {'1097'} {'1098'} {'1099'} {'1100'}];

path='C:\Users\ilu3\Dropbox (GaTech)\ME-DboxMgmt-Dixon-Brandon\Turning
Point (H15203)\Structure scans (Summer 2018)\';

filetype='.obj';
side = 'right'; % or 'left';

WristXcoords=xlsread('C:\Users\ilu3\Dropbox (GaTech)\ME-DboxMgmt-Dixon-
Brandon\Turning Point (H15203)\Structure scans (Summer
2018)\WristXcoord_final.xlsx','WristX_Coordinates','B7:GS7');

for i=1:length(ID)
    fn=[path ID{i} side filetype];
    obj=readObj(fn);
    %obj x is length of arm, y is height, z is depth front to back

    objSort = sortrows(obj.v,[1 -2 -3]);
    %sort points in descending order based on x values then y then z
    middleFinger=objSort(1,:);

    %% remove trunk
    % rotate the object
    theta = 1*(pi/3+pi/2); % rotation angle
    transmatrix = [cos(theta),sin(theta),0,0; - ...
        sin(theta),cos(theta),0,0;0,0,1,0;0,0,0,1];
    transformation = affine3d(transmatrix);
    ptCloud = pointCloud(obj.v,'Normal',obj.vn);
    ptCloudOut = pctransform(ptCloud, transformation);
```

```
data_all=ptCloudOut.Location; %pull data location points

[r c]=size(data_all);
ind=rot90(1:r,3);
data_all_origInd=[data_all, ind];

%% Aligning x-coordinates
dataAlign=horzcat(round(data_all_origInd(:,1),2),...
     data_all_origInd(:,2:end));
     %move points to nearest cm in x direction
dataRotate4 = sortrows(dataAlign,[1 -2 -3]);
%sort points in descending order based on x values then y then z

origInd=dataRotate4(:,4);
dataRotate=dataRotate4(:,1:3);

armX=unique(dataRotate(:,1)); %find all unique x coordinates
armX=sort(armX,'ascend');
armLowerBound = zeros(length(armX),3);

for n = 1:length(armX)
    tempArm = find(dataRotate(:,1) == armX(n));
    armLowerBound(n,:) = dataRotate(tempArm(end),:);
end

[m,inde] = max(armLowerBound(:,2));
armArmPit = armLowerBound(inde,:);
ArmandPit=[dataRotate;armArmPit];
ArmandPitPtCloud = pointCloud(ArmandPit);

% Truncate
index = ArmandPitPtCloud.Location(1:end - ...
     1,1)>=ArmandPitPtCloud.Location(end,1);
ArmRot=ArmandPitPtCloud.Location(index,:);
ArmRotPtCloud = pointCloud(ArmRot);
% Rotate the point cloud back
theta=-theta;
transmatrix = [cos(theta),sin(theta),0,0; - ...
     sin(theta),cos(theta),0,0;0,0,1,0;0,0,0,1];
     %update to rotate back
transformation = affine3d(transmatrix);
ArmPtCloudOut = pctransform(ArmRotPtCloud,transformation);
% performs operation on point cloud
PitCloudOut = pctransform(ArmandPitPtCloud,transformation);

rotatedArmPit=PitCloudOut.Location(end,:);
order=[index origInd];
sortedorder=sortrows(order,2);
logic=logical(sortedorder(:,1));

ArmPtCloudOut2=obj.v(logic,:);
ArmPtCloudNorm=obj.vn(logic,:);
ArmIndex2=ArmPtCloudOut2(:,1)<=(rotatedArmPit(1,1)-.01);

Arm2=ArmPtCloudOut2(ArmIndex2,:);
```

```
    ArmNorm2=ArmPtCloudNorm(ArmIndex2,:);
    ArmPtCloudIL2 = pointCloud(Arm2,'Normal',ArmNorm2);
    dataAlignXYZ=horzcat(round(ArmPtCloudIL2.Location(:,1),2), ...
         ArmPtCloudIL2.Location(:,2:3));
         %move points to nearest cm in x direction

    %% Identify wrist manually
    % [RWristX,~] = ginput(1);
    % RWristX = round(RWristX,2);

    %% Identify wrist with final x-coordinate from FinalWristX.m
    if strcmp(side, 'left') == 1
        WristX = WristXcoords(i);
    elseif strcmp(side, 'right') == 1
        WristX = WristXcoords(i+100);
    end

    %% Removing hand
    objXYZ_Align = dataAlignXYZ;
    objInd_Align = objXYZ_Align(:,1)>=WristX;
    objXYZ_Align = objXYZ_Align(objInd_Align,:); %truncated the hand
    objNorm_Align = ArmPtCloudIL2.Normal(objInd_Align,:);
    %truncate normals associated with hand
    object_Align = pointCloud(objXYZ_Align,'Normal',objNorm_Align);
    %create pointCloud type with normals

    % non aligned objXYZ
    objXYZ_nonAlign_Index = ArmPtCloudIL2.Location(:,1)>=WristX;
    objXYZ_nonAlign = ArmPtCloudIL2.Location(objXYZ_nonAlign_Index,:);
    objNorm_nonAlign = ArmPtCloudIL2.Normal(objXYZ_nonAlign_Index,:);
    object_nonAlign = ...
         pointCloud(objXYZ_nonAlign,'Normal',objNorm_nonAlign);

    % Save arm point cloud
    vs = 'final';

    % Save .mat file
    mat_fn = [path vs '\' ID{i} side vs '.mat'];
    save(mat_fn)
end
```

A.1.2 FeatureExtraction.m

```
%% FEATUREEXTRACTION.M
%% THIS FUNCTION EXTRACTS FEATURES FROM TRUNCATED ARMS
path = 'C:\Users\ilu3\Dropbox (GaTech)\ME-DboxMgmt-Dixon-
Brandon\Turning Point (H15203)\Structure scans (Summer 2018)\';

ID = [{'1001'} {'1002'} {'1003'} {'1004'} {'1005'} {'1006'} ...
      {'1007'} {'1008'} {'1009'} {'1010'} {'1011'} {'1012'} ...
      {'1013'} {'1014'} {'1015'} {'1016'} {'1017'} {'1018'} ...
      {'1019'} {'1020'} {'1021'} {'1022'} {'1023'} {'1024'} ...
      {'1025'} {'1026'} {'1027'} {'1028'} {'1029'} {'1030'} ...
```

```
      {'1031'} {'1032'} {'1033'} {'1034'} {'1035'} {'1036'} ...
      {'1037'} {'1038'} {'1039'} {'1040'} {'1041'} {'1042'} ...
      {'1043'} {'1044'} {'1045'} {'1046'} {'1047'} {'1048'} ...
      {'1049'} {'1050'} {'1051'} {'1052'} {'1053'} {'1054'} ...
      {'1055'} {'1056'} {'1057'} {'1058'} {'1059'} {'1060'} ...
      {'1061'} {'1062'} {'1063'} {'1064'} {'1065'} {'1066'} ...
      {'1067'} {'1068'} {'1069'} {'1070'} {'1071'} {'1072'} ...
      {'1073'} {'1074'} {'1075'} {'1076'} {'1077'} {'1078'} ...
      {'1079'} {'1080'} {'1081'} {'1082'} {'1083'} {'1084'} ...
      {'1085'} {'1086'} {'1087'} {'1088'} {'1089'} {'1090'} ...
      {'1091'} {'1092'} {'1093'} {'1094'} {'1095'} {'1096'} ...
      {'1097'} {'1098'} {'1099'} {'1100'}];
len_IDnums = length(ID);

vs = 'final';
filetype = '.mat';

%% load lymphedema outcomes
outcomes_fn='C:\Users\ilu3\Dropbox (GaTech)\ME-DboxMgmt-Dixon-
Brandon\Turning Point (H15203)\Structure scans (Summer
2018)\LEOutcomes.xlsx';
[num text raw] = xlsread(outcomes_fn);
outcomes=raw;

%% initialize the features output
titles = [{'titles'}];
% % angles=[{'angles'}];              % forearm angle
anglexy=[{'angle_xy'}];
anglexz=[{'angle_xz'}];
normals=[{'normals_XYZ'}];            % normals of arm points from scan
normalx=[{'normalx'}];
normalx_avg = [{'normalx_avg'}];
normalx_med = [{'normalx_med'}];
normalx_std = [{'normalx_std'}];
normalx_range = [{'normalx_range'}];
normalx_kurt = [{'normalx_kurt'}];
normalx_skew = [{'normalx_skew'}];
normaly=[{'normaly'}];
normaly_avg = [{'normaly_avg'}];
normaly_med = [{'normaly_med'}];
normaly_std = [{'normaly_std'}];
normaly_range = [{'normaly_range'}];
normaly_kurt = [{'normaly_kurt'}];
normaly_skew = [{'normaly_skew'}];
normaly_alpha = [{'normaly_alpha'}];
normaly_beta = [{'normaly_beta'}];
normalz=[{'normalz'}];
normalz_avg = [{'normalz_avg'}];
normalz_med = [{'normalz_med'}];
normalz_std = [{'normalz_std'}];
normalz_range = [{'normalz_range'}];
normalz_kurt = [{'normalz_kurt'}];
normalz_skew = [{'normalz_skew'}];
normalz_alpha = [{'normalz_alpha'}];
normalz_beta = [{'normalz_beta'}];
circularities=[{'circularity'}];          % circularity
```

```
circularities_ratio=[{'circularity_ratio_shouldertowrist'}];
circularities_avg=[{'circularities_avg'}];
circularities_med=[{'circularities_med'}];
circularities_std=[{'circularities_std'}];
circularities_range = [{'circularities_range'}];
circularities_kurt=[{'circularities_kurt'}];
circularities_skew=[{'circularities_skew'}];
perimeters=[{'perimeter'}];                    % cross section perimeters
perimeters_ratio = [{'perimeter_ratio_shouldertowrist'}];
perimeters_avg = [{'perimeters_avg'}];
perimeters_med = [{'perimeters_med'}];
perimeters_std = [{'perimeters_std'}];
perimeters_range = [{'perimeters_range'}];
perimeters_kurt = [{'perimeters_kurt'}];
perimeters_skew = [{'perimeters_skew'}];
areas=[{'areas'}];                             % areas
area_avg = [{'area_avg'}];
area_med = [{'area_med'}];
area_std = [{'area_std'}];
area_range = [{'area_range'}];
area_kurt = [{'area_kurt'}];
area_skew = [{'area_skew'}];
volumes_disc = [{'volumes_disc'}];
titles_circ = [{'circRatio_2to1'}, {'circRatio_3to1'}, ...
    {'circRatio_4to1'}, {'circRatio_5to1'}, {'circRatio_6to1'}, ...
    {'circRatio_7to1'}, {'circRatio_3to2'}, {'circRatio_4to2'}, ...
    {'circRatio_5to2'}, {'circRatio_6to2'}, {'circRatio_7to2'}, ...
    {'circRatio_4to3'}, {'circRatio_5to3'}, {'circRatio_6to3'}, ...
    {'circRatio_7to3'}, {'circRatio_5to4'}, {'circRatio_6to4'}, ...
    {'circRatio_7to4'}, {'circRatio_6to5'}, {'circRatio_7to5'}, ...
    {'circRatio_7to6'}];
circRatios = titles_circ';
titles_peri = [{'periRatio_2to1'}, {'periRatio_3to1'}, ...
    {'periRatio_4to1'}, {'periRatio_5to1'}, {'periRatio_6to1'}, ...
    {'periRatio_7to1'}, {'periRatio_3to2'}, {'periRatio_4to2'}, ...
    {'periRatio_5to2'}, {'periRatio_6to2'}, {'periRatio_7to2'}, ...
    {'periRatio_4to3'}, {'periRatio_5to3'}, {'periRatio_6to3'}, ...
    {'periRatio_7to3'}, {'periRatio_5to4'}, {'periRatio_6to4'}, ...
    {'periRatio_7to4'}, {'periRatio_6to5'}, {'periRatio_7to5'}, ...
    {'periRatio_7to6'}];
periRatios = [titles_peri'];
curvatures = [{'curvatures'}];
% curvatures based on findPointsNormal.m file
curvature_avg = [{'curvature_avg'}];
curvature_med = [{'curvature_med'}];
curvature_std = [{'curvature_std'}];
curvature_range = [{'curvature_range'}];
curvature_kurt = [{'curvature_kurt'}];
curvature_skew = [{'curvature_skew'}];
curvature_mu = [{'curvature_mu'}];
curvature_lambda = [{'curvature_lambda'}];

%% extracting features
for n=1:1:2
    if n==1
        side='left';
    else
```

```
    side='right';
end

for m=1:1:len_IDnums
    mat_fn = [path vs '\' ID{m} side vs filetype];
    load(mat_fn, 'objXYZ_Align', 'objXYZ_nonAlign', ...
        'objNorm_Align','objNorm_nonAlign')

    armID=[ID{m} side];
    titles=[titles {armID}];

    % FOREARM ANGLE; one-double output
    [angle_xy, angle_xz]=forearm_angle(objXYZ_Align);
    anglexy = [anglexy {angle_xy}];
    anglexz = [anglexz {angle_xz}];
    % NORMAL PER COORDINATE DIRECTION
    normals=[normals {objNorm_nonAlign}]; %vector %v2 and v3
    normalx=[normalx {objNorm_nonAlign(:,1)}]; %vector
    normalx_avg=[normalx_avg {mean(objNorm_nonAlign(:,1))}];
        %double
    normalx_med=[normalx_med {median(objNorm_nonAlign(:,1))}];
        %double
    normalx_std=[normalx_std {std(objNorm_nonAlign(:,1))}];
        %double
    normalx_range=[normalx_range {range(objNorm_nonAlign(:,1))}];
        %double
    normalx_kurt=[normalx_kurt {kurtosis(objNorm_nonAlign(:,1))}];
        %double
    normalx_skew=[normalx_skew {skewness(objNorm_nonAlign(:,1))}];
        %double
    normaly=[normaly {objNorm_nonAlign(:,2)}]; %vector
    normaly_avg = [normaly_avg {mean(objNorm_nonAlign(:,2))}];
        %double
    normaly_med=[normaly_med {median(objNorm_nonAlign(:,2))}];
        %double
    normaly_std=[normaly_std {std(objNorm_nonAlign(:,2))}];
        %double
    normaly_range=[normaly_range {range(objNorm_nonAlign(:,2))}];
        %double
    normaly_kurt=[normaly_kurt {kurtosis(objNorm_nonAlign(:,2))}];
        %double
    normaly_skew=[normaly_skew {skewness(objNorm_nonAlign(:,2))}];
        %double
    normaly_dist = fitdist((objNorm_nonAlign(:,2)+1)/2,'beta');
    normaly_alpha = [normaly_alpha {normaly_dist.a}];
    normaly_beta = [normaly_beta {normaly_dist.b}];
    normalz=[normalz {objNorm_nonAlign(:,3)}]; %vector
    normalz_avg = [normalz_avg {mean(objNorm_nonAlign(:,3))}];
        %double
    normalz_med=[normalz_med {median(objNorm_nonAlign(:,3))}];
        %double
    normalz_std=[normalz_std {std(objNorm_nonAlign(:,3))}];
        %double
    normalz_range=[normalz_range {range(objNorm_nonAlign(:,3))}];
        %double
    normalz_kurt=[normalz_kurt {kurtosis(objNorm_nonAlign(:,3))}];
```

```
    %double
normalz_skew=[normalz_skew {skewness(objNorm_nonAlign(:,3))}];
    %double
normalz_dist = fitdist((objNorm_nonAlign(:,3)+1)/2,'beta');
normalz_alpha = [normalz_alpha {normalz_dist.a}];
normalz_beta = [normalz_beta {normalz_dist.b}];

% CIRCULARITY; output is an array
[k, area, perimeter, circ, volume_disc]= ...
    circularity_v6(objXYZ_nonAlign);

volumes_disc = [volumes_disc {sum(volume_disc(1:end-1))}];

perimeters = [perimeters {(perimeter)}]; %vector
perimeters_avg = [perimeters_avg {mean(perimeter)}]; %double
perimeters_med = [perimeters_med {median(perimeter)}]; %double
perimeters_std = [perimeters_std {std(perimeter)}]; %double
perimeters_range = [perimeters_range {range(perimeter)}];
    %double
perimeters_kurt = [perimeters_kurt {kurtosis(perimeter)}];
    %double
perimeters_skew = [perimeters_skew {skewness(perimeter)}];
    %double
circularities = [circularities {(circ)}]; %vector
circularities_avg = [circularities_avg {mean(circ)}]; %double
circularities_med = [circularities_med {median(circ)}]; %double
circularities_std = [circularities_std {std(circ)}]; %double
circularities_range = [circularities_range {range(circ)}];
    %double
circularities_kurt = [circularities_kurt {kurtosis(circ)}];
    %double
circularities_skew = [circularities_skew {skewness(circ)}];
    %double
areas = [areas {(area)}]; %vector
area_avg = [area_avg {mean(area)}]; %double
area_med = [area_med {median(area)}]; %double
area_std = [area_std {std(area)}]; %double
area_range = [area_range {range(area)}]; %double
area_kurt = [area_kurt {kurtosis(area)}]; %double
area_skew = [area_skew {skewness(area)}]; %double

% RATIOS; output is an array
[circularity_ratios, perimeter_ratios] = ...
    ratios(objXYZ_nonAlign);
% ratios are a horizonal array
circRatios = [circRatios num2cell(circularity_ratios)'];
periRatios = [periRatios num2cell(perimeter_ratios)'];

% CURVATURE is per vertex (point in the 3D point cloud)
[normals, curvature] = findPointNormals(objXYZ_nonAlign);
curvatures = [curvatures {(curvature)}]; %vector
curvature_avg = [curvature_avg {mean(curvature)}]; %double
curvature_med = [curvature_med {median(curvature)}]; %double
curvature_std = [curvature_std {std(curvature)}]; %double
curvature_range = [curvature_range {range(curvature)}]; %double
curvature_kurt = [curvature_kurt {kurtosis(curvature)}];
```

```
            %double
        curvature_skew = [curvature_skew {skewness(curvature)}];
            %double
        curvature_dist = fitdist(abs(curvature)+1e-16, ...
            'InverseGaussian'); %inversegaussiandistribution
        curvature_mu = [curvature_mu {curvature_dist.mu}]; %double
        curvature_lambda = [curvature_lambda {curvature_dist.lambda}];
            %double
    end
end

%% write to .xlsx
%single double outputs
data_single=[titles;outcomes;anglexy;anglexz;normalx_avg; ...
      normalx_med;normalx_std;normalx_range;normalx_kurt; ...
      normalx_skew;normaly_avg;normaly_med;normaly_std; ...
      normaly_range;normaly_kurt;normaly_skew;normaly_alpha; ...
      normaly_beta;normalz_avg;normalz_med;normalz_std; ...
      normalz_range;normalz_kurt;normalz_skew;normalz_alpha; ...
      normalz_beta;volumes_disc;perimeters_avg;perimeters_med; ...
      perimeters_std;perimeters_range;perimeters_kurt; ...
      perimeters_skew;area_avg;area_med;area_std;area_range; ...
      area_kurt;area_skew;circularities_avg;circularities_med; ...
      circularities_std;circularities_range;circularities_kurt; ...
      circularities_skew;periRatios; circRatios;curvature_avg; ...
      curvature_med;curvature_std;curvature_range;curvature_kurt; ...
      curvature_skew;curvature_mu; curvature_lambda];
xlswrite([path '20190213_features_v1.xlsx'], data_single, ...
      'singleOutputs');
xlswrite([path '20190213_features_v1.xlsx'], data_single', ...
      'sO_transposed');
```

A.1.3 forearm_angle.m

```
%% FOREARM_ANGLE.M
%% THIS FUNCTION TAKES IN THE OBJECT FILE AND OUTPUTS THE FOREARM ANGLE
FROM THE XY PLANE AND FROM THE XZ PLANE.

function [angle_y, angle_z]=forearm_angle(objXYZ)
%objXYZ should be the arm cleaved at the shoulder and the wrist

    %compress image into x-y view by deleting the z-coordinate
    objXY=objXYZ(:,1:2);

    %find the min and max x-coordinates
    minX = min(objXY(:,1));
    maxX = max(objXY(:,1));

    %x-range of interest, first 33% of larm length
    forearmX = round((maxX-minX)/3,2)+minX; %add minX to find the
    actual location of X of the forearm of interest
```

```
%initializing variables
maxypts=[];
minypts=[];

%compress image into x-z view by deleting the y-coordinate
objXZ=[objXYZ(:,1), objXYZ(:,3)];
maxzpts=[];
minzpts=[];

%initiate cell array
bin_XY = {};
bin_XZ = {};
rows=0;

%bin points by x coordinate
for i=minX:0.01:forearmX
    i=round(i,2);
    ind_xy=[];
    ind_xz=[];
    ind_xy=objXY(:,1)==i;
    ind_xz=objXZ(:,1)==i;
    bin_xy=[];
    bin_xz=[];
    bin_xy = objXY(ind_xy,:);
    bin_xz = objXZ(ind_xz,:);
    [r,~]=size(bin_xy);
    rows=rows+r;
    bin_XY = [bin_XY {bin_xy}]; %concatonate cell array
    bin_XZ = [bin_XZ {bin_xz}];
end

%find the max y and min y at each x of the forearm
for j=1:length(bin_XY)
    %the top and bottom of arm (in y plane)
    maxypt=max(bin_XY{j}(:,2));
    minypt=min(bin_XY{j}(:,2));
    maxypts=[maxypts maxypt];
    minypts=[minypts minypt];
    %the front and back of arm (in z plane)
    maxzpt=max(bin_XZ{j}(:,2));
    minzpt=min(bin_XZ{j}(:,2));
    maxzpts=[maxzpts maxzpt];
    minzpts=[minzpts minzpt];
end

x_coord=minX:0.01:forearmX;

%create lines
%the top and bottom of arm (in y plane)
p_maxy=polyfit(x_coord, maxypts,1);
f_maxy=polyval(p_maxy,x_coord); %for plotting
p_miny=polyfit(x_coord, minypts,1);
f_miny=polyval(p_miny,x_coord); %for plotting
%the front and back of arm (in z plane)
p_maxz=polyfit(x_coord, maxzpts,1);
f_maxz=polyval(p_maxz,x_coord); %for plotting
```

```
    p_minz=polyfit(x_coord, minzpts,1);
    f_minz=polyval(p_minz,x_coord); %for plotting

    %angle of inclination (theta)
    %the top and bottom of arm (in y plane)
    angle_maxy=atand(p_maxy(1));
    angle_miny=atand(p_miny(1));
    %the front and back of arm (in z plane)
    angle_maxz=atand(p_maxz(1));
    angle_minz=atand(p_minz(1));

    %angle between two lines
    %the top and bottom of arm (in y plane)
    angle_y=abs(angle_maxy-angle_miny); %units: degrees
    %the front and back of arm (in z plane)
    angle_z=abs(angle_maxz-angle_minz);

end
```

A.1.4 circularity.m

```
%% CIRCULARITY.M
%% THIS FUNCTION TAKES IN THE OBJECT FILE AND OUTPUTS THE CROSS-
SECTIONAL AREAS, CROSS-SECTIONAL PERIMETERS, CROSS-SECTIONAL
CIRCULARITIES, VOLUME, AND ARM LENGTH.

function [k,area,perimeter,circ,volume_disc,armLen]= ...
      circularity(objXYZ)
    %objXYZ should be the arm cleaved at the shoulder and the wrist
    minX = min(objXYZ(:,1));
    maxX = max(objXYZ(:,1));
    [r,~]=size(objXYZ);
    objXYZ = sortrows(objXYZ, [1 2 3], {'ascend' 'ascend' 'ascend'});
    round = 0;
    t=0.01; % in meters
    rows=0;
    round = round +1;
    slice=[minX:t:maxX maxX];
    slice_num=length(slice)-1;
    bin_X = {}; %initiate cell array
    bin_size=zeros(1,slice_num);
    for p=2:slice_num
    %all except the last slice because it's not the same thickness
        ind_i = [];
        ind_i = objXYZ(:,1)<slice(p) & objXYZ(:,1)>=slice(p-1);
        bin=[];
        bin = objXYZ(ind_i,:);
        [r,~]=size(bin);
        bin_size(p-1) = r;
        rows=rows+r;
```

```
    bin_X = [bin_X {bin}]; %concatonate cell array
end
    ind_i=objXYZ(:,1)>=slice(end-1);
    bin=[];
    bin=objXYZ(ind_i,:);
    [r,~]=size(bin);
    rows = rows+r;
    bin_size(end) = r;
    bin_X = [bin_X {bin}];

len=length(bin_X);
k = num2cell(zeros(1,len));

area = zeros(1,len);
perimeter = zeros(1,len);
circ = zeros(1,len);
volume_step = zeros(1,len);

for j=1:length(bin_X) %length of the arm in cms
    r=size(bin_X{1,j});
    if r(1)<10 | std(bin_X{1,j}(:,2))==0 | std(bin_X{1,j}(:,3))==0
    else
        % boundary
        k{j}=boundary(bin_X{1,j}(:,2),bin_X{1,j}(:,3));
        y=bin_X{1,j}(:,2);
        z=bin_X{1,j}(:,3);

        % points from boundary function
        tempk=k{j};
        yz_boundary = [y(tempk) z(tempk)];
        %k incl the first point as the last point also to complete
        circle

        % calculating AREA
        area(j) = polyarea(yz_boundary(:,1), yz_boundary(:,2));

        % calculating VOLUME
        volume_step(j) = area(j)*t; %m^2 * m so units is m^3

        % calculate distance between points
        peri = 0;
        for p=2:length(yz_boundary)
            dist=sqrt((yz_boundary(p,1)-yz_boundary((p-1),1))^2 ...
                    + (yz_boundary(p,2)-yz_boundary((p-1),2))^2);
            peri = peri + dist;
        end
        perimeter(j) = peri;
        circ(j) = (perimeter(j) .^ 2) ./ (4 * pi * area(j));
        if circ(j) > 2
            k{j}=boundary(bin_X{1,j}(:,2),bin_X{1,j}(:,3),0.1);
            y=bin_X{1,j}(:,2);
            z=bin_X{1,j}(:,3);
            tempk=k{j};
            yz_boundary = [y(tempk) z(tempk)];
            area(j) = polyarea(yz_boundary(:,1), yz_boundary(:,2));
            volume_step(j) = area(j)*.01;
```

```
                peri = 0;
                for m=2:length(yz_boundary)
                    dist = sqrt((yz_boundary(m,1)- ...
                              yz_boundary((m-1),1))^2 + ...
                              (yz_boundary(m,2)- ...
                              yz_boundary((m-1),2))^2);
                    peri = peri + dist;
                end
                perimeter(j) = peri;
                circ(j) = (perimeter(j) .^ 2) ./ (4 * pi * area(j));
            else
            end
        end
        % finishing calculation for VOLUME
         t_last=maxX-slice(end-1);
        volume_step(end) = area(end)*t_last;
        volume_disc = sum(volume_step);
        slices = slice_num;
        bin_sizes = median(bin_size);
        armLen = maxX - minX;
    end

    % for slices too small
    if area(end)==0
        area=area(1:end-1);
        perimeter=perimeter(1:end-1);
        circ=circ(1:end-1);
        armLen = armLen - t;
    else
    end
end
```

A.2 Table of Local Geometry Features

Table 12 Local Geometry Features

Base features created	Vector size per scan	Feature Vector
Angles	1x2	x-y x-z
Minimum Curvature (per region)	1x36	36 Regions
Maximum Curvature (per region)	1x36	36 Regions
Mean Curvature (per region)	1x36	36 Regions
Gaussian Curvature (per region)	1x36	36 Regions
PCA	1x3	S1

		S2 S3
Volume	1x1	-
Arm Length	1x1	-
Average Cross-sectional area	1x1	-
Base features created	**Vector size per scan**	**Statistical Representation**
Curvature (per point)	1xV*	Average Median Standard Deviation Range Skewness Kurtosis Mu Lambda
Normal_x-coordinate	1xV*	Average Median Standard Deviation Range Skewness Kurtosis
Normal_y-coordinate	1xV*	Average Median Standard Deviation Range Skewness Kurtosis Alpha Beta
Normal_z-coordinate	1xV*	Average Median Standard Deviation Range Skewness Kurtosis Alpha Beta
Perimeter	1xL**	Average Median Standard Deviation Range Skewness Kurtosis
Area	1xL**	Average

		Median Standard Deviation Range Skewness Kurtosis
Circularity	1xL**	Average Median Standard Deviation Range Skewness Kurtosis
SDF	1xV*	Average Median Standard Deviation Range Skewness Kurtosis

* V represents the number of vertices in the arm scan

** L represents the number of 1 cm slices in the arm scan (equals to the length of the arm in cm)

A.3 Aim 2 Model Results

Table 13 Three-class patient classification features and p-values

Features	**p-values**
volumes_disc_DiffRL	4.30E-06
volumearmLen_DiffRL	1.50E-05
perimeters_avg_DiffRL	3.13E-05
perimeters_med_DiffRL	0.012436
perimeters_std_DiffRL	0.010408
area_avg_DiffRL	3.44E-05
area_med_DiffRL	0.018359
area_std_DiffRL	0.004867
periRatio_5to1_DiffRL	0.054304
periRatio_5to4_DiffRL	0.03452
circRatio_7to2_DiffRL	0.069468
circRatio_7to4_DiffRL	0.065403
circRatio_7to5_DiffRL	0.019412
curvature_avg_DiffRL	0.042712
curvature_med_DiffRL	0.000115
curvature_mu_DiffRL	0.042712

curvature_lambda_DiffRL	0.028521

Table 14 Three-class patient classification training set outcomes

	1-1	1-2	1-3	2-1	2-2	2-3	3-1	3-2	3-3	Acc	Sen	Spec
Fine Tree	8	0	5	0	2	3	6	3	23	0.66	0.556	0.719
Medium Tree	8	0	5	0	2	3	6	3	23	0.66	0.556	0.719
Coarse Tree	8	0	5	0	2	3	6	3	23	0.66	0.556	0.719
Linear SVM	7	0	6	0	1	4	1	0	31	0.78	0.444	0.969
Quad SVM	8	0	5	0	1	4	1	2	29	0.76	0.500	0.906
Cubic SVM	7	0	6	0	1	4	5	4	23	0.62	0.444	0.719
Fine Gaussian SVM	0	0	13	0	0	5	0	0	32	0.64	0.000	1.000
Med Gaussian SVM	3	0	10	0	0	5	0	0	32	0.7	0.167	1.000
Coarse Gauss SVM	1	0	12	0	0	5	0	0	32	0.66	0.056	1.000
Fine KNN	9	0	4	0	1	4	7	4	21	0.62	0.556	0.656
Medium KNN	8	0	5	0	0	5	4	0	28	0.72	0.444	0.875
Coarse KNN	0	0	13	0	0	5	0	0	32	0.64	0.000	1.000
Cosine KNN	11	0	2	0	0	5	6	0	26	0.74	0.611	0.813
Cubic KNN	4	0	9	0	0	5	3	0	29	0.66	0.222	0.906
Weighted KNN	9	0	4	0	0	5	3	0	29	0.76	0.500	0.906
Boosted Trees	0	0	13	0	0	5	0	0	32	0.64	0.000	1.000
Bagged Trees	7	0	6	0	1	4	2	1	29	0.74	0.444	0.906
Subspace Disc	8	1	4	0	1	4	1	0	31	0.8	0.529	0.939
Subspace KNN	3	0	10	0	1	4	8	1	23	0.54	0.222	0.719
RUSBoosted Trees	11	0	2	0	4	1	6	11	15	0.6	0.833	0.469
Linear Disc(Full)	9	1	3	0	2	3	3	3	26	0.74	0.647	0.788
Quad Disc (Diag)	10	0	3	0	1	4	4	1	27	0.76	0.611	0.844

* 1-1, 1-2, etc represent the [true-predicted] labels. 1 represents left lymphedema; 2 represents right lymphedema; 3 represents non-lymphedema. To calculate sensitivity and specificity the following outcomes were denoted as True Positive = [1-1, 2-2], True Negative = [3-3], False Positive = [3-1, 3-2], False Negative = [1-2, 1-3, 2-1, 2-3]

** Acc = accuracy, Sen = sensitivity, Spec = specificity

Table 15 Three-class patient classification testing set outcomes

	1-1	1-2	1-3	2-1	2-2	2-3	3-1	3-2	3-3	Acc	Sen	Spec
Medium Tree	5	0	8	1	2	2	8	1	23	0.6	0.412	0.697

Linear SVM	6	0	7	0	2	3	6	0	26	0.68	0.444	0.813
Quad SVM	7	0	6	0	3	2	5	0	27	0.74	0.556	0.844
Fine KNN	9	0	4	0	4	1	10	0	22	0.7	0.722	0.688
Cosine KNN	9	0	4	0	0	5	10	0	22	0.62	0.500	0.688
Weighted KNN	6	0	7	0	0	5	7	0	25	0.62	0.333	0.781
Subspace Disc	7	0	6	0	3	2	7	1	24	0.68	0.556	0.750
RUSBoosted Trees	8	1	4	0	3	2	9	6	17	0.56	0.647	0.515
Linear Disc (Full)	5	4	4	1	3	1	7	2	23	0.62	0.615	0.622
Quad Disc (Diag)	7	0	6	0	4	1	5	2	25	0.72	0.611	0.781

* 1-1, 1-2, etc represent the [true-predicted] labels. 1 represents left lymphedema; 2 represents right lymphedema; 3 represents non-lymphedema. To calculate sensitivity and specificity the following outcomes were denoted as True Positive = [1-1, 2-2], True Negative = [3-3], False Positive = [3-1, 3-2], False Negative = [1-2, 1-3, 2-1, 2-3]

** Acc = accuracy, Sen = sensitivity, Spec = specificity

Table 16 Two-class patient classification features and p-values

Features	**p-values**
Angle_xy_DiffLSVol	0.094102
Normalx_std_DiffLSVol	0.049193
armlength_DiffLSVol	0.065481

Table 17 Two-class patient classification training set outcomes

	TN	**TP**	**FN**	**FP**	**Accuracy**	**Sensitivity**	**Specificity**
Fine Tree	12	4	5	4	0.640	0.444	0.750
Medium Tree	12	4	5	4	0.640	0.444	0.750
Coarse Tree	12	4	5	4	0.640	0.444	0.750
Logistic Regression	12	3	6	4	0.600	0.333	0.750
Linear SVM	12	5	4	4	0.680	0.556	0.750
Quad SVM	9	3	6	7	0.480	0.333	0.563
Cubic SVM	6	4	5	10	0.400	0.444	0.375
Fine Gaussian SVM	16	1	8	0	0.680	0.111	1.000
Med Gaussian SVM	12	2	7	4	0.560	0.222	0.750
Coarse Gaussian SVM	16	0	9	0	0.640	0.000	1.000
Fine KNN	8	2	7	8	0.400	0.222	0.500

Medium KNN	13	2	7	3	0.600	0.222	0.813
Coarse KNN	16	0	9	0	0.640	0.000	1.000
Cosine KNN	13	1	8	3	0.560	0.111	0.813
Cubic KNN	14	2	7	2	0.640	0.222	0.875
Weighted KNN	10	4	5	6	0.560	0.444	0.625
Boosted Trees	16	0	9	0	0.640	0.000	1.000
Bagged Trees	9	5	4	7	0.560	0.556	0.563
Subspace Discriminant	13	2	7	3	0.600	0.222	0.813
Subspace KNN	11	2	7	5	0.520	0.222	0.688
RUSBoosted Trees	11	4	5	5	0.600	0.444	0.688
Linear Discriminant (Full)	12	4	5	4	0.640	0.444	0.750
Quad Discriminant (Full)	11	4	5	5	0.600	0.444	0.688

Table 18 Two-class patient classification testing set outcomes

	TN	**TP**	**FN**	**FP**	**Accuracy**	**Sensitivity**	**Specificity**
Medium Tree	35	12	15	13	0.627	0.444	0.729
Logistic Regression	30	8	19	18	0.507	0.296	0.625
Linear SVM	33	12	15	15	0.600	0.444	0.688
Bagged Trees	36	10	17	12	0.613	0.370	0.750
RUSBoosted Trees	35	11	16	13	0.613	0.407	0.729
Quad Discriminant (Full)	39	8	19	9	0.627	0.296	0.813

Table 19 Arm classification features and p-values

Features	**p-values**
normalx_std	0.06453
normalz_avg	0.091204
normalz_std	0.035487
normalz_beta	0.053697
volumes_disc	0.062921
perimeters_avg	0.050218
perimeters_med	0.055631
area_avg	0.044657
area_med	0.055213
area_std	0.080998
area_range	0.074063
circularities_avg	0.019324

circularities_med	0.083057
circularities_std	0.093598
curvature_avg	0.000116
curvature_med	0.000815
curvature_std	7.62E-06
curvature_range	0.003987
curvature_mu	0.000116
curvature_lambda	0.047023

Table 20 Arm classification training set outcomes

	TN	TP	FN	FP	Accuracy	Sensitivity	Specificity
Fine Tree	34	3	6	7	0.740	0.333	0.829
Medium Tree	34	3	6	7	0.740	0.333	0.829
Coarse Tree	34	3	6	7	0.740	0.333	0.829
Logistic Regression	32	3	6	9	0.700	0.333	0.780
Linear SVM	40	1	8	1	0.820	0.111	0.976
Quad SVM	35	4	5	6	0.780	0.444	0.854
Cubic SVM	35	2	7	6	0.740	0.222	0.854
Fine Gaussian SVM	41	0	9	0	0.820	0.000	1.000
Med Gaussian SVM	39	1	8	2	0.800	0.111	0.951
Coarse Gaussian SVM	41	0	9	0	0.820	0.000	1.000
Fine KNN	33	5	4	8	0.760	0.556	0.805
Medium KNN	40	1	8	1	0.820	0.111	0.976
Coarse KNN	41	0	9	0	0.820	0.000	1.000
Cosine KNN	37	1	8	4	0.760	0.111	0.902
Cubic KNN	41	0	9	0	0.820	0.000	1.000
Weighted KNN	39	1	8	2	0.800	0.111	0.951
Boosted Trees	41	0	9	0	0.820	0.000	1.000
Bagged Trees	34	3	6	7	0.740	0.333	0.829
Subspace Discriminant	39	3	6	2	0.840	0.333	0.951
Subspace KNN	36	1	8	5	0.740	0.111	0.878
RUSBoosted Trees	31	5	4	10	0.720	0.556	0.756
Linear Discriminant (Full)	34	3	6	7	0.740	0.333	0.829
Quad Discriminant (Diag)	36	4	5	5	0.800	0.444	0.878

Table 21 Arm classification testing set outcomes

	TN	TP	FN	FP	Accuracy	Sensitivity	Specificity
Quad SVM	108	4	23	15	0.747	0.148	0.878
Fine KNN	99	5	22	24	0.693	0.185	0.805
RUSBoosted Trees	89	14	13	34	0.687	0.519	0.724
Quad Discriminant (Diag)	100	10	17	23	0.733	0.370	0.813

REFERENCES

1. Olszewski WL. The lymphatic system in body homeostasis: physiological conditions. *Lymphat Res Biol*. 2003;1(1):11-21. doi:10.1089/15396850360495655.

2. Gwendalyn J. Randolph, Angeli V, Swartz MA. Dendritic-cell trafficking to lymph nodes through lymphatic vessels. *Nat Rev Immunol*. 2005;5:617-628.

3. Dixon JB. Lymphatic lipid transport: sewer or subway? *Trends Endocrinol Metab*. 2010;21(8):480-487. doi:10.1016/j.tem.2010.04.003.

4. Swartz MA. The physiology of the lymphatic system. *Adv Drug Deliv Rev*. 2001;50(1-2):3-20. http://www.ncbi.nlm.nih.gov/pubmed/11489331.

5. Mortimer PS, Rockson SG. New developments in clinical aspects of lymphatic disease. *J Clin Invest*. 2014;124(3):915-921. doi:10.1172/JCI71608.

6. Mortimer PS. The Pathophysiology of Lymphedema. *Cancer Suppl*. 1998;83(12):2798-2802.

7. Zuther JE, Norton S. *Lymphedema Management: The Comprehensive Guide for Practitioners*. 4th Editio. New York: Thieme; 2018.

8. Velanovich V, Szymanski W. Quality of life of breast cancer patients with lymphedema. *Am J Surg*. 1999;177(3):184-7; discussion 188. http://www.ncbi.nlm.nih.gov/pubmed/10219851.

9. Beaulac SM, McNair L a, Scott TE, LaMorte WW, Kavanah MT. Lymphedema and

quality of life in survivors of early-stage breast cancer. *Arch Surg*. 2002;137:1253-1257. doi:10.1001/archsurg.137.11.1253.

10. Ferrandina G, Mantegna G, Petrillo M, et al. Quality of life and emotional distress in early stage and locally advanced cervical cancer patients : A prospective , longitudinal study. *Gynecol Oncol*. 2012;124(3):389-394. doi:10.1016/j.ygyno.2011.09.041.

11. Korpan MI, Crevenna R, Fialka-Moser V. Lymphedema: A therapeutic approach in the treatment and rehabilitation of cancer patients. *Am J Phys Med Rehabil*. 2011;90(SUPPL.5):69-75. doi:10.1097/PHM.0b013e31820be160.

12. Gerber L, Lampert M, Wood C, et al. Comparison of pain, motion, and edema after modified radical mastectomy vs. local excision with axillary dissection and radiation. *Breast Cancer Res Treat*. 1992;21(2):139-145. doi:10.1007/BF01836960.

13. Moffatt CJ, Franks PJ, Doherty DC, et al. Lymphoedema: An underestimated health problem. *QJM - Mon J Assoc Physicians*. 2003;96(10):731-738. doi:10.1093/qjmed/hcg126.

14. Shaw C, Mortimer P, Judd PA. A randomized controlled trial of weight reduction as a treatment for breast cancer-related lymphedema. *Cancer*. 2007;110(8):1868-1874. doi:10.1002/cncr.22994.

15. Casley-Smith JR. Lymphedema initiated by aircraft flights. *Aviat Space Environ Med*. 1996;61(1):52-56.

16. Clark B, Sitzia J, Harlow W. Incidence and risk of arm oedema following treatment for breast cancer: a three-year follow-up study. *QJM - Mon J Assoc Physicians*. 2005;98(5):343-348. doi:10.1093/qjmed/hci053.

17. Petrek JA, Pressman PI, Smith RA. Lymphedema: current issues in research and management. *CA - A Cancer J Clin*. 2000;50(5):292-307. http://www.ncbi.nlm.nih.gov/pubmed/11075239.

18. Loudon L, Petrek J. Lymphedema in women treated for breast cancer. *Cancer Pract*. 2000;8(2):65-71.

19. Siegel RL, Miller KD, Jemal A. Cancer statistics, 2017. *CA Cancer J Clin*. 2017;67(1):7-30. doi:10.3322/caac.21387.

20. Rockson SG. Lymphedema. *Vasc Med*. 2016;21(1):77-81. doi:10.1177/1358863X15620852.

21. Morrell RM, Halyard MY, Schild SE, Ali MS, Gunderson LL, Pockaj BA. Breast Cancer-Related Lymphedema. *Mayo Clin Proc*. 2005;80(11):1480-1484. doi:http://dx.doi.org/10.4065/80.11.1480.

22. Ribeiro Pereira ACP, Koifman RJ, Bergmann A. Incidence and risk factors of lymphedema after breast cancer treatment: 10 years of follow-up. *The Breast*. 2017;36:67-73. doi:10.1016/j.breast.2017.09.006.

23. Kwan ML, Yao S, Lee VS, et al. Race/ethnicity, genetic ancestry, and breast cancer-related lymphedema in the Pathways Study. *Breast Cancer Res Treat*.

2016;159(1):119-129. doi:10.1007/s10549-016-3913-x.

24. Sherman KA, Kilby CJ, Elder E, Ridner SH. Factors associated with professional healthcare advice seeking in women at risk for developing breast cancer-related lymphedema. *Patient Educ Couns*. 2018;101(3):445-451. doi:10.1016/j.pec.2017.10.010.

25. Jammallo LS, Miller CL, Horick NK, et al. Factors associated with fear of lymphedema after treatment for breast cancer. *Oncol Nurs Forum*. 2014;41(5):473-483. doi:10.1188/14.ONF.473-483.

26. Norman SA, Localio AR, Potashnik SL, et al. Lymphedema in breast cancer survivors: Incidence, degree, time course, treatment, and symptoms. *J Clin Oncol*. 2009;27(3):390-397. doi:10.1200/JCO.2008.17.9291.

27. Fu MR. Breast cancer-related lymphedema: Symptoms, diagnosis, risk reduction, and management. *World J Clin Oncol*. 2014;5(3):241-247. doi:10.5306/wjco.v5.i3.241.

28. Ivens D, Hoe AL, Podd TJ, Hamilton CR, Taylor I, Royle GT. Assessment of morbidity from complete axillary dissection. *Br J Cancer*. 1992;66(1):136-138. doi:10.1038/bjc.1992.230.

29. Hinrichs CS, Watroba NL, Rezaishiraz H, et al. Lymphedema Secondary to Postmastectomy Radiation: Incidence and Risk Factors. *Ann Surg Oncol*. 2004;11(6):573-580. doi:10.1245/ASO.2004.04.017.

30. Ahmed RL, Prizment A, Lazovich D, Schmitz KH, Folsom AR. Lymphedema and quality of life in breast cancer survivors: The Iowa Women's Health Study. *J Clin Oncol*. 2008;26(35):5689-5696. doi:10.1200/JCO.2008.16.4731.

31. McWayne J, Heiney SP. Psychologic and social sequelae of secondary lymphedema: A review. *Cancer*. 2005;104(3):457-466. doi:10.1002/cncr.21195.

32. Chance-Hetzler J, Armer J, Van Loo M, et al. Prospective Lymphedema Surveillance in a Clinic Setting. *J Pers Med*. 2015;5(3):311-325. doi:10.3390/jpm5030311.

33. Swenson KK, Nissen MJ, Leach JW, Post-White J. Case-control study to evaluate predictors of lymphedema after breast cancer surgery. *Oncol Nurs Forum*. 2009;36(2):185-193. doi:HQ16X6622407521W [pii]\r10.1188/09.ONF.185-193.

34. Tsai RJ, Dennis LK, Lynch CF, Snetselaar LG, Zamba GKD, Scott-Conner C. The risk of developing arm lymphedema among breast cancer survivors: a meta-analysis of treatment factors. *Ann Surg Oncol*. 2009;16(7):1959-1972. doi:10.1245/s10434-009-0452-2.

35. Cemal Y, Pusic A, Mehrara BJ. Preventative Measures for Lymphedema: Separating Fact from Fiction. *J Am Coll Surg*. 2011;213(4):543-551. doi:10.1016/j.jamcollsurg.2011.07.001.

36. Soran A, D'Angelo G, Begovic M, et al. Breast cancer-related lymphedema - What are the significant predictors and how they affect the severity of lymphedema? *Breast J*. 2006;12(6):536-543. doi:10.1111/j.1524-4741.2006.00342.x.

37. Helyer LK, Varnic M, Le LW, Leong W, McCready D. Obesity is a risk factor for developing postoperative lymphedema in breast cancer patients. *Breast J*. 2010;16(1):48-54. doi:10.1111/j.1524-4741.2009.00855.x.

38. Ahmed RL, Schmitz KH, Prizment AE, Folsom AR. Risk factors for lymphedema in breast cancer survivors, the Iowa Women's Health Study. *Breast Cancer Res Treat*. 2011;130(3):981-991. doi:10.1007/s10549-011-1667-z.

39. Ridner SH, Dietrich MS, Stewart BR, Armer JM. Body mass index and breast cancer treatment-related lymphedema. *Support Care Cancer*. 2011;19(6):853-857. doi:10.1007/s00520-011-1089-9.

40. Meeske K a, Sullivan-Halley J, Smith AW, et al. Risk factors for arm lymphedema following breast cancer diagnosis in Black women and White women. *Breast Cancer Res Treat*. 2009;113(2):383-391. doi:10.1007/s10549-008-9940-5.

41. McLaughlin SA, Bagaria S, Gibson T, et al. Trends in risk reduction practices for the prevention of lymphedema in the first 12 months after breast cancer surgery. *J Am Coll Surg*. 2013;216(3):380-389. doi:10.1016/j.jamcollsurg.2012.11.004.

42. The International Society of Lymphology. The Diagnosis and Treatment of Peripheral Lymphedema: 2016 Consensus Document of the International Society of Lymphology. *Lymphology*. 2016;49:170-184. https://www.internationalsocietyoflymphology.org/wp-content/uploads/2017/12/20106-35060-1-PB.pdf.

43. Stillwell G. Treatment of Postmastectomy Lymphedema. *Mod Treat*.

1969;6(2):396-412.

44. Lai L, Binkley J, Jones V, et al. Implementing the Prospective Surveillance Model (PSM) of Rehabilitation for Breast Cancer Patients with 1-Year Postoperative Follow-up, a Prospective, Observational Study. *Ann Surg Oncol*. 2016;23(10):3379-3384. doi:10.1245/s10434-016-5315-z.

45. Zaleska M, Olszewski WL, Durlik M. The Effectiveness of Intermittent Pneumatic Compression in Long-Term Therapy of Lymphedema of Lower Limbs. *Lymphat Res Biol*. 2014;12(2):103-109. doi:10.1089/lrb.2013.0033.

46. Adams KE, Rasmussen JC, Darne C, et al. Direct evidence of lymphatic function improvement after advanced pneumatic compression device treatment of lymphedema. *Biomed Opt Express*. 2010;1(1):114-125. doi:10.1364/BOE.1.000114.

47. Pappas CJ, O'Donnell TF. Long-term results of compression treatment for lymphedema. *J Vasc Surg*. 1992;16(4):555-564. doi:10.1016/0741-5214(92)90163-3.

48. Moseley a L, Carati CJ, Piller NB. A systematic review of common conservative therapies for arm lymphoedema secondary to breast cancer treatment. *Ann Oncol*. 2007;18(4):639-646. doi:10.1093/annonc/mdl182.

49. Ramos SM, O'Donnell LS, Knight G. Edema volume, not timing, is the key to success in lymphedema treatment. *Am J Surg*. 1999;178(4):311-315. doi:10.1016/S0002-9610(99)00185-3.

50. Tiwari A, Cheng K, Button M, Myint F, Hamilton G. Differential Diagnosis, Investigation, and Current Treatment of Lower Limb Lymphedema. *Arch Surg*. 2003;138(1):152-161.

51. Koshima I, Narushima M, Yamamoto Y, Mihara M, Iida T. Recent advancement on surgical treatments for lymphedema. *Ann Vasc Dis*. 2012;5(4):409-415. doi:10.3400/avd.ra.12.00080.

52. Committee NMA. *The Diagnosis and Treatment of Lymphedema*.; 2011.

53. Sander AP, Hajer NM, Hemenway K, Miller AC. Upper-extremity volume measurements in women with lymphedema: A comparison of measurements obtained via water displacement with geometrically determined volume. *Phys Ther*. 2002;82(12):1201-1212.

54. Deltombe T, Jamart J, Recloux S, et al. Reliability and limits of agreement of circumferential, water displacement, and optoelectronic volumetry in the measurement of upper limb lymphedema. *Lymphology*. 2007;40(1):26-34. doi:10.3109/0284186X.2014.952389.

55. Armer JM, Stewart BR. A comparison of four diagnostic criteria for lymphedema in a post-breast cancer population. *Lymphat Res Biol*. 2005;3(4):208-217. doi:10.1089/lrb.2005.3.208.

56. Jung M, Jeon JY, Yun GJ, Yang S, Kwon S, Seo YJ. Reference values of bioelectrical impedance analysis for detecting breast cancer-related lymphedema. *Medicine (Baltimore)*. 2018;97(44):e12945. doi:10.1097/MD.0000000000012945.

57. Dylke ES, Schembri GP, Bailey DL, et al. Diagnosis of upper limb lymphedema: development of an evidence-based approach. *Acta Oncol (Madr)*. 2016;55(12):1477-1483. doi:10.1080/0284186X.2016.1191668.

58. Newcastle and York External Assessment Centre. *L -De x U400 for Lymphoedema after Breast Cancer Treatment*.; 2017.

59. Bundred NJ, Stockton C, Keeley V, et al. Comparison of multi-frequency bioimpedance with perometry for the early detection and intervention of lymphoedema after axillary node clearance for breast cancer. *Breast Cancer Res Treat*. 2015;151(1):121-129. doi:10.1007/s10549-015-3357-8.

60. Witte CL, Witte MH, Unger EC, et al. Advances in Imaging of Lymph Flow Disorders. *Radiographics*. 2000;20(6):1697-1719. doi:10.1148/radiographics.20.6.g00nv141697.

61. Society AC. *Understanding Lymphedema – For Cancers Other Than Breast Cancer What Is Lymphedema ? Signs of Lymphedema*.; 2013.

62. Armer JM. The Problem of Post-Breast Cancer Lymphedema: Impact and Measurement Issues. *Cancer Invest*. 2005;23(1):76-83. doi:10.1007/s11171-008-2009-8.

63. Stout NL, Binkley JM, Schmitz KH, et al. A prospective surveillance model for rehabilitation for women with breast cancer. *Cancer*. 2012;118(SUPPL.8):2191-2200. doi:10.1002/cncr.27476.

64. Armer JM, Hulett JM, Bernas M, Ostby P, Stewart BR, Cormier JN. Best-Practice Guidelines in Assessment, Risk Reduction, Management, and Surveillance for Post-Breast Cancer Lymphedema. *Curr Breast Cancer Rep*. 2013;5(2):134-144. doi:10.1007/s12609-013-0105-0.

65. Norman SA, Miller LT, Erikson HB, Norman MF, McCorkle R. Development and validation of a telephone questionnaire to characterize lymphedema in women treated for breast cancer. *Phys Ther*. 2001;81(6):1192-1205. http://www.ncbi.nlm.nih.gov/pubmed/11380275.

66. Armer JM, Radina ME, Porock D, Culbertson SD. Predicting Breast Cancer-Related Lymphedema Using Self-Reported Symptoms. *Nurs Res*. 2003;52(6).

67. Carter J, Raviv L, Appollo K, Baser RE, Iasonos A, Barakat RR. A pilot study using the Gynecologic Cancer Lymphedema Questionnaire (GCLQ) as a clinical care tool to identify lower extremity lymphedema in gynecologic cancer survivors. *Gynecol Oncol*. 2010;117(2):317-323. doi:10.1016/j.ygyno.2010.01.022.

68. Bernas MJ, Askew RL, Armer JM, Cormier JN. Lymphedema: How do we diagnose and reduce the risk of this dreaded complication of breast cancer treatment? *Curr Breast Cancer Rep*. 2010;2(1):53-58. doi:10.1007/s12609-010-0009-1.

69. Stout Gergich NL, Pfalzer LA, McGarvey C, Springer B, Gerber LH, Soballe P. Preoperative assessment enables the early diagnosis and successful treatment of lymphedema. *Cancer*. 2008;112(12):2809-2819. doi:10.1002/cncr.23494.

70. Binkley JM, Harris SR, Levangie PK, et al. Patient perspectives on breast cancer

treatment side effects and the prospective surveillance model for physical rehabilitation for women with breast cancer. *Cancer*. 2012;118(SUPPL.8):2207-2216. doi:10.1002/cncr.27469.

71. Dorr DA, Wilcox A, Burns L, Brunker CP, Narus SP, Clayton PD. Implementing a Multidisease Chronic Care Model in Primary Care Using People and Technology. *Dis Manag*. 2006;9(1):1-15. doi:https://doi.org/10.1089/dis.2006.9.1.

72. Stanton AWB, Northfield JW, Holroyd B, Mortimer PS, Levick JR. Validation of an optoelectronic limb volumeter (Perometer). *Lymphology*. 1997;30:77-97.

73. Stanton AW., Badger C, Sitzia J. Non-invasive assessment of the lymphedematous limb. *Lymphology*. 2000;33(3):122-135.

74. Sharkey AR, King SW, Kuo RY, Bickerton SB, Ramsden AJ, Furniss D. Measuring Limb Volume: Accuracy and Reliability of Tape Measurement Versus Perometer Measurement. *Lymphat Res Biol*. 2017;00(00):lrb.2017.0039. doi:10.1089/lrb.2017.0039.

75. Hwang JH, Kwon JY, Lee KW, et al. Changes in lymphatic function after complex physical therapy for lymphedema. *Lymphology*. 1999;32(1):15-21. http://search.proquest.com/professional/docview/592133456?accountid=137925.

76. Perrin M, Guex JJ. Edema and Leg Volume: Methods of Assessment. *Angiology*. 2000;51(1):9-12. doi:10.1177/000331970005100103.

77. Moreira R, Magalhães A, Oliveira H. A Kinect-Based System for Upper-Body

Function Assessment in Breast Cancer Patients. *J Imaging*. 2015;1(1):134-155. doi:10.3390/jimaging1010134.

78. Öhberg F, Zachrisson A, Holmner-Rocklöv Å. Three-Dimensional Camera System for Measuring Arm Volume in Women with Lymphedema Following Breast Cancer Treatment. *Lymphat Res Biol*. 2014;12(4):267-274. doi:10.1089/lrb.2014.0026.

79. Lu G, Han K, Desouza GN, Armer J, Shyu CR. A new algorithm for 3D registration and its application in self-monitoring and early detection of lymphedema. *IRBM*. 2014;35(6):370-384. doi:10.1016/j.irbm.2014.10.003.

80. Buffa R, Mereu E, Lussu P, et al. A new, effective and low-cost three-dimensional approach for the estimation of upper-limb volume. *Sensors*. 2015;15(6):12342-12357. doi:10.3390/s150612342.

81. Hameeteman M, Verhulst AC, Vreeken RD, Maal TJJ, Ulrich DJO. 3D stereophotogrammetry in upper-extremity lymphedema: An accurate diagnostic method. *J Plast Reconstr Aesthetic Surg*. 2016;69(2):241-247. doi:10.1016/j.bjps.2015.10.011.

82. Hoevenaren IA, Verhulst AC, Hameeteman M, Vreeken RD, Maal TJJ, Ulrich DJO. Three-dimensional stereophotogrammetry as an accurate tool for analyzing lymphedema of the hand. *JPRAS Open*. 2016;10:40-46. doi:10.1016/j.jpra.2016.07.002.

83. Verhulst AC, Wesselius TS, Glas HH, Vreeken RD, Ulrich DJO, Maal TJJ. Accuracy and reproducibility of a newly developed tool for volume measurements

of the arm using 3D stereophotogrammetry. *J Plast Reconstr Aesthetic Surg*. 2017;70(12):1753-1759. doi:10.1016/j.bjps.2017.07.016.

84. Karakashian K, Shaban L, Pike C, van Loon R. Investigation of Shape with Patients Suffering from Unilateral Lymphoedema. *Ann Biomed Eng*. 2017. doi:10.1007/s10439-017-1929-y.

85. Landau MJ, Kim JS, Gould DJ, Patel KM. Vectra 3D Imaging for Quantitative Volumetric Analysis of the Upper Limb: A Feasibility Study for Tracking Outcomes of Lymphedema Treatment. *Plast Reconstr Surg*. 2018;141(1):80e-84e. doi:10.1097/PRS.0000000000003912.

86. Koban KC, Schenck TL, Giunta RE. Using Mobile 3D Scanning Systems for Objective Evaluation of Form, Volume, and Symmetry in Plastic Surgery: Intraoperative Scanning and Lymphedema Assessment. In: *Proceedings of the 7th International Conference on 3D Body Scanning Technologies*. Lugano; 2016. doi:10.15221/16.

87. Yahathugoda C, Weiler MJ, Rao R, et al. Use of a novel portable 3D scanner to measure limb volume and circumference in patients with filarial lymphedema. *Am J Trop Med Hyg*. 2017. doi:https://doi.org/10.4269/ajtmh.17-0504.

88. Bahadori M, Teymourzadeh E, Ravangard R, Raadabadi M. Factors affecting the overcrowding in outpatient healthcare. *J Educ Health Promot*. 2017;6(21). doi:10.4103/2277-9531.204742.

89. Hull MM. Lymphedema in women treated for breast cancer. *Semin Oncol Nurs*.

2000;16(3):226-237. doi:l 0.1053/sone.2000.8117.

90. Taylor R, Jayasinghe UW, Koelmeyer L, Ung O, Boyages J. Reliability and Validity of Arm Volume Measurements for Assessment of Lymphedema. *Phys Ther*. 2006;86(2):205-214. doi:10.1093/ptj/86.2.205.

91. Landis JR, Koch GG. The Measurement of Observer Agreement for Categorical Data. *Biometrics*. 1977;33(1):159-174. doi:10.2307/2529310.

92. Watson PF, Petrie A. Method agreement analysis: A review of correct methodology. *Theriogenology*. 2010;73(9):1167-1179. doi:10.1016/j.theriogenology.2010.01.003.

93. McLaughlin SA, Staley AC, Vicini F, et al. Considerations for Clinicians in the Diagnosis, Prevention, and Treatment of Breast Cancer-Related Lymphedema: Recommendations from a Multidisciplinary Expert ASBrS Panel: Part 1: Definitions, Assessments, Education, and Future Directions. *Ann Surg Oncol*. 2017;24(10):2818-2826. doi:10.1245/s10434-017-5982-4.

94. Mayrovitz HN. Limb volume estimates based on limb elliptical vs. circular cross section models. *Lymphology*. 2003;36(3):140-143. http://www.ncbi.nlm.nih.gov/pubmed/14552033.

95. Tan CW, Coutts F, Bulley C. Measurement of lower limb volume: Agreement between the vertically oriented perometer and a tape measure method. *Physiotherapy*. 2013;99(3):247-251. doi:10.1016/j.physio.2012.12.004.

96. Lu IM, Dixon JB. Assessment of Upper Extremity Swelling Among Breast Cancer Survivors with a Commercial Infrared Sensor. *Lymphat Res Biol*. 2019;0(0). doi:https://doi.org/10.1089/lrb.2018.0010.

97. Bergmark K, Åvall-Lundqvist E, Dickman PW, Henningsohn L, Steineck G. Lymphedema and bladder-emptying difficulties after radical hysterectomy for early cervical cancer and among population controls. *Int J Gynecol Cancer*. 2006;16(3):1130-1139. doi:10.1111/j.1525-1438.2006.00601.x.

98. Lymphoedema Framework. *Best Practice for the Management of Lymphoedema*. London; 2006. http://www.woundsinternational.com/pdf/content_175.pdf.

99. Brown JC, John GM, Sega S, Chu CS, Schmitz KH. Physical Activity and Lower Limb Lymphedema among Uterine Cancer Survivors. *Med Sci Sport Exerc*. 2013;45(11):2091-2097. doi:10.1249/MSS.0b013e318299afd4.

100. Sawan S, Mugnai R, Lopes A de B, Hughes A, Edmondson RJ. Lower-Limb Lymphedema and Vulval Cancer Feasibility of Prophylactic Compression Garments and Validation of Leg Volume Measurement. *Int J Gynecol Cancer*. 2009;19(9):1649-1654. doi:10.1111/IGC.0b013e3181a8446a.

101. Moreira R, Magalhaes A, Oliveira HP. A Kinect-Based System to Assess Lymphedema Impairments in Breast Cancer Patients. *Pattern Recognit Image Anal*. 2015;9117:228-236. doi:10.1007/978-3-319-19390-8_26.

102. Ko DSC, Lerner R, Klose G, Cosimi AB. Effective treatment of lymphedema of the extremities. *Arch Surg*. 1998;133(4):452-458.

http://www.ncbi.nlm.nih.gov/pubmed/9565129.

103. Fukushima T, Tsuji T, Sano Y, et al. Immediate effects of active exercise with compression therapy on lower-limb lymphedema. *Support Care Cancer*. 2017;25(8):2603-2610. doi:10.1007/s00520-017-3671-2.

104. Fu MR, Wang Y, Li C, et al. Machine learning for detection of lymphedema among breast cancer survivors. *mHealth*. 2018;4(17):1-11. doi:10.21037/mhealth.2018.04.02.

105. Armer JM, Ballman K V, McCall L, et al. Lymphedema symptoms and limb measurement changes in breast cancer survivors treated with neoadjuvant chemotherapy and axillary dissection: results of American College of Surgeons Oncology Group (ACOSOG) Z1071 (Alliance) substudy. *Support Care Cancer*. July 2018. doi:10.1007/s00520-018-4334-7.

106. Taylor Z. findPointNormals.m. 2015.

107. Taylor Z, Nieto J, Johnson D. Multi-Modal Sensor Calibration Using a Gradient Orientation Measure. *J F Robot*. 2015;32(5):675-695. doi:10.1002/rob.

108. Shapira L, Shamir A, Cohen-Or D. Consistent mesh partitioning and skeletonisation using the Shape Diameter Function. *Vis Comput*. 2008;24:249-259. doi:10.1007/s00371-007-0197-5.

109. Goltner E, Gass P, Haas JP, Schneider P. The importance of volumetry, lymphscintigraphy and computer tomography in the diagnosis of brachial edema

after mastectomy. *Lymphology*. 1988;21(3):134-143.

110. Lu G, DeSouza GN, Armer J, Anderson B, Shyu C-R. A System for Limb-Volume Measurement using 3D Models from an Infrared Depth Sensor. *Proc 2013 Ieee Symp Comput Intell Healthc E-Health*. 2013;M:64-69.

111. Lautenschläger I, Dombrowsky H, Frerichs I, et al. A model of the isolated perfused rat small intestine. *Am J Physiol Gastrointest Liver Physiol*. 2010;298(2):G304-13. doi:10.1152/ajpgi.00313.2009.

112. Binkley J, Weiler M, Frank N, Bober L, Dixon J, Stratford P. Reliability and Convergent Validity of the LymphaTech System to Assess Arm Volume in Patients During and After Treatment for Breast Cancer. *Phys Ther*. 2019;In Press.

113. Stout NL, Pfalzer LA, Springer B, et al. Breast Cancer–Related Lymphedema: Comparing Direct Costs of a Prospective Surveillance Model and a Traditional Model of Care. *Phys Ther*. 2012;92(1):152-163. doi:http://dx.doi.org/10.2522/ptj.20100167.

114. Shih Y-CT, Xu Y, Cormier JN, et al. Incidence, Treatment Costs, and Complications of Lymphedema After Breast Cancer Among Women of Working Age: A 2-Year Follow-Up Study. *J Clin Oncol*. 2009;27(12):2007-2014. doi:10.1200/jco.2008.18.3517.